Subglacial volcanic and geothermal activity
Measurement and modelling of heat flow

Hannah Iona Reynolds

Faculty of Earth Sciences
University of Iceland
2017

Subglacial volcanic and geothermal activity
Measurement and modelling of heat flow

Hannah Iona Reynolds

Dissertation submitted in partial fulfilment of a
Philosophiae Doctor degree in Geophysics

Advisor
Magnús Tumi Gudmundsson

PhD Committee
Magnús Tumi Gudmundsson, University of Iceland
Freysteinn Sigmundsson, University of Iceland
Gudni Axelsson, Iceland Geosurvey

Opponents
Lionel Wilson, Lancaster University
Shaul Hurwitz, U.S. Geological Survey

Faculty of Earth Sciences
School of Engineering and Natural Sciences
University of Iceland
Reykjavik, December 2017

Subglacial volcanic and geothermal activity: Measurement and modelling of heat flow
Subglacial volcanic and geothermal activity
Dissertation submitted in partial fulfillment of a *Philosophiae Doctor* degree in Geophysics

Copyright © 2017 Hannah Iona Reynolds
All rights reserved

Faculty of Earth Sciences
School of Engineering and Natural Sciences
University of Iceland
Sturlugata 7
101 Reykjavík
Iceland

Telephone: 525 4000

Bibliographic information:
Hannah Iona Reynolds, 2017, *Subglacial volcanic and geothermal activity: Measurement and modelling of heat flow*, PhD dissertation, Faculty of Earth Sciences, University of Iceland, 90 pp.

Author ORCID: 0000-0003-2326-3594
ISBN: 978-9935-9306-7-5

Printing: Háskólaprent
Reykjavik, Iceland, December 2017

Abstract

Thermal anomalies are observed at many volcanoes, resulting from geothermal and magmatic activity, and are usually difficult to quantify since the measurement of heat fluxes from the ground to the atmosphere is subject to large uncertainties. However, many of Iceland's volcanoes are ice-covered, and this study exploits the special situation that the overlying ice acts as a calorimeter, where estimates of heat release can be made based on the volume of ice melted over a specified time period. This provides opportunities to estimate thermal signals to considerable accuracy. The general aim of this thesis is to advance the understanding and interpretation of thermal signals at ice-covered volcanoes in Iceland, and how they are linked to intrusive and volcanic activity. Three study areas are focused on: Grímsvötn, Bárdarbunga and Dyngjujökull.

Ice calorimetry is used to derive the heat output from Grímsvötn for 1998–2016, using annual mapping of ice surface, providing the most detailed study of the thermal output of Grímsvötn to date. The average heat released over the 18 year period is estimated to be 1.8 GW, whereof about 0.6 GW is composed of peaks above the base flux from melting during eruptions and associated geothermal anomalies. Peaks in geothermal activity were associated with all three eruptions which took place during the study period.

In August 2014, a period of seismic unrest began at the subglacial caldera of Bárdarbunga, and was followed by the propagation of a lateral dyke to the north, beneath the Dyngjujökull glacier, that resulted in a subaerial fissure eruption at Holuhraun. Ice surface depressions were observed above the path of the dyke beneath Dyngjujökull, and around the caldera rim at Bárdarbunga. Rates of heat transfer and duration of thermal signals show that subglacial eruptions rapidly generated the depressions at Dyngjujökull. The depressions around the Bárdarbunga caldera rim formed during and following an episode of caldera collapse, due to associated changes in permeability and possibly intrusive activity. In the two-year period following the onset of increased seismicity in the area, the total power from Bárdarbunga caldera cauldrons averaged ~270 MW.

The surface thermal signals produced by shallow intrusions were investigated with numerical modelling, using HYDROTHERM. Permeability was found to provide strong control on the surface heat flux, as was the initial temperature of the porous matrix. Lower initial temperatures result in buffering of the heat transfer to the surface, creating a muted thermal signal. High-permeability pathways were found to significantly increase the magnitude of the surface heat flux, and reduce the onset time for the signal.

Útdráttur

Merki um útstreymi varma í eldfjöllum eru algeng, og geta stafað af eldgosum eða jarðhitavirkni. Ef frá eru talin sjálf eldgosin, er oft erfitt að meta umfang og afl slíks útstreymis til andrúmsloftsins þar sem óvissa í mælingum eru mikil. Þegar eldfjöll eru hulin jökli gegnir þó öðru máli, þar sem ísinn getur virkað eins og varmamælir þar sem hægt er að meta með þokkalegri nákvæmni bæði afl og orku út frá magni íss sem bráðnar yfir tiltekið tímabil. Markmið þessa verkefnis er að auka skilning á eðli og umfangi varmaútstreymis af þessu tagi í eldstöðvum undir jökli á Íslandi, einkum að varpa ljósi á hvernig slík varmafrávik tengjast innskotum grunnt í jarðskorpunni og eldgosum undir jökli. Rannsóknin beinist að þremur svæðum: Grímsvötnum, Bárðarbungu og Dyngjujökli.

Bræðsla íss í Grímsvötnum yfir tímabilið 1998 til 2016 er metin út frá árlegri kortlagningu yfirborðs jökulsins. Með samanburði kortanna fæst nákvæmasta mat sem hingað til hefur verið gert á varmaafli Grímsvatna. Rannsóknin leiðir í ljós að yfir þetta 18 ára tímabil var varmaaflið um 1.8 GW, þar sem um þriðjungur eða 0.6 GW er meðaltal nokkurra toppa í varmaflæði sem urðu í eldgosum og aukinni jarðhitavirkni, bæði fyrir gos og í kjölfar þeirra. Slíkir toppar í jarðhitavirkni fylgdu öllum þremur eldgosunum sem urðu í Grímsvatnaöskjunni á tímabilinu.

Um miðjan ágústmánuð 2014 hófst jarðskjálftavirkni í Bárðarbunguöskjunni og í kjölfar hennar varð til berggangur í jarðskorpunni undir Dyngjujökli sem náði frá Bárðarbungu norður í Holuhraun. Sigkatlar mynduðust í Dyngjujökli yfir ganginum og á nokkrum stöðum á brúnum Bárðarbunguöskjunnar. Afl varmaflæðisins og tiltölulega skammur líftími þess undir kötlunum í Dyngjujökli verður ekki skýrt nema með litlum eldgosum upp á jökulbotninn. Aftur á móti benda líkanreikningar til þess að sigkatlar í brúnum Bárðarbungu hafi orsakast af breytingum í berglekt samfara sigi öskjunnar auk þess sem grunn innskot gætu hafa átt þátt í að auka jarðhitann. Á tveggja ára tímabili frá því að umbrotin í Bárðarbungu hófust, er meðalafl jarðhitans þar um 270 MW.

Varmaflæði frá grunnum kvikuinnskotum var kannað með tölulegum reikningum með forritinu HYDROTHERM. Niðurstöðurnar sýna að tveir þættir ráða mestu um hve mikið varmaflæði verður upp til yfirborðs: Lekt bergsins og hiti bergs og grunnvatns áður en innskotið verður til. Sé lektin mikil veldur það háu varmaflæði. Hár hiti fyrir innskot veldur því að lítinn viðbótarvarma þarf til að auka mjög varmaflæðið. Ef hiti í berginu er lágur áður en innskotið myndast, fer varmi innskotsins í að hita upp umhverfið, berg og grunnvatn, án þess að verulega aukinn varmaflutningur verði til yfirborðs. Ef sprungur og/eða þröng svæði með háa lekt myndast eða eru til staðar ofan við lóðrétt innskot verður öflugt varmaflæði um þau sem skilar sér hratt upp til yfirborðs. Suma sigkatlana í Bárðarbungu virðist vera hægt að skýra með slíkum hálektarsvæðum.

For Alasdair

Table of Contents

List of Figures

Acknowledgements

I would like to begin by thanking Magnús Tumi for being the most welcoming, inspiring, kind and patient supervisor a student could ask for. Thank you for the opportunities you have given me through the project. It has been a genuine pleasure working with you.

Whenever I've had a question about anything regarding past fieldwork, data, or even life itself, Dísa has always been there to provide an answer. I never failed to leave her office with a smile on my face – thank you for brightening my days. My work has benefitted greatly from the expertise of my co-authors Finnur, Eyjólfur, and Guðni. Thank you for the effort you have put into both our work and advising me. Thanks also to Tobi, you have been a great colleague and even better friend.

I was very lucky to be a part of the NEMOH initial training network, and I would like to thank both the organisers and the other fellows. You are all such enthusiastic and friendly people to work with - I have loved travelling and exploring volcanoes with you, and learnt a lot.

Life in Askja would not have been the same without my wonderful officemates, thank you all, with a special mention to Vincent and Werner who have been a constant source of humour, support, and sibling-like abuse since day one. I would like to thank each and every one of my Askja friends, both the Earth and Life scientists, amongst whom I'm sure I have made life-long friends. Sharing the building with you has made my time as a PhD student immeasurably more enjoyable. Thanks also to the Folda and Flóki graduate student societies who have organised some great celebrations.

I would like to especially thank my flatmates. First and foremost, Becca, who I lived with for almost the entire time I have been in Iceland. We had such amazing times (particularly the many, many parties) – thank you for the laughs in the good times and the support in the bad. I also want to give a big shout out to my current flatmates, Kate, Rob, and Pippin.

I feel very lucky to have had Will by my side throughout this project. His love and support towards me have been limitless and very much appreciated – thank you, Will!

Finally, thank you to all my friends and family in the UK, moving abroad has made me appreciate you even more. A special thanks to Rachel, Mhairi, and Simon, who have been on the other end of countless messages and phone calls to keep any homesickness at bay. Mum and Dad, you inspired me to do a PhD and have supported me in every way possible, through the whole journey. I would not have made it to where I am today without you.

This PhD project was funded by the EU Seventh Framework Marie Curie project NEMOH (no. 289976), the Research Fund of the University of Iceland, and Landsvirkjun power company. Fieldwork subsequent to the Holuhraun eruption was supported with crisis response funding from the Icelandic government through the Civil Protection Department of the National Commissioner of the Iceland Police, and through the European Community's Seventh Framework project FUTUREVOLC (no. 308377).

1 Introduction

Intrusive and volcanic activity transfers heat to the shallow crust and to the surface. The heat of intrusions in the shallow crust heats up the surrounding country rock and groundwater, and contributes to the formation of geothermal areas. At ice-covered volcanoes, the heat from shallow intrusions can lead to melting at the base of the glacier and possibly flooding when the meltwater is released. Heat can be transferred from intrusions to the surrounding country rock, the groundwater, the hydrosphere and the atmosphere in a variety of ways. Consequently, thermal signals from sub-surface magmatic sources are usually difficult to quantify, and the measurement of heat fluxes from the ground to the atmosphere is subject to large uncertainties. Many of Iceland's volcanoes are ice-covered, resulting in the special situation where the overlying ice acts as a calorimeter. This study exploits this and the opportunity it presents to estimate these signals to a much-improved accuracy.

The general aim of this thesis is to advance the understanding of heat transfer within the shallow crust in volcanic settings in the presence of magma, and how it is related to geothermal activity. In particular, the interpretation of thermal signals at ice-covered volcanoes in Iceland is explored, and how they link with intrusive and volcanic activity. The effects of intrusions and minor subglacial eruptions are explored using analytical and numerical models, and the results are presented in three papers:

Paper I **Reynolds, HI**, Gudmundsson, MT, Högnadóttir, Th, Pálsson, F. Thermal power of Grímsvötn, Iceland, from 1998 to 2016: quantifying the effects of volcanic activity and geothermal anomalies. Submitted to the Journal of Volcanology and Geothermal Research.

Paper II **Reynolds, HI**, Gudmundsson, MT, Högnadóttir, Th, Magnússon, E, Pálsson, F. (2017) Subglacial volcanic activity above a lateral dyke path during the 2014–2015 Bárdarbunga-Holuhraun rifting episode, Iceland. *Bulletin of Volcanology*, 79:38 doi: 10.1007/s00445-017-1122-z

Paper III **Reynolds, HI**, Gudmundsson, MT, Högnadóttir, Th, Axelsson, G. Changes in geothermal activity at Bárdarbunga, Iceland, following the 2014–15 caldera collapse, investigated using geothermal system modelling. To be submitted to the Journal of Geophysical Research.

A detailed time-series of annual ice-surface changes at Grímsvötn volcano that exists from 1998, was extended to 2016 during this study, providing a long-term record during which three volcanic eruptions took place. This time-series is used in paper I to estimate the thermal

fluctuations at Grímsvötn over the 18-year period, and define precursory and post-eruptive events associated with eruptions.

In August 2014, a period of seismic unrest began at the subglacial caldera of Bárdarbunga, and was followed by a lateral dyke that propagated ~45 km to the north, beneath the Dyngjujökull glacier, and resulted in a subaerial fissure eruption at Holuhraun. Several ice-surface features were observed during this period: a slow caldera collapse at Bárdarbunga over ~6 months, three ice cauldrons which formed very rapidly at Dyngjujökull above the path of the dyke, and ice cauldrons which formed around the Bárdarbunga caldera rim. The ice cauldrons observed from the onset of this event provided an opportunity to study melting associated with subglacial eruptions and increased geothermal activity, and shaped the rest of the PhD project. The evolutions of the ice cauldrons at Dyngjujökull and Bárdarbunga form the datasets of papers II and III, respectively.

The nature of the heat source required to generate the thermal signals observed at Bárdarbunga is unknown, and paper III includes a numerical study to investigate the surface heat flux generated by magmatic intrusions, conducted using HYDROTHERM (U.S.G.S. software). Insight gained from this work can be applied to other subglacial volcanoes where thermal variations are observed.

Alongside my main research project, I was fortunate to be involved in several related studies, which led to the following publications:

- Montanaro, C., Scheu, B., Gudmundsson, M.T., Vogfjörd, K., **Reynolds, H.I.**, Dürig, T., Strehlow, K., Rott, S., Reuschlé, T. and Dingwell, D.B. (2016). Multidisciplinary constraints of hydrothermal explosions based on the 2013 Gengissig lake events, Kverkfjöll volcano, Iceland. *Earth and Planetary Science Letters*, *434*, pp.308-319.

- Gudmundsson MT, Jónsdóttir K, Hooper A, Holohan EP, Halldórsson SA, Ófeigsson BG, Cesca S, Vogfjörd KS, Sigmundsson F, Högnadóttir Th, Einarsson P, Sigmarsson O, Jarosch AH, Jónasson K, Magnússon E, Hreinsdóttir S, Bagnardi M, Parks MM, Hjörleifsdóttir V, Pálsson F, Walter TR, Schöpfer MPJ, Heimann S, **Reynolds HI**, Dumont S, Bali E, Gudfinnsson GH, Dahm T, Roberts MJ, Hensch M, Belart JMC, Spaans K, Jakobsson S, Gudmundsson GB, Fridriksdóttir HM, Drouin V, Dürig T, Aðalgeirsdóttir G, Riishuus MS, Pedersen GBM, van Boeckel T, Oddsson B, Pfeffer MA, Barsotti S, Bergsson B, Donovan A, Burton MR, Aiuppa A (2016) Gradual caldera collapse at Bárdarbunga volcano, Iceland, regulated by lateral magma outflow. *Science*, 353(6296): aaf8988.

- Pedersen GBM, Höskuldsson A, Dürig T, Thordarson T, Jónsdóttir I, Riishuus MS, Óskarsson BV, Dumont S, Magnusson E, Gudmundsson MT, Sigmundsson F, Drouin VJPB, Gallagher C, Askew R, Guðnason J, Moreland WM, Nikkola P, **Reynolds HI**, Schmith J (2017) Lava field evolution and emplacement dynamics of the 2014–2015 basaltic fissure eruption at Holuhraun, Iceland. *J Volcanol Geotherm Res*. doi:10.1016/j.jvolgeores.2017.02.027

1.1 Research aims

This study focuses on variations of thermal signals at ice covered volcanoes in Iceland, and the nature of the heat sources producing these signals. The research aims evolved during the project, due to opportune events associated with the Bárdarbunga-Holuhraun eruption in 2014–15. The main objective of this thesis is to advance the general understanding of heat flow at volcanoes, and how it relates to movement and emplacement of magma. To achieve this overarching aim, the specific aims were set as:

- Collect/extend and present time series data of thermal activity at Grímsvötn (1998–2016), Bárdarbunga (2014–2017) and Dyngjujökull (2014–2015), collected through airborne radar altimetry profiling and ground-based GPS surveys.
- Identify characteristics of the thermal signals, e.g. the onset time, duration, and magnitude, which constrain the possible heat sources.
- Explore the effects of different intrusion depths, pre-intrusion bedrock/groundwater temperatures, and high-permeability fracture zones on the onset times of convection and the heat flux magnitude at the ice-bedrock boundary, and compare results to observed thermal signals.

1.2 Geothermal systems at subglacial volcanoes

Geothermal systems generally form in areas with relatively high heat flow, and high permeability to allow for fluid circulation. Stimac et al. (2015, p. 800) list the principle categories of geothermal resources as follows: (1) igneous systems related to high permeability areas over magmatic intrusions within the shallow crust; (2) tectonic systems linked to fluid circulation along fracture systems; (3) deep sedimentary aquifers and geo-pressured systems; (4) engineered geothermal systems; and (5) supercritical systems.

This work principally discusses magmatic intrusion-related geothermal systems, where cool groundwater is heated within permeable bedrock, and a convecting system is established where rising groundwater transports heat from magma reservoirs or intrusions to the surface (e.g. Hurwitz et al., 2003; Hayba and Ingebritsen, 2007). Monitoring geothermal activity at volcanoes gives necessary insight into the associated volcanic and phreatic hazards, and the hydrothermal systems below. Fumaroles, hot springs, and bubbling mud pools characterise the surface expression of many geothermal areas (e.g. Hochstein and Bromley, 2001; 2005). Thermal signals from subsurface magmatic sources, however, are usually difficult to quantify since the measurement of heat flux from the ground is subject to large uncertainties due to heat loss to the atmosphere. Subglacial geothermal fields present a unique opportunity to calculate the surface heat flux to a much improved accuracy, as all of the thermal energy is spent melting ice (Jarosch and Gudmundsson, 2007; Jarosch et al., 2008).

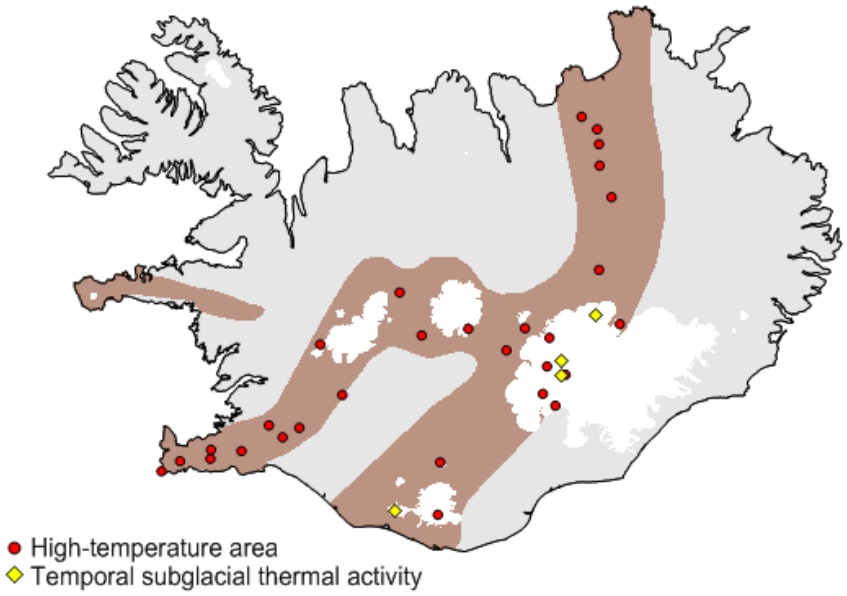

Figure 1-1 Map of high-temperature geothermal areas (data from Orkustofnun report - Energy Statistics in Iceland 2013), and temporal subglacial thermal activity, in Iceland.

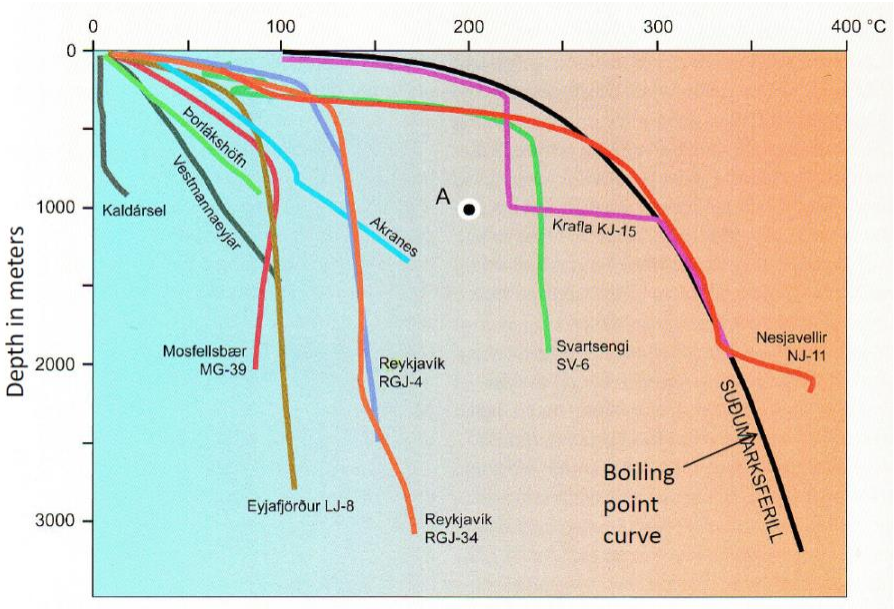

Figure 1-2 Temperature profiles from boreholes at various locations in Iceland. The point labelled 'A' separates the low- and high-temperature geothermal areas, with profiles on the left being low-temperature and profiles on the right being high-temperature. Four profiles are from places outside geothermal areas (Kaldársel, Vestmannaeyjar, Þorlákshöfn, and Akranes) (after Pálmason 2005).

Thermal signals are observed at many ice covered volcanoes in Iceland (figures 1-1 and 1-2) and worldwide (Major and Newhall, 1989). Notable examples outside Iceland include the ice caves observed at Mount St. Helens and Mount Rainier in the U.S.A. (Kiver and Mumma, 1971; Anderson et al., 1998; Zimbelman et al., 2000), and at Mount Erebus in Antarctica (Giggenbach, 1976). Several thermal features evolved at Redoubt volcano, Alaska, in the build-up to the 2009 eruption, including ice surface depressions, wide-spread subsidence, and punctures created by steam (Bleick et al., 2013).

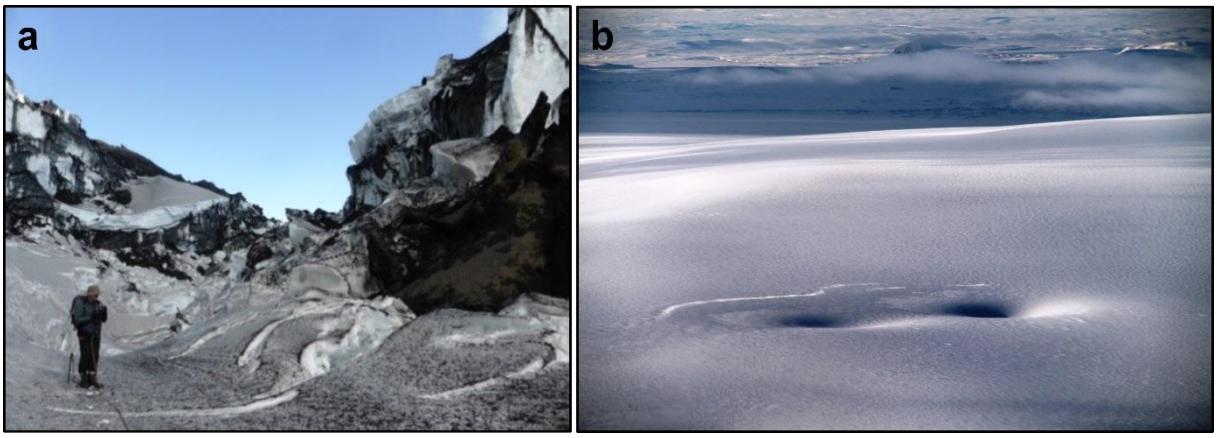

Figure 1-3 a) Inside an ice cauldron at Grímsvötn in 2014, and b) an aerial photograph of a SE-NW oriented double cauldron formed at Bárdarbunga in 2014, which has an approximate length of 1 km and width of 0.5-0.7 km.

Ice cauldrons are shallow depressions which form on the glacier surface due to basal melting (figure 1-3), as a manifestation of heat flux from below (e.g. Björnsson 1976; Jarosch and Gudmundsson, 2007); the melting ice acts as a calorimeter, allowing estimations of heat flux magnitude to be made. The source of heat may either be a subglacial eruption or geothermal activity above shallow magmatic intrusions. Several types of thermal signals are observed, with the onset time, duration, and location of the resulting cauldrons all being important factors. Geothermally generated cauldrons tend to produce a sustained signal over months, years, or decades.

1.3 Subglacial volcanism

Subglacial eruptions melt the overlying ice, producing large volumes of meltwater in a relatively short time due to their high rate of heat output. Ice cauldrons resulting from subglacial eruptions have a high initial growth rate, generated by a thermal pulse as ice is in contact with magma, and followed by a sharply decreasing melt rate as the eruption deposit cools.

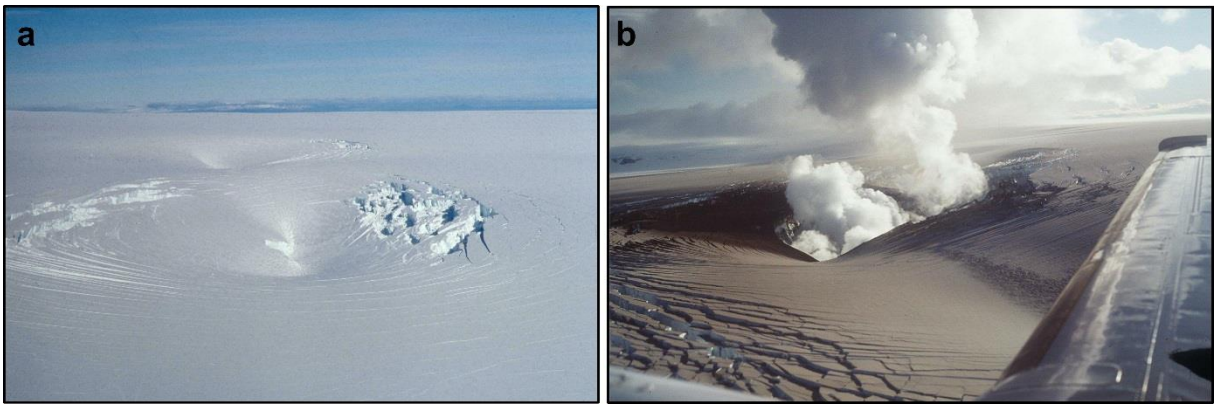

Figure 1-4 Aerial photographs of the Gjálp eruption in 1996. a) The ice cauldrons which formed during the initial phase of the eruption, and b) the plume after the eruption had melted through the full ice thickness.

Eruptions at fully- or partially-subglacial volcanoes are common in Iceland, making up 60% of the eruptions known to have taken place in the last 1100 years (Thordarson and Larsen, 2007). The 1996 eruption at Gjálp was located between Bárdarbunga and Grímsvötn, beneath 600–750 m of ice (figure 1-4). The entire eruption lasted for 13 days, but it melted through the ice thickness within 31 hours. This was the first eruption to be monitored in detail using airborne radar altimeter profiling, and was subsequently the subject of many thermal studies concerning the heat output and heat flux, as well as the heat transfer mechanisms (e.g. Gudmundsson et al., 1997; Gudmundsson et al., 2004; Jarosch et al., 2008). These studies confirmed that the heat transfer rate during a subglacial eruption is very high, with an average heat flux of 1 MW m^{-2} during the initial phase of the eruption (Jarosch et al., 2008). The Eyjafjallajökull eruption of 2010 produced a higher heat flux, of 4 MW m^{-2}, during its initial subglacial phase. It has been estimated that during explosive subglacial eruptions, 70–80% of the heat content of the magma is released to the surroundings prior to burial of the erupted particles, producing the observed high heat fluxes (Gudmundsson, 2003; Woodcock et al., 2012). The rapid ice melting may cause jökulhlaups (glacial outburst floods), which pose a risk to the surrounding communities and infrastructure (Gudmundsson et al., 2008; Edwards et al., 2015).

While most well-studied subglacial eruptions melt through the ice thickness to become subaerial after the initial phase, some evidence has been found of smaller, fully subglacial eruptions; e.g. field observations provide evidence of an effusive subglacial rhyolitic eruption at Bláhnúkur, Torfajökull, Iceland (Tuffen et al., 2001). During relatively small events, it is not clear whether the heat source is geothermal or a small subglacial eruption, and this uncertainty is explored in Paper I.

Confining pressure is a critical factor in eruption style and is principally controlled by the lithostatic load generated by the ice thickness. Several estimates have been published for the pressure threshold, above which only effusive activity will occur, from 3 to 5 MPa which corresponds to ~320–550 m of ice (Wilson and Head, 2002; Gudmundsson et al., 2004; Tuffen, 2007).

1.4 Areas of study

The work presented in this thesis is focused on three study areas: two central volcanoes, Grímsvötn and Bárdarbunga, both of which lie beneath Vatnajökull, and Dyngjujökull glacier which is located in the Northern part of Vatnajökull (figure 1-5).

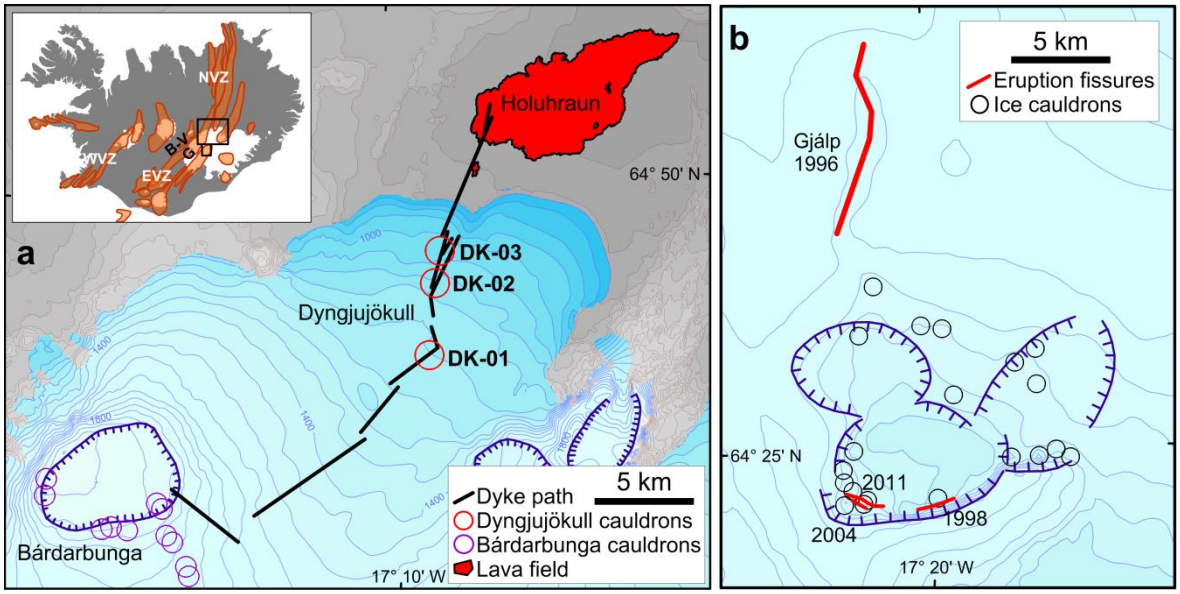

Figure 1-5 Location of study areas. (a) The north-western part of Vatnajökull. The segmented black line marks the path of the dyke (after Sigmundsson et al., 2015). Ice cauldrons are denoted by purple circles (Bárdarbunga) and red circles (Dyngjujökull). The inset map shows the location of (a) and (b), the Bárdarbunga-Veidivötn (B-V) and Grímsvötn (G) volcanic systems, and the volcanic zones in Iceland (orange). (b) The Grímsvötn area, with the eruption sites of 1998, 2004 and 2011 are marked within the caldera, and the Gjálp fissure to the north. Ice cauldrons are denoted by black circles.

1.4.1 Grímsvötn

Grímsvötn lies beneath the centre of Vatnajökull, to the north of the Grímsvötn volcanic system, which has been the most volcanically active system in Iceland in historic times (Larsen et al., 1998; Thordarson and Larsen 2007). Most of the eruptions originate from the caldera at Grímsvötn, which has produced six eruptions in the past 100 years (e.g. Björnsson and Gudmundsson, 1993; Oddsson et al., 2012; Jude-Eton et al., 2012; Hreinsdóttir et al., 2014), including three which are included in this study (1998, 2004, and 2011). Grímsvötn comprises three caldera structures (figure 1-5), with a partially subglacial lake located in the main caldera (Björnsson and Einarsson, 1990; Gudmundsson and Milsom, 1997). Meltwater from the Grímsvötn and Gjálp area collects in the lake, and is released periodically as a jökulhlaup. However, for the last 20 years, leakage from the lake has for extended periods kept the lake level low (Björnsson, 2003; Institute of Earth Sciences unpublished data), disrupting the pattern of accumulation of meltwater and sudden lake drainage, characteristic for Grímsvötn during the 19th and 20th centuries (Björnsson, 1988).

Grímsvötn is one of the most geothermally active calderas in the world, with sustained heat output for centuries in the Gigawatts range (Björnsson, 1988). The geothermal activity is easily

visible in the area, with ice cauldrons forming around the caldera rims and steaming areas in the exposed bedrock and around the edges of the open parts of the lake. Geothermal activity at Grímsvötn has been the subject of many studies. Sigvaldason (1965) published the first estimates of the heat output at Grímsvötn, followed by studies by Björnsson (1974 and 1988), and a detailed record of the heat output between 1922 and 1991 by Björnsson and Gudmundsson (1993).

1.4.2 Bárdarbunga

Bárdarbunga is a subglacial central volcano located in the north-west of Vatnajökull. It is part of the Bárdarbunga-Veidivötn volcanic system, which has produced more than 20 known eruptions in the last 1200 years (Larsen et al., 1998; Óladóttir et al., 2011). It has a large caldera approximately 65 km^2 in area, with a thickness of 700–800 m of ice at its deepest point (Björnsson and Einarsson, 1990). Ice cauldrons had been observed on the Bárdarbunga caldera rims prior to the 2014–15 event, both at the western and south-eastern parts of the caldera rim. The western cauldron has been sustained for decades and is geothermally generated (Eíriksdóttir, 2012). The south-eastern cauldrons were formed after the Gjálp eruption in 1996 and were shorter-lived (Gudmundsson et al., 2004), and may have formed due to minor subglacial eruptive activity (Kristmannsdóttir et al., 1999).

The 2014–15 Bárdarbunga-Holuhraun eruption was preceded by increased seismic activity within the Bárdarbunga caldera starting 16 August 2014. During the following two weeks, the seismic activity traced the path of a lateral dyke for more than 45 kilometres, beneath Dyngjujökull outlet glacier and to the site of the Holuhraun lavas which lie to the north of Vatnajökull (Sigmundsson et al., 2015). A small fissure eruption took place at Holuhraun on 29 August 2014, lasting approximately 4 hours. The main eruption began on 31 August with a large, effusive fissure eruption at the same location, which lasted for 6 months and produced a lava field ~1.4 km^3 in area (Gíslason et al., 2015; Pedersen et al., 2017, Dirscherl et al., 2017). Ice subsidence was observed within the Bárdarbunga caldera during the eruption, with no evidence of significant basal melting, representing a slow caldera collapse (Gudmundsson et al., 2016). On 27 August, four ice cauldrons were observed in a line orientated radially outward from the south-east caldera margin. These cauldrons were mostly short-lived, except the one closest to Bárdarbunga which was active for a period of years. The heat output of pre-existing minor subglacial geothermal areas at the caldera rim increased following the onset of increased seismic activity in the area, and new cauldrons formed in the years following (figure 1-6). These cauldrons remained active for between 6 months and several years.

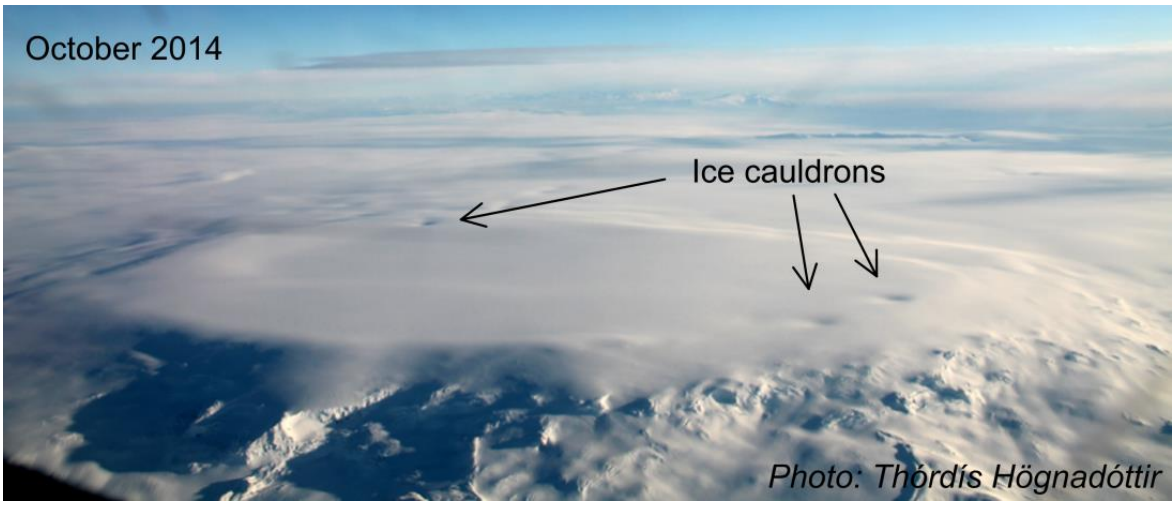

Figure 1-6 An aerial view of Bárdarbunga caldera from October 2014, showing the subsidence bowl which resulted from the down-sag of the caldera, and ice cauldrons which formed around the caldera rims.

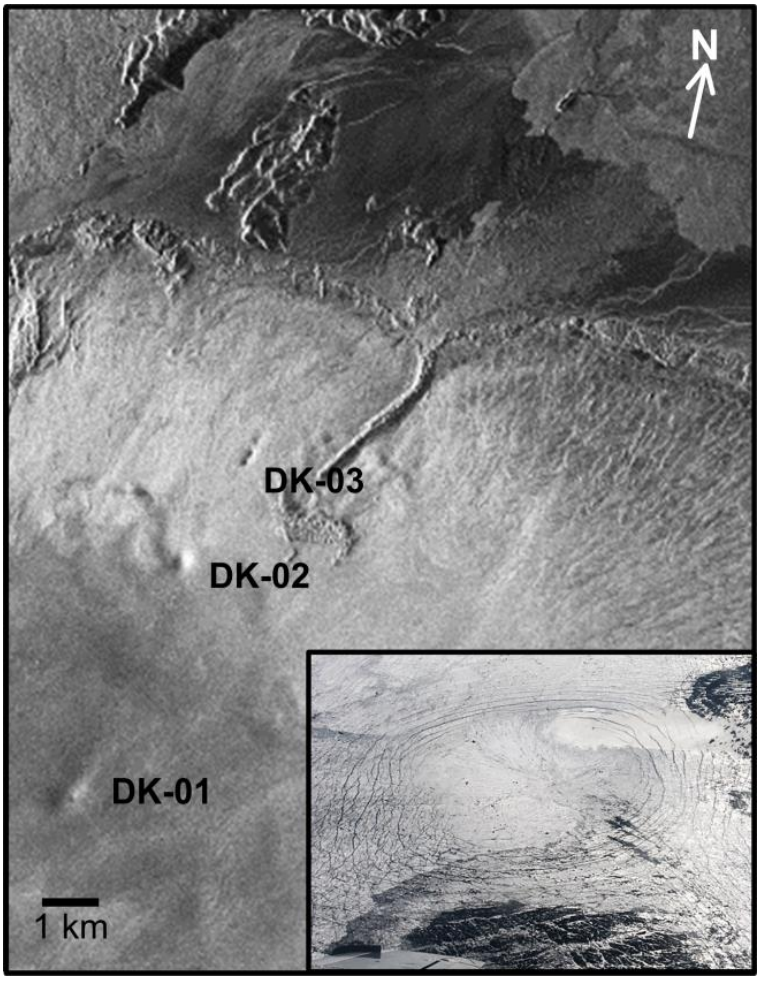

Figure 1-7 TerraSAR-X image of Dyngjujökull showing the three ice cauldrons which formed above the path of the dyke. The inset shows an aerial photograph of the subsidence at DK-02, taken on 5 September 2014.

1.4.3 Dyngjujökull

Dyngjujökull is an outlet glacier located to the north of Vatnajökull (figure 1-5). As stated in section 1.4.1, a dyke propagated from Bárdarbunga to the eruption site at Holuhraun in 2014, beneath the Dyngjujökull glacier. During the dyke propagation, movement on a graben above the magma flow path was identified from subsidence on the surface of Dyngjujökull and new fractures north of the glacier, extending to the eruption site at Holuhraun (Sigmundsson et al., 2015; Hjartardóttir et al., 2016; Rossi et al., 2016). Three ice cauldrons formed within the graben, above the path of the dyke (figure 1-7). The ice cauldrons formed very rapidly, with a high initial heat flux over a period of days, and reached their maximum volume within two months. No recent volcanic or geothermal activity is known to have occurred beneath Dyngjujökull.

2 Methods

2.1 Ice surface monitoring

Time series data of ice cauldron evolution exist for several volcanoes in Iceland, revealing thermal fluctuations in subglacial geothermal areas during intrusive events and periods of seismic unrest. These datasets are extended routinely, with additional monitoring during, and subsequent to, volcanic activity and periods of unrest.

Changes in the glacier surface are generally first identified by visual inspection of the ice surface, during observation flights or using satellite images (Gudmundsson et al., 1997; 2004; 2007; 2016; Magnússon et al., 2012; Bleick et al., 2013; Sigmundsson et al., 2015). In Iceland, the evolution of these features is primarily monitored by repeated airborne radar altimetry profiling, supplemented by satellite images. Ground-based GPS profiling is also used where depressions are not crevassed, particularly for more complex features, to map the ice surface in more detail.

Airborne altimetry measurements are made on board a low-flying aircraft (at approximately 100 m altitude), using a C-band radar altimeter to record the aircraft altitude, and kinematic or sub-metre differential GPS to simultaneously record the precise position (figure 2-1). Data collection is limited by weather conditions and the availability of the aircraft. An absolute accuracy of 3 m is achieved, with a relative consistency of 1–2 m. This method is outlined in detail by Gudmundsson et al. (2007). The penetration depth of the radar is dependent on the temperature and density of the surface layer, which varies over the year. In summer, the radar is reflected by the glacier surface, yet in winter it may penetrate several metres (Gudmundsson et al., 2016, supplements). For this reason, the ice surface profiles cannot always be used as an absolute measurement of ice surface elevation, but can be used to monitor the relative changes of ice cauldrons, compared to the ice surface beyond the edges of the depression.

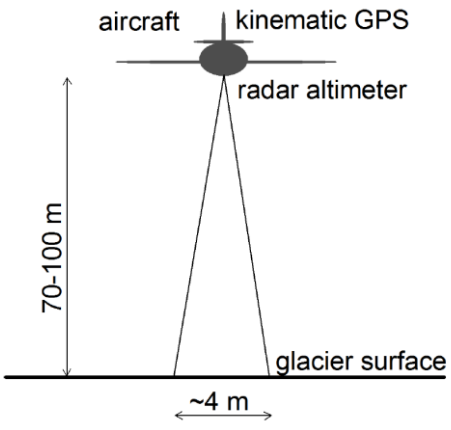

Figure 2-1 Schematic diagram of the altimeter beam spreading at the optimum flying height of 70-100 m (after Gudmundsson et al., 2007).

2.2 Calorimetry

An ice surface map is created by interpolating the profile data, and used to calculated the volume of features on the ice surface. Previous maps may be subtracted from the new map to reveal temporal variations in the ice surface, and allow the volume change of surface features to be calculated (figure 2-2). The mass of ice melted can be estimated from the observed volume change (Jarosch and Gudmundsson, 2007). In the simplest case:

$$\dot{m}_b = \rho_i \dot{V}_i \tag{1}$$

with ρ_i the density of the ice, $\dot{V}_i$ the rate of change of the volume of ice, and $\dot{m}_b$ the mass loss due to basal melting. When this method is applied to a single ice cauldron or a very limited area, ice flow into the depression may skew the results if not accounted for. This is done by adding an underestimation factor, U, so that

$$\dot{m}_b = (U + 1)\rho_i \dot{V}_i \tag{2}$$

Jarosch and Gudmundsson (2007) found that a value of U = 0.23 is appropriate to correct for the underestimation. If a map of the ice surface prior to the development of thermal features is available the total volume can be calculated; otherwise each successive map is subtracted from the previous one to show the change in volume with time (figure 2-2).

The mass of melted ice corresponds to the thermal signal at the base of the glacier, and is used to estimate the heat flux by calculating the thermal energy required for melting the ice. If melting at the base is assumed to correspond exactly to the ice volume change on the surface, we assume that all meltwater drains instantaneously. In the case of subglacial eruptions, the volume of volcanic products must be corrected for when calculating the volume of ice melted. The glaciers in Iceland are temperate, meaning that the ice is at its melting point throughout, so only the latent heat of fusion is required to melt the ice. Therefore, the heat flux (Q) required to generate the ice cauldrons can be estimated using calorimetry, considering the mass of ice melted and the latent heat of fusion of water (L_w).

$$Q = \dot{m}_b L_w \tag{3}$$

In the case of a subglacial eruption, the volume flux of magma ($\dot{V}_m$) required to generate the observed heat flux is estimated using:

$$\dot{V}_m = \frac{\rho_i L_i \dot{V}_i}{\rho_m (L_m + C_m \Delta T)} \tag{4}$$

where ρ_m, L_m and C_m are the density, latent heat of fusion and specific heat capacity of magma, respectively. ΔT is the change in temperature of the cooling magma. This assumes full-efficiency of heat transfer from the magma to the ice which may not be reached, due to heat loss to the bedrock beneath or to meltwater, and this should therefore be considered a minimum value for the volume of magma required. Not all the heat released need result in melting directly

above the vents. A fraction of the heat may be advected by meltwater flow. Data from recent eruptions shows that this heat is released as ice melting above the flow-path of the water (Gudmundsson et al., 2004; Magnússon et al., 2012; Oddsson et al., 2016b).

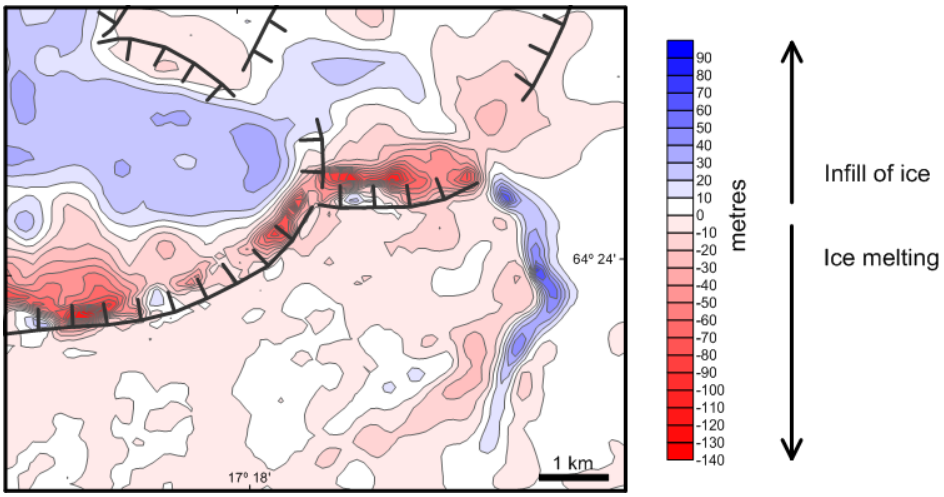

Figure 2-2 An example map of changes in ice surface elevation at Grímsvötn, between 1998 and 2010. Red areas represent developing ice cauldrons where ice has melted at the base of the glacier. Blue represents areas of ice infill. In the western part, this is due to uplift of the ice surface caused by higher lake level, while in the area east of the caldera the increase is due to recovery of the glacier following the formation of an ice canyon over the path of the jökulhlaup of 1996 associated with the Gjálp eruption.

2.3 Heat transfer

There are three fundamental mechanisms for heat transfer: conduction, convection, and radiation (e.g. Turcotte and Schubert, 2002). The heat flux per unit area, q, transferred through each mechanism will be defined below.

Conductive heat transport is a diffusive process which occurs when there is a spatial variation in temperature in a medium (solid, liquid or gas). Kinetic energy is transmitted between molecules during collisions. Conductive heat flux is expressed by Fourier's law as:

$$q_{cond} = -k\frac{dT}{dy} \tag{5}$$

where k is the coefficient of thermal conductivity, and $\frac{dT}{dy}$ is the temperature gradient in the direction of temperature variation. Convection occurs due to temperature variations in a liquid or gas, and involves the motion of relatively hot/cold fluid into a cooler/hotter region due to buoyancy forces. The basic equation for heat flux due to convection is:

$$q_{conv} = h(T_1 - T_2) \tag{6}$$

where h is the convection heat transfer coefficient, T_1 is the higher temperature, and T_2 is the lower temperature. Radiation is defined as the transmission of energy in the form of electromagnetic waves, and can be expressed using the Stefan-Boltzmann law as:

$$q_{rad} = \varepsilon \sigma T^4 \quad (7)$$

where ε is the emissivity of the material, and σ is the Stefan-Boltzmann constant (5.67×10^{-8} W m^{-2} K^{-4}). Radiation is not a significant process in water dominated systems; rather, conduction is the main heat transfer mechanism in solids (e.g. lava blocks or volcanic glass particles), and convection the dominant process in a fluid-filled porous matrix (e.g. geothermal systems).

This section considers the dominant heat transfer mechanisms for three scenarios: a magmatic intrusion in the shallow crust beneath a glacier; an effusive subglacial eruption; and an explosive/fragmentation dominated subglacial eruption (figure 2-3).

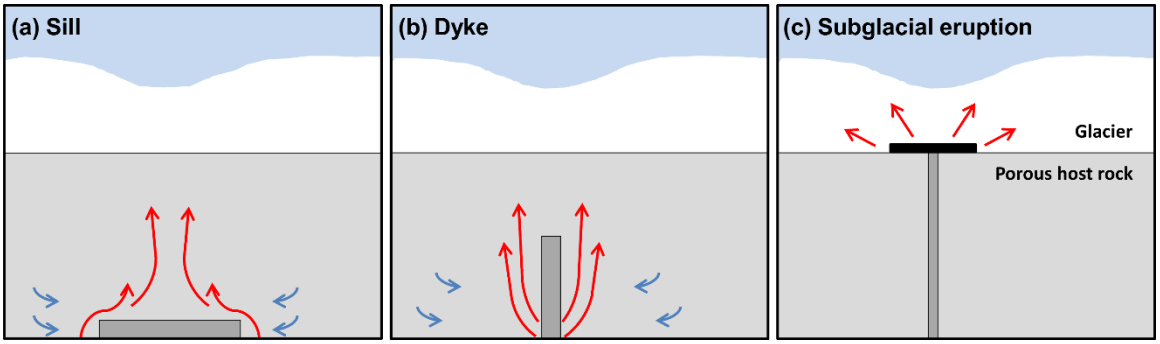

Figure 2-3 Conceptual model showing both sill and dyke style magmatic intrusions emplaced within a porous host-rock (a and b), where heat is transferred towards the surface by conduction and groundwater convection, generating heat flux beneath the glacier. The third image (c) shows a subglacial eruption scenario.

When a shallow magmatic intrusion is formed in the uppermost crust beneath a glacier, heat is transferred from the intrusion to the bedrock both by conduction and convection (figure 2-3). At the magma-bedrock boundary, the dominant mechanism of heat transfer is dependent on the physical state of the bedrock; if the bedrock has very low permeability then conduction will dominate, but if the bedrock is permeable then single- or two-phase hydrothermal convection will transport heat more efficiently. In the latter case heat is transported towards the bedrock-ice boundary via convection, and the time scale for the thermal signal to reach the surface depends primarily on the depth and geometry of the intrusion, the permeability of the bedrock, and the initial temperature of the country rock and groundwater. Where the ice temperature is below the water-freezing point, some minor heat conduction will take place within the ice, but most of the heat melts the ice.

Should the magma body reach the surface and result in a subglacial eruption, the style of eruption heavily influences which heat transfer mechanism is dominant, and the rate of heat transfer. A useful parameter to use when considering the heat transfer is the "efficiency", defined as the ratio of heat released from magma per unit time and the total heat content of the magma which erupted during the same time period (Gudmundsson, 2003; Gudmundsson et al., 2004). Models of subglacial effusive basaltic eruptions which form pillow lava have indicated

a thermal efficiency of 10–45%, dependent on the eruption rate as the longer the lava pillows are in direct contact with the ice/meltwater, the higher the efficiency (Gudmundsson, 2003). Experiments where ice and molten lava come in to direct contact show that the heat flux was highest in the first 10 s but dropped by an order of magnitude within several minutes (Oddsson et al., 2016a).

During an explosive subglacial eruption, fragmentation generates small particles, creating a large surface contact area between magma and water. The erupted products cool far more quickly than with an effusive eruption, with 70–80% of the initial heat within the erupted product transferred within the settling time (Gudmundsson, 2003; Woodcock et al., 2012)

2.4 Heat flow modelling

2.4.1 Darcy groundwater flow

As groundwater is heated, convection cells develop which carry heat towards the surface. Darcy's law can be employed to estimate the fluid velocity of the groundwater, assuming that the flow remains of single-phase liquid water, as it rises due to increased buoyancy, from a heated area around the intrusion towards the relatively cold bedrock-ice interface. The Darcy velocity (q_w) gives the volumetric flow rate per unit area (Ingebritsen and Sanford, 1999), and can be estimated as:

$$q_w = \frac{k\rho_{w,0}g\alpha_w(T_{boiling}-T_{surface})}{\mu_w} \quad (8)$$

where k is intrinsic permeability, $\rho_{w,0}$ is water density, g is the gravitational acceleration, α_w the linear coefficient of thermal expansion for water at 0 °C, and μ_w the dynamic viscosity of water. The bedrock-ice interface is considered to have a temperature, $T_{surface}$, of 0 °C, the freezing point of water. $T_{boiling}$ is the boiling point of water at the depth of the intrusion, as this is the highest temperature the groundwater can reach without becoming superheated or develop into a two-phase fluid. However, steam can play a significant role in heat transfer in hydrothermal areas, and this can be addressed using numerical modelling software such as HYDROTHERM (see below) and MUFITS (Afanasyev et al., 2015).

2.4.2 Cooling of magmatic intrusions – HYDROTHERM

HYDROTHERM is a numerical modelling program available from the U.S.G.S., which simulates multi-phase ground-water flow and thermal energy transport, at temperatures of up to 1200 °C (Hayba and Ingebritsen, 1997; Kipp et al., 2008). HYDROTHERM version 3.2.0 was used to simulate heat flow from a shallow magmatic intrusion to the surrounding bedrock, focusing on the surface heat flux.

Two governing partial differential equations are solved: the water-component flow equation, which combines the conservation of mass of the groundwater in both liquid and gas phase and Darcy's law for fluid flow in porous media (equation 9); and the thermal-energy transport

equation, which is formed using the conservation of enthalpy for both the groundwater and the porous medium (equation 10). For the spatial and temporal discretization of the equations, finite-difference techniques are employed.

The equation for groundwater flow is given by:

$$\frac{\partial}{\partial t}[\phi(\rho_w S_w + \rho_s S_s)] - \nabla \cdot \frac{\mathbf{k} k_{rw} \rho_w}{\mu_w}[\nabla p_w + \rho_w g \hat{\mathbf{e}}_z] - \nabla \cdot \frac{\mathbf{k} k_{rs} \rho_s}{\mu_s}[\nabla p_s + \rho_s g \hat{\mathbf{e}}_z] = 0 \quad (9)$$

The subscripts refer to the phase of the water, where *w* and *s* refer to liquid water and steam, respectively. Here, ϕ is the porosity, ρ the fluid density, S the saturation of water or steam with $S_w + S_s = 1$, $\mathbf{k}$ the porous-medium permeability tensor, k_r the relative permeability, μ the fluid viscosity, p_w is the fluid pressure in the liquid phase, p_s the fluid pressure in the steam phase, g the gravitational constant, $\hat{\mathbf{e}}_z$ the unit vector in the z-direction (upwards), t is the time, and ∇ is the spatial gradient (Kipp et al., 2008).

The heat transfer equation is given by:

$$\frac{\partial}{\partial t}[\phi(\rho_w h_w S_w + \rho_s h_s S_s) + (1-\phi)\rho_r h_r] - \nabla \cdot K_a \mathbf{I} \nabla T + \nabla \cdot \phi(S_w \rho_w h_w \mathbf{v}_w + S_s \rho_s h_s \mathbf{v}_s) - q_{sh} = 0 \quad (10)$$

The subscript *r* refers to the porous-matrix solid phase. Here, h is the specific enthalpy, ρ_r the density of the porous-matrix solid phase, K_a the effective thermal conductivity of the bulk porous medium, $\mathbf{I}$ the identity matrix of rank 3, T the temperature, and q_{sh} is the flow-rate intensity of an enthalpy source (Kipp et al., 2008).

Two-dimensional symmetric models, where a heat source is emplaced at shallow depths, are used to explore the heat flux produced in a medium of homogeneous permeability, and the effect of anisotropy in the form of a highly permeable (fault) zone as a pathway for fluid and energy flow. The effects of pre-intrusion temperatures are explored, and different upper boundary pressures based on those exerted by different glacier thicknesses. The results from an example model are displayed in figure 2-4.

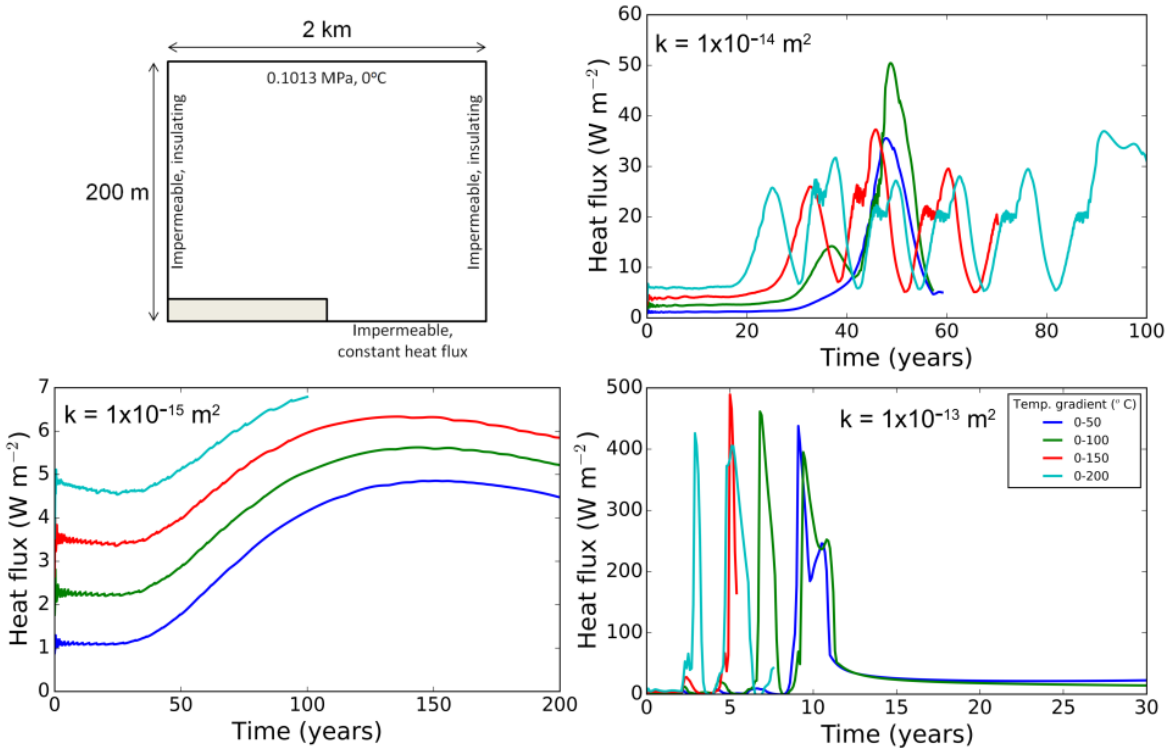

Figure 2-4 An example model of a cooling intrusion in HYDROTHERM, with results for varying bedrock permeabilities (k) and initial temperature gradients. The initial temperature increases linearly from 0 °C at the surface to the temperature labelled in the legend at 200 m depth. The heat flux magnitude and the onset time of the surface signal are highly dependent on both permeability and the pre-intrusion temperatures.

2.4.3 Cooling of lava flows - COMSOL

COMSOL Multiphysics is commercial modelling software that can be used to simulate physics-based problems using finite element modelling. COMSOL version 4.3b was used to simulate a lava flow cooling and solidifying under ice. The initial temperature of the lava body was set to 1200 °C, with a phase change temperature of 1100 °C and a transition interval between the phases of 100 °C to simulate gradual crystallisation. The upper boundary of the lava flow was considered to be in contact with glacial ice and held at 0 °C. A thermal conductivity of 2 W m^{-1} K^{-1} was used for the lava.

3 Paper I: Thermal power of Grímsvötn, Iceland, from 1998 to 2016: quantifying the effects of volcanic activity and geothermal anomalies

3.1 Summary

Paper I investigates the fluctuations in geothermal activity at Grímsvötn volcano, Iceland. A record of heat output at Grímsvötn between 1998 and 2016 is presented, using annual measurements which allow for a more detailed study than those previously carried out. We split Grímsvötn into sub-areas, quantifying the geothermal activity in terms of spatial distribution. This study covers a period of high volcanic activity, during which three eruptions took place within the caldera, and explores the relationship between observed thermal signals to volcanic activity and eruption sites.

Grímsvötn lies beneath the centre of the Vatnajökull ice cap, Iceland, and has for centuries been one of the most powerful geothermal areas in the world as well as being Iceland's most active volcano. Calorimetric studies of its heat output have suggested long-term heat release of 2–4 GW. Three caldera structures have been identified at Grímsvötn, and a partially subglacial lake is located within the main caldera. Ice cauldrons form preferentially around the caldera rims, and are a manifestation of geothermal activity beneath the glacier.

Annual mapping of the ice surface is used to monitor ice volume changes, combined with results of mass-balance monitoring over this same period. Corrections are made for changes in the subglacial lake level, and the area of open water. We present a detailed study of the ice surface changes which occur from 1998–2016 (figure 3-1). Melting due to volcanic eruptions and associated geothermal melting are quantified for one year intervals over the study period, and precursory and post-eruptive increases in geothermal activity are identified. We estimate the average heat release of the area for the study period, splitting it into the base geothermal heat flux, and the contributions from volcanic melting and geothermal anomalies.

3.2 Main results

- A net ice loss of about 1.1 km^3 (a mass of 1×10^{12} kg is observed for the Grímsvötn drainage basin over the survey period. Ice cauldrons are observed around the caldera rims, with the majority of the heat flux generated along the southern, south-eastern and south-western caldera walls.
- Some increase in geothermal activity was observed preceding all eruptions.

- Thermal anomalies were observed following all three eruptions, lasting 2–3 years. After the 1998 eruption a thermal anomaly of 650 MW was observed during the following two years; similarly, thermal anomalies of 500 MW and 450 MW were observed in the two years after the 2004 and 2011 eruptions, respectively. These thermal signals suggest a post-eruption link to increased geothermal activity at the caldera walls.
- The average thermal power of volcanic eruptions and associated shorter-term increases in geothermal power over the survey period is estimated as ~600 MW.
- The average base geothermal heat flux for the Grímsvötn area was estimated to be 1200 MW and the average total power of Grímsvötn from volcanic and geothermal sources ~1800 MW.

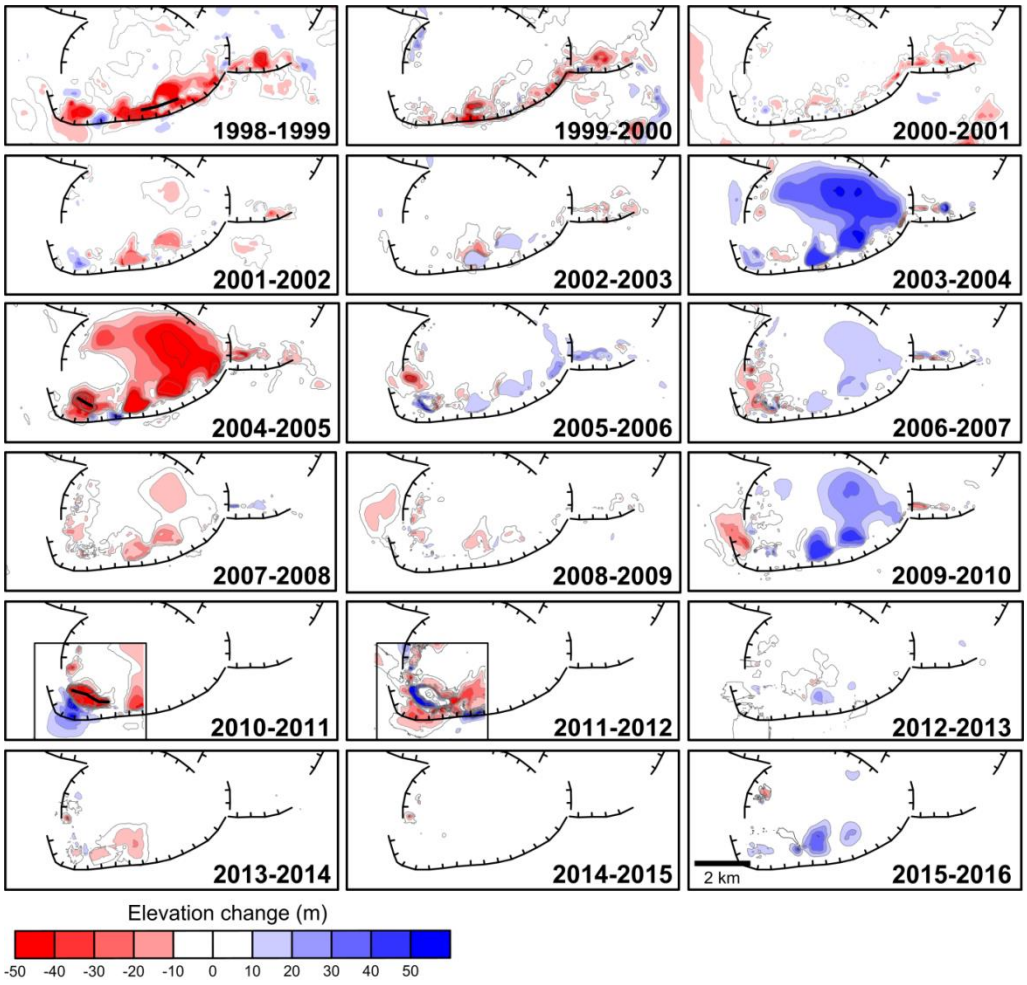

Figure 3-1 Differential maps showing the change in ice elevation over a one year period, as labelled. The red parts represent a lowering of the ice surface, due to ice melting or a decrease in the water level of the lake, and the blue areas show uplift of the ice, or infill of previous depressions. Black lines show eruption fissures in 1998–1999, 2004–2005, and 2010–2011. Data collection was limited following the 2011 eruption, so the 2010–2011 and 2011–2012 differential maps cover a smaller area.

4 Paper II: Subglacial volcanic activity above a lateral dyke path during the 2014–2015 Bárdarbunga-Holuhraun rifting episode, Iceland

4.1 Summary

The rifting episode associated with the Bárdarbunga-Holuhraun eruption in 2014–2015 included the first observations of major dyke propagation under ice. Three shallow ice depressions (ice cauldrons) with volumes ranging from 1 to 18 million m^3 formed in Dyngjujökull glacier above the 48 km long lateral path of the magma, at 4, 7, and 12 km from the northern glacier edge. Aircraft-based radar altimetry profiling was used to map the evolution of the cauldrons and construct a time series of the heat transfer rates. Out of the three scenarios explored: (1) onset or increase of hydrothermal activity; (2) convection within vertical fissures filled with water overlying intruded magma; and (3) subglacial eruptions, the last option emerges as the only plausible mechanism to explain the rapid heat transfer observed in a location far from known geothermal areas. Radio echo sounding data (collected and interpreted by E. Magnusson and F. Pálsson) indicate that the smallest cauldron was formed due to an intrusion into the glacier below, and are the first data ever recorded of this type of event.

4.2 Main results

- Three ice cauldrons, ranging from 1 to 18 million m^3 in volume, formed on Dyngjujökull glacier at the end of August and beginning of September 2014, associated with the slow collapse of Bárdarbunga caldera and the Holuhraun fissure eruption. The southernmost cauldron is located about 20 km to the SSW of the main eruption site.
- Neither convection of groundwater within the bedrock, nor heating of fluid-filled cracks within the bedrock or ice, could have produced enough heat to generate the observed ice cauldrons.
- The Dyngjujökull cauldrons were generated as a result of small, most likely effusive subglacial eruptions during the Holuhraun 2014–2015 event.
- Radio-echo soundings of the northernmost cauldron (DK-03) reveal that it was likely to have formed when a dyke intruded into the base of the glacier, penetrating approximately 50 m.

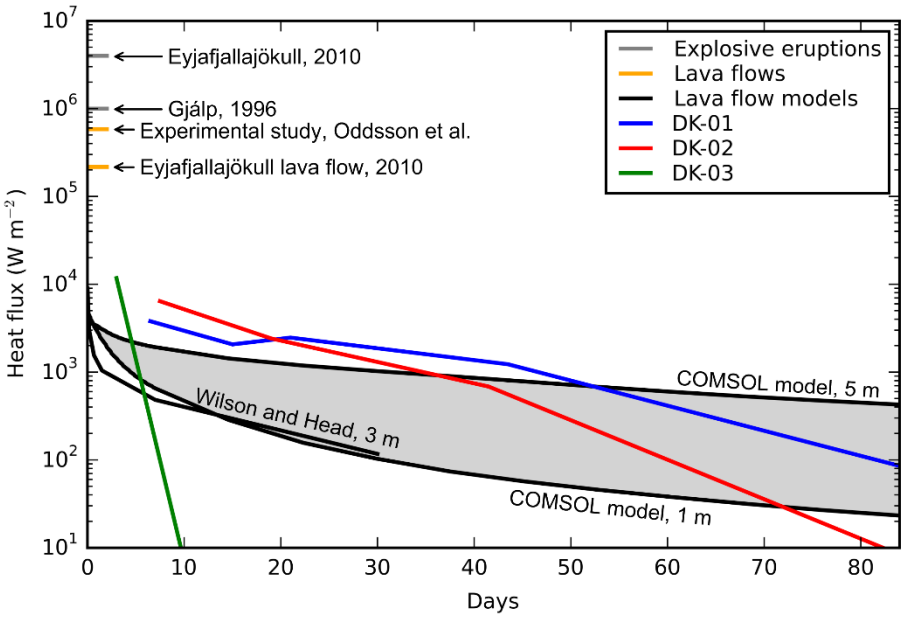

Figure 4-1 Comparison of observed heat flux for the ice cauldrons observed on Dyngjujökull, with empirical data for the initial subglacial phase of the Eyjafjallajökull 2010 and Gjálp 1996 explosive eruptions (Jarosch et al., 2008; Magnusson et al., 2012), and for the Eyjafjallajökull 2010 lava flow (Oddsson et al., 2016b). Modelling results are also displayed: experimental study data from Oddsson et al., (2016a), and numerical models of subglacial lava flow cooling from Wilson and Head (2007) and using COMSOL Multiphysics. The shaded area shows the heat flux expected for lava flows between 1 and 5 m thick (using COMSOL); the Wilson and Head model is for a 3-m-thick lava flow. Original figure published in Reynolds et al., 2017, paper II.

5 Paper III: Changes in geothermal activity at Bárdarbunga, Iceland, following the 2014-15 caldera collapse, investigated using geothermal system modelling.

5.1 Summary

A rifting event began at the subglacial central volcano Bárdarbunga in August 2014, resulting in a caldera collapse, a lateral dyke which propagated ~48 km to produce a large fissure eruption at Holuhraun, and several smaller eruptions above the path of the dyke. During the start of the activity in August 2014, four ice cauldrons (shallow depressions on the ice surface) formed on the south-eastern flank of Bárdarbunga caldera. These cauldrons very quickly reached their maximum size and then declined, indicating creation in minor subglacial eruptions. Ice cauldrons also formed around the rim of Bárdarbunga caldera. Three cauldrons formed within months of the start of the activity, three formed almost one year later, and another cauldron formed at the beginning of 2017. The shortest-lived of these cauldrons was active for seven months, while several continue to increase in volume at the time of writing. The total thermal power from the cauldrons, during the two-year period following the onset of increased activity, is estimated to be ~270 MW. We use the numerical modelling software HYDROTHERM for simulations of fluid flow and heat transport to assess the potential surface heat flux produced by shallow magmatic intrusions. The bedrock parameter space is explored to investigate the control of bedrock permeability anisotropy and initial temperature on the surface thermal signal.

5.2 Main results

- Six ice cauldrons formed at the Bárdarbunga caldera rim in the two years following the onset of increased seismicity in the area in 2014. A seventh ice cauldron was observed at the beginning of 2017, 2.5 years after the start of the event.
- The maximum volume of the individual ice cauldrons ranged between 1.0±0.2 and 17±2 million m^3.
- The ice cauldrons around the caldera rim formed due to increased geothermal activity. HYDROTHERM was used to investigate the potential surface heat flux produced by shallow magmatic intrusions, and compared to the observed thermal signals.
- It was found that permeability provides strong control on the surface heat flux, as does the initial temperature of the porous matrix where lower temperatures result in a muted surface thermal signal compared to the higher initial temperatures.
- Modelling results show that high-permeability pathways have a very significant effect on both the magnitude of the surface heat flux, and the onset time for the signal. The distribution of ice cauldrons suggests that these high permeability pathways correspond to fault zones associated with the caldera collapse.

- The smaller ice cauldrons (BB-04 and BB-05) could have been produced by the total thermal output according to the modelling results and the delay in onset time may be a result of limited permeability. However, the thermal signals measured at BB-01 and BB-02 can only be partly explained by the modelling results, suggesting that additional heating mechanisms must contribute to these signals, e.g. from deeper intrusions or increased permeability at greater depth than modelled in this study.
- In contrast, the cauldrons which formed in August 2014 to the southeast of the caldera display characteristics of minor subglacial eruptions, as they initially grew very rapidly followed by a gradual decline.

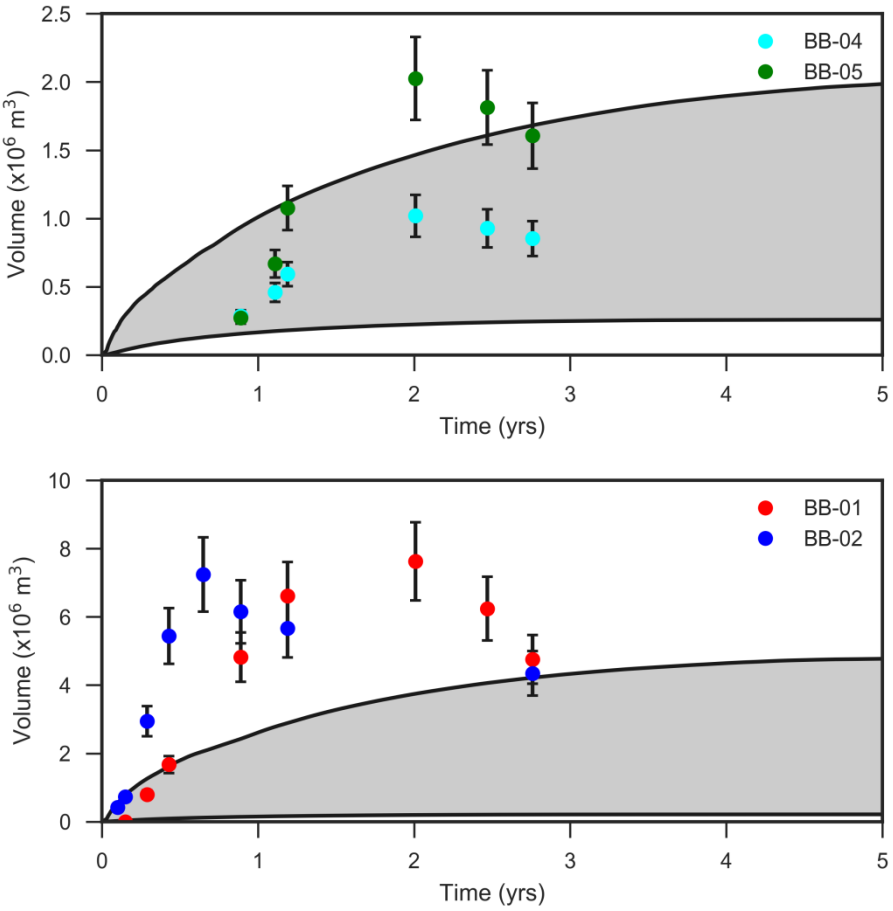

Figure 5-1 Modelling results converted to the equivalent volume of melted ice, for a vertical intrusion 500 m below the surface, of width 5 m, plotted with the observed volumes of ice cauldrons. The permeability of the high permeability zone is 1×10^{-12} m^2, and the pre-intrusion bedrock temperature gradient is 0–200 °C over the uppermost 200 m. a) Shaded area gives range in ice melt for an intrusion of between 100 and 300 m in length beneath an ice thickness of 150 m, plotted with the volume of BB-04 and BB-05. b) Shaded area gives the potential ice melt based on an intrusion of between 100 and 800 m in length below an ice thickness of 300 m, plotted with the volume of BB-01 and BB-02.

6 Concluding remarks

Thermal signals from sub-surface magmatic sources are usually difficult to quantify since the measurement of heat fluxes from the ground to the atmosphere is subject to large uncertainties. Many of Iceland's volcanoes are ice-covered, and this study exploits the special situation that the overlying ice acts as a calorimeter, presenting the opportunity to estimate thermal signals to a much-improved accuracy. Observed thermal data were used to distinguish the signals from subglacial eruptions and increased geothermal activity at three study areas: Grímsvötn, Dyngjujökull, and Bárdarbunga. To explore the relationship between shallow magmatic intrusions and increased permeability and initial bedrock temperature, simulations were performed using HYDROTHERM.

Transient signals are observed at both Grímsvötn and Bárdarbunga, with ice cauldrons forming around the rims of the calderas. These thermal signals last for months to decades. At Grímsvötn, thermal signals due to geothermal activity are observed following all three eruptions which took place during the study period, on the time scale of several years. Areas of previously established geothermal activity at Bárdarbunga caldera reactivated or increased in power within a month of the start of the caldera collapse in 2014. Ice cauldrons also formed around the Bárdarbunga caldera rim in places where geothermal activity had not previously been observed, with an onset time of 1 to 2 years. The increase in geothermal activity at Bárdarbunga accompanying and following the caldera collapse may be due to the formation of high-permeability pathways caused by faulting, and possible intrusive activity within the faults.

In contrast to the geothermally generated thermal signals, subglacial volcanic activity at Dyngjujökull and to the south-east of Bárdarbunga caldera produced sudden, high magnitude signals. The transfer of heat from volcanic products is not instantaneous, but the signal decreases significantly in the days following the eruptions, and is undetectable within months.

Modelling results show that cold groundwater has a strong buffering effect on any surface thermal signals produced by a magmatic intrusion, as the heat is mostly absorbed into heating the groundwater and bedrock, with far less heat transferred to the surface. However, an intrusion into a hot area can lead to a strong response, as groundwater boils and pulses of steam are produced, efficiently transferring the heat towards the surface due to buoyancy. Zones of high permeability (fissure systems) allow for rapid heat transfer from the intrusion to the surface.

This work enhances the general understanding of thermal signals at ice-covered volcanoes in Iceland, and the interpretation of the heat sources generating the observed signals. The work also sheds light on how the sub-surface temperature and permeability affect the surface thermal signals produced by magmatic intrusions.

References

Afanasyev A, Costa A, Chiodini G (2015) Investigation of hydrothermal activity at Campi Flegrei caldera using 3D numerical simulations: extension to high temperature processes. J Volcanol Geotherm Res 299:68–77.

Anderson CH, Behrens CJ, Floyd GA, Vining MR (1998) Crater Firn Caves of Mount St. Helens, Washington. J Caves and Karst Stud 60:44–50.

Björnsson H (1976) Subglacial water reservoirs, jökulhlaups and volcanic eruptions. Jökull 25:1–15.

Björnsson H (1988) Hydrology of Ice Caps in Volcanic Regions. Soc Sci Isl, Rit 40. 139 pp.

Björnsson H, Einarsson P (1990) Volcanoes beneath Vatnajökull, Iceland: evidence from radio-echo sounding, earthquakes and jökulhlaups. Jökull 40:147–148.

Björnsson H, Guðmundsson MT (1993) Variations in the thermal output of the subglacial Grímsvötn caldera, Iceland. Geophys Res Lett 20(19):2127–2130.

Bleick HA, Coombs ML, Cervelli PF, Bull KF, Wessels RL (2013) Volcano-ice interactions precursory to the 2009 eruption of Redoubt Volcano, Alaska. J Volcanol Geotherm Res 259:373–388.

Dirscherl M, Rossi C (2017) Geomorphometric analysis of the 2014–2015 Bárðarbunga volcanic eruption, Iceland. Remote Sensing of Environment. doi: 10.1016/j.rse.2017.10.027

Edwards BR, Gudmundsson MT, Russell JK (2015) Glaciovolcanism. In Sigurðsson H, Houghton B, McNutt S, Rymer H, Stix J, editors, Encyclopedia of Volcanoes, pp. 377–393. Elsevier, Boston.Eiríksdóttir VS (2012) Þróun sigkatla í Bárðarbungu (Bachelor´s thesis). Retrieved from http://skemman.is/stream/get/1946/11961/30211/1/BS.pdf

Giggenbach WF (1976) Geothermal ice caves on Mt Erebus, Ross Island, Antarctica. New Zeal J Geol Geophys 19:365–372, doi:10.1080/00288306.1976.10423566.

Gíslason SR, Stefánsdóttir G, Pfeffer MA, Barsotti S, Jóhannsson T, Galeczka I, Bali E, Sigmarsson O, Stefánsson A, Keller NS, Sigurdsson Á, Bergsson B, Galle B, Jacobo VC, Arellano S, Aiuppa A, Jónasdóttir EB, Eiríksdóttir ES, Jakobsson S, Guðfinnsson GH, Halldórsson SA, Gunnarsson H, Haddadi B, Jónsdóttir I, Thordarson T, Riishuus M, Högnadóttir Th, Dürig T, Pedersen GBM, Höskuldsson Á, Gudmundsson MT (2015) Environmental pressure from the 2014–15 eruption of Bárðarbunga volcano, Iceland. Geochem Perspect Lett 1(0):84–93.

Gudmundsson MT, Sigmundsson F, Björnsson H (1997) Ice–volcano interaction of the 1996 Gjálp subglacial eruption, Vatnajökull, Iceland. Nature 389:954–957.

Guðmundsson MT, Milsom J (1997) Gravity and magnetic studies of the subglacial Grímsvötn volcano, Iceland. Implications for crustal and thermal structure. J Geophys Res 102: 7691–7704.

Gudmundsson MT (2003) Melting of ice by magma-ice-water interactions during subglacial eruptions as an indicator of heat transfer in subaqueous eruptions. In White JDL, Smellie JL, Clague AD, editors, Explosive Subaqueous Volcanism, pp. 61–72. American Geophysical Union.

Gudmundsson MT, Sigmundsson F, Björnsson H, Högnadóttir Th (2004) The 1996 Eruption at Gjálp, Vatnajökull Ice Cap, Iceland: Efficiency of Heat Transfer, Ice Deformation and Subglacial Water Pressure. Bull Volcanol 66(1):46–65, doi:10.1007/s00445-003-0295-9.

Gudmundsson MT, Högnadóttir Th, Kristinsson AB, Gudbjörnsson S (2007) Geothermal activity in the subglacial Katla caldera, Iceland, 1999–2005, studied with radar altimetry. Annals of Glaciology 45:66–72.

Gudmundsson MT, Larsen G, Höskuldsson Á, Gylfason ÁG (2008) Volcanic hazards in Iceland. Jökull 58:251–268.

Gudmundsson MT, Jónsdóttir K, Hooper A, Holohan EP, Halldórsson SA, Ófeigsson BG, Cesca S, Vogfjörd KS, Sigmundsson F, Högnadóttir Th, Einarsson P, Sigmarsson O, Jarosch AH, Jónasson K, Magnússon E, Hreinsdóttir S, Bagnardi M, Parks MM, Hjörleifsdóttir V, Pálsson F, Walter TR, Schöpfer MPJ, Heimann S, Reynolds HI, Dumont S, Bali E, Gudfinnsson GH, Dahm T, Roberts MJ, Hensch M, Belart JMC, Spaans K, Jakobsson S, Gudmundsson GB, Fridriksdóttir HM, Drouin V, Dürig T, Aðalgeirsdóttir G, Riishuus MS, Pedersen GBM, van Boeckel T, Oddsson B, Pfeffer MA, Barsotti S, Bergsson B, Donovan A, Burton MR, Aiuppa A (2016) Gradual caldera collapse at Bárdarbunga volcano, Iceland, regulated by lateral magma outflow. Science 353(6296): aaf8988.

Hayba DO, Ingebritsen SE (1997) Multiphase groundwater flow near cooling plutons. J Geophys Res 102(B6):12,235–12,252.

Hjartardóttir ÁR, Einarsson P, Gudmundsson MT, Högnadóttir Th (2016) Fracture movements and graben subsidence during the 2014 Bárðarbunga dike intrusion in Iceland. J Volcanol Geotherm Res 310:242–252.

Hochstein MP, Bromley CJ (2001) Steam cloud characteristics and heat output of fumaroles. Geothermics 30:547–559.

Hochstein MP, Bromley CJ (2005) Measurement of heat flux from steaming ground. Geothermics 34:133–160.

Hreinsdóttir S, Sigmundsson F, Roberts MJ, Björnsson H, Grapenthin R, Arason P, Árnadóttir T, Hólmjárn J, Geirsson H, Bennett RA, Gudmundsson MT, Oddsson B, Ófeigsson BG, Villemin T, Jónsson T, Sturkell E, Höskuldsson Á, Larsen G, Thordarson T, Óladóttir BA (2014) Volcanic plume height correlated with magma pressure change at Grímsvötn Volcano, Iceland. Nature Geoscience 7:214–218, doi:10.1038/ngeo2044.

Hurwitz S, Kipp KL, Ingebritsen SE, Reid ME (2003) Groundwater flow, heat transport, and water table position within volcanic edifices: Implications for volcanic processes in the Cascade Range. J Geophys Res Solid Earth 108(B12):2557.

Ingebritsen SE, Sandford WE (1999) Groundwater in Geologic Processes. Cambridge University Press.

Jarosch AH, Gudmundsson MT (2007) Numerical studies of ice flow over subglacial geothermal heat sources at Grímsvötn, Iceland, using Full Stokes equations. J Geophys Res 112:F02008, doi:10.1029/2006JF000540.

Jarosch AH, Gudmundsson MT, Högnadóttir Th, Axelsson G (2008) Progressive cooling of the hyaloclastite ridge at Gjálp, Iceland, 1996–2005. J Volcanol Geotherm Res 170:218–229.

Jude-Eton TC, Thordarson T, Gudmundsson MT, Oddsson B (2012) Dynamics, stratigraphy and proximal dispersal of supraglacial tephra during the ice-confined 2004 eruption at Grímsvötn Volcano, Iceland. Bull Volcanol 74(5):1057–1082.

Kipp KL Jr., Hsieh PA, Charlton SR (2008) Guide to the revised ground-water flow and heat transport simulator: HYDROTHERM — Version 3: U.S. Geological Survey Techniques and Methods 6–A25, 160 p.

Kiver E, Mumma M (1971) Summit firn caves, Mount Rainier, Washington. Science 173:320–322.

Kristmannsdóttir H, Björnsson A, Pálsson S, Sveinbjörnsdóttir ÁE (1999) The Impact of the 1996 Subglacial Volcanic Eruption in Vatnajökull on the River Jökulsá Á Fjöllum, North Iceland. J Volcanol Geotherm Res 92(3–4):359–372, doi:10.1016/S0377-0273(99)00056-6.

Larsen G, Gudmundsson MT, Björnsson H (1998) Eight centuries of periodic volcanism at the center of the Iceland hotspot revealed by glacier tephrostratigraphy. Geology 26:943–946.

Magnusson E, Gudmundsson MT, Roberts MJ, Sigurdsson G, Höskuldsson F, Oddsson B (2012) Ice-volcano interactions during the 2010 Eyjafjallajökull eruption, as revealed by airborne imaging radar. J Geophys Res 117:B07405.

Major JJ, Newhall CG (1989) Snow and ice perturbtion during historical volcanic-eruptions and the formation of lahars and floods – a global review. Bull Volcanol 52:1–27.

Oddsson B, Gudmundsson MT, Larsen G, Karlsdóttir S (2012) Monitoring of the plume from the basaltic phreatomagmatic 2004 Grímsvötn eruption—Application of weather radar and comparison with plume models. Bull Volcanol 74(6):1395–1407.

Oddsson B, Gudmundsson MT, Sonder I, Zimanowski B, Schmid A (2016a) Experimental studies of heat transfer at the dynamic magma ice/water interface: Application to subglacially emplaced lava. J Geophys Res-Sol Ea 121(5):3261–3277.

Oddsson B, Gudmundsson MT, Edwards BR, Thordarson T, Magnússon E, Sigurðsson G (2016b) Subglacial lava propagation, ice melting and heat transfer during emplacement of an intermediate lava flow in the 2010 Eyjafjallajökull eruption. Bull Volcanol 78(7):1–17.

Óladóttir BA, Larsen G, Sigmarsson O (2011) Holocene volcanic activity at Grímsvötn, Bárdarbunga and Kverkfjöll subglacial centres beneath Vatnajökull, Iceland. Bull Volcanol 73(9):1187–1208.

Orkustofnun (2013) Energy Statistics in Iceland 2013. Accessed 2 August 2016. http://www.os.is/gogn/os-onnur-rit/orkutolur_2013-enska.pdf

Pedersen GBM, Höskuldsson A, Dürig T, Thordarson T, Jónsdóttir I, Riishuus MS, Óskarsson BV, Dumont S, Magnusson E, Gudmundsson MT, Sigmundsson F, Drouin VJPB, Gallagher C, Askew R, Guðnason J, Moreland WM, Nikkola P, Reynolds HI, Schmith J (2017) Lava field evolution and emplacement dynamics of the 2014–2015 basaltic fissure eruption at Holuhraun, Iceland. J Volcanol Geotherm Res 450:155–169, doi:10.1016/j.jvolgeores.2017.02.027.

Rossi C, Minet C, Fritz T, Eineder M, Bamler R (2016) Temporal monitoring of subglacial volcanoes with TanDEM-X—application to the 2014–2015 eruption within the Bárðarbunga volcanic system, Iceland. Remote Sens Environ 181:186–197.

Sigmundsson F, Hooper A, Hreinsdottir S, Vogfjord KS, Ofeigsson BG, Heimisson ER, Dumont S, Parks M, Spaans K, Gudmundsson GB, Drouin V, Arnadottir T, Jonsdottir K, Gudmundsson MT, Hognadottir Th, Fridriksdottir HM, Hensch M, Einarsson P, Magnusson E, Samsonov S, Brandsdottir B, White RS, Agustsdottir Th, Greenfield T, Green RG, Hjartardottir AR, Pedersen R, Bennett RA, Geirsson H, La Femina PC, Bjornsson H, Palsson F, Sturkell E, Bean CJ, Mollhoff M, Braiden AK, Eibl EPS (2015) Segmented lateral dyke growth in a rifting event at Bardarbunga volcanic system, Iceland. Nature 517(7533):191–195.

Sigvaldason GE (1965) The Grímsvötn area. Chemical analysis of jökulhlaup water. Jökull 15:125–128.

Stimac J, Goff F, Goff CJ (2015) Intrusion-Related Geothermal Systems, in Sigurdsson H, Houghton B, McNutt S, Rymer H, Stix J, editors, The Encyclopedia of Volcanoes, pp. 377–393, Elsevier, Boston. Sturkell E, Einarsson P, Roberts MJ, Geirsson H, Gudmundsson MT, Sigmundsson F, Pinel V, Gudmundsson GB, Ólafsson H, Stefansson R (2008) Seismic and geodetic insights into magma accumulation at Katla subglacial volcano, Iceland: 1999 to 2005. J Geophys Res–Sol Ea 113(B3).

Thordarson T, Larsen G (2007) Volcanism in Iceland in historical time: Volcano types, eruption styles and eruptive history. Journal of Geodynamics 43(1):118–152.

Tuffen H, Gilbert J, McGarvie D (2001) Products of an effusive subglacial rhyolite eruption: Bláhnúkur, Torfajökull, Iceland. BullVolcanol 63(2):179–190.

Tuffen H (2007) Models of ice melting and edifice growth at the onset of subglacial basaltic eruptions. J Geophys Res 112:B03203.

Turcotte DL, Schubert G (2002) Geodynamics. Cambridge University Press, 2nd edition.
Wilson L, Head JW (2002) Heat transfer and melting in subglacial basaltic volcanic eruptions: implications for volcanic deposit morphology and meltwater volumes. Geological Society, London, Special Publications, 202(1):5–26.
Wilson L, Head JW (2007) Heat transfer in volcano–ice interactions on earth. Ann Glaciol 45(1):83–86.
Woodcock DC, Gilbert JS, Lane SJ (2012) Particle-water heat transfer during explosive volcanic eruptions. J Geophys Res-Sol Ea 117(B10).
Zimbelman DR, Rye RO, Landis GP (2000) Fumaroles in ice caves on the summit of Mount Rainier—preliminary stable isotope, gas, and geochemical studies. J Volcanol Geotherm Res 97:457–473, doi: 10.1016/S0377-0273(99)00180-8.

Paper I

Thermal power of Grímsvötn, Iceland, from 1998 to 2016: quantifying the effects of volcanic activity and geothermal anomalies

Hannah Iona Reynolds, Magnús Tumi Gudmundsson, Thórdís Högnadóttir, Finnur Pálsson
Manuscript in preparation for Journal of Volcanology and Geothermal Research

Thermal power of Grímsvötn, Iceland, from 1998 to 2016: quantifying the effects of volcanic activity and geothermal anomalies

Hannah I. Reynolds*, Magnús T. Gudmundsson, Thórdís Högnadóttir, Finnur Pálsson

Nordvulk, Institute of Earth Sciences, University of Iceland, Sturlugata 7, Reykjavík 101, ICELAND.

*corresponding author: hir10@hi.is

Keywords: Volcano-ice interaction, Ice cauldrons, Heat flux, Grímsvötn

Abstract

Grímsvötn lies beneath the centre of the Vatnajökull ice cap, Iceland, and has for centuries been one of the most powerful geothermal areas in the world as well as being Iceland's most active volcano. Calorimetric studies of its heat output have suggested long-term heat release of 2–4 GW. We have performed a detailed study of the heat release of Grímsvötn over the period 1998–2016, which includes the eruptions of 1998, 2004 and 2011. Annual mapping of the ice surface is used to monitor ice volume changes, combined with results of mass-balance monitoring over this same period. We estimate an average heat release of 1800 MW, whereof about 1200 MW is the base geothermal heat flux. The remaining 600 MW is an average over the study period, composed of peaks above the base flux from melting during eruptions and associated geothermal anomalies. The most intense melting occurs at the eruption sites during eruptions. Less intense signals lasting several months to years are due to increased geothermal melting creating new ice cauldrons and deepening of pre-existing ones. Such thermal anomalies were observed both as precursors to the eruptions, and in the 2–3 years following. The strongest signal followed the 1998 eruption which produced an average of 650 MW in the two years following. After the 2004 eruption a thermal anomaly of 500 MW was observed in the following years, and an average signal of 450 MW followed the 2011 eruption. These thermal signals demonstrate a post-eruption link to increased geothermal activity at the caldera walls.

1. Introduction

Grímsvötn is a central volcano beneath the Vatnajökull ice cap and has a partly ice-filled caldera (figures 1). It lies near the northern end of the Grímsvötn volcanic system, which has been the most active in Iceland in historical time, accounting for ~38% of the confirmed eruptions, with most of these eruptions occurring within the Grímsvötn caldera (Larsen et al., 1998; Thordarson and Larsen 2007). In the 100 year period before 2017, eruptions have been recorded within the Grímsvötn caldera in 1922, 1934, 1983, 1998, 2004, and 2011 (e.g. Thorarinsson, 1974; Gudmundsson and Björnsson, 1993; Oddsson et al., 2012; Jude-Eton et al., 2012; Hreinsdóttir et al., 2014) and in Gjálp, 10–15 km to the north of the caldera, in 1938 and 1996 (Gudmundsson and Björnsson, 1993; Gudmundsson, 1997; Gudmundsson et al., 2004). The last three caldera eruptions occurred during the period covered by this study.

Grímsvötn is one of the most geothermally active calderas in the world, with sustained heat output in the order of Gigawatts for centuries (Björnsson and Gudmundsson, 1993; Björnsson 1988). Three caldera structures have been identified at Grímsvötn (Saemundsson, 1982; Björnsson and Einarsson, 1991; Gudmundsson and Milsom, 1997), and a partially subglacial lake is located within the main caldera, with patches of open water along the southern and south-eastern caldera walls. Prior to the current period of high volcanic activity, which began with the Gjálp eruption in 1996, meltwater generated by subglacial geothermal activity and surface ablation collected in the subglacial lake. The lake level would rise by 70–130 m over a period of 4–6 years, before being released as a glacial flood, known as a jökulhlaup. Jökulhlaups from Grímsvötn tended to last 2–3 weeks, although larger floods usually have a shorter duration (Björnsson 2003). Over the last two decades, changes in the location of geothermal activity have resulted in sustained leakage and reduced storage, leading to less regular variations in lake level and smaller jökulhlaups (Jarosch and Gudmundsson, 2007; IES unpublished data).

The long-term geothermal activity at Grímsvötn is manifested as a 12-15 km wide depression in the glacier surface with the caldera at the centre. This depression is an ice drainage basin, with ice flowing into the depression where it may melt due to the geothermal heat (e.g. Björnsson, 2003; Björnsson and Gudmundsson, 1993). Within this wider depression, individual spots of high subglacial geothermal activity are manifested as ice cauldrons, which are depressions in the glacier surface and form due to melting at the glacier base. In Grímsvötn ice cauldrons are typically less than 1 km in diameter and 10-100 m deep. Ice cauldrons form primarily around the caldera edges at Grímsvötn, and vary in their dimensions and growth rate. When ice melts at the glacier base it may either accumulate beneath the glacier, or drain continuously. At Grímsvötn, both scenarios are observed, with meltwater accumulating in the subglacial lake, but other geothermal areas beyond the edges of the lake drain continuously (Björnsson 1988). Ice cauldrons provide an opportunity to use the ice as a calorimeter in cases where meltwater drains from the area.

Thermal signals are observed at many ice covered volcanoes in Iceland, including Bárdarbunga and Kverkfjöll which are also located beneath Vatnajökull (figure 1) (Björnsson and Einarsson, 1991; Gudmundsson et al., 2016, Montanaro et al., 2016), and worldwide (Major and Newhall, 1989). Notable examples outside of Iceland include the ice caves observed at Mount St. Helens and Mount Rainier in the U.S.A. (Kiver and Mumma, 1971; Anderson et al., 1998; Zimbelman et al., 2000), and at Mount Erebus in Antarctica (Giggenbach, 1976). Thermal features have been known to act as precursors to volcanic activity, e.g. at Redoubt volcano, Alaska, where ice surface depressions, wide-spread subsidence, and punctures created by steam evolved during the build-up to the 2009 eruption (Bleick et al., 2013).

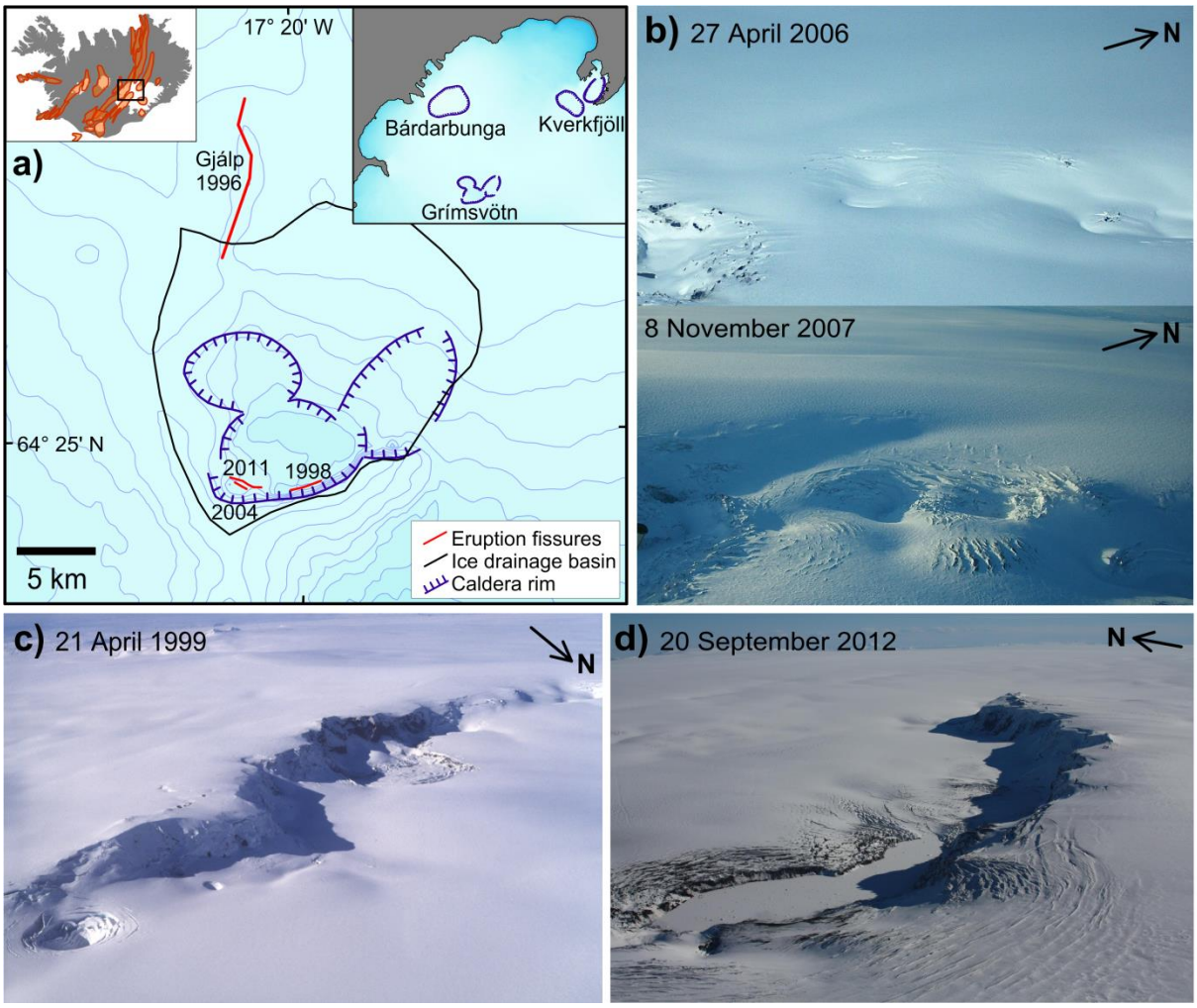

Figure 1: a) Grímsvötn and the surrounding area. Red lines denote the eruption fissures from the 1996 Gjálp eruption, and the 1998, 2004 and 2011 eruptions at Grímsvötn. The black line marks the average margin of the Grímsvötn ice drainage basin over the study period. The first inset map (left) shows Iceland with the volcanic zones shaded orange; the box marks the area of the second inset map (right), which shows the three central volcanoes beneath North-east Vatnajökull. b) Photographs of the West caldera wall taken 18 month apart, showing the growth of ice cauldrons in this area. c) The south caldera wall, looking south-west. An ice cauldron can be seen clearly in the East (left in the photograph) which developed after the 1998 eruption. d) The south caldera wall, looking east. The flat area at the foot of the caldera wall towards the west is the subaerial part of the glacial lake.

Monitoring geothermal activity at volcanoes gives necessary insight into the associated volcanic hazards, and the hydrothermal systems below. Thermal signals from subsurface magmatic sources are usually difficult to quantify since the measurement of heat flux from the ground is subject to large uncertainties due to heat loss to the atmosphere. Subglacial geothermal fields present a unique opportunity to calculate the surface heat flux to a much-improved accuracy, as almost all of the thermal energy is spent melting ice (Jarosch and Gudmundsson, 2007; Jarosch et al., 2008).

A record of heat output at Grímsvötn between 1998 and 2016 is presented, using annual measurements which allow for a more detailed study than those previously carried out. We split Grímsvötn into sub-areas, quantifying the geothermal activity in terms of spatial distribution.

This study covers a period of high volcanic activity, during which three eruptions took place within the caldera, and explores the relationship between observed thermal signals to volcanic activity and eruption sites.

2. Methods

2.1 Ice surface monitoring

Over the survey period, ice surface elevation at Grímsvötn was mapped annually, always at the same time of year, in June, before summer ablation starts. Thus, seasonal elevation variations due to surface melting caused by meteorological factors should not affect the comparison. The ice surface was surveyed using a differential GPS between 1998 and 2004, with elevation accuracy of 2-3 m, and a kinematic GPS from 2005 onwards, with an elevation accuracy of ~0.1 m. The GPS instruments were mounted on snowmobiles to cover large distances, or carried on foot in areas where the terrain is steep or crevassed. The survey lines are displayed in appendix A. It is not possible to cover the entire area of Grímsvötn in detail, so active geothermal areas and recent eruption sites are focussed on. These data are supplemented by airborne radar altimetry profiling. Airborne altimetry measurements are made on board a low-flying aircraft (approximately 100 m elevation), using a C-band radar altimeter to record the aircraft elevation, and kinematic GPS or sub-meter differential GPS to simultaneously record the precise position. The surface elevation measurements obtained through altimetry profiling achieve an absolute accuracy of 3 m and a relative accuracy of 1-2 m (Gudmundsson et al., 2007; 2016). Ice surface maps are prepared each year, by manually interpolating the elevation data to ensure detailed coverage of areas of interest. An InSAR map of western Vatnajökull from the summer of 1998, and a high resolution (accuracy ~0.1 m) LiDAR map obtained in the summer of 2012 , are also used (Magnússon et al. 2005; Jóhannesson et al., 2013). The mapping after 2012 has been done by recording changes relative to the LiDAR map.

2.2 Calorimetry

Changes in the ice surface elevation are used to calculate the geothermal energy released at the base of the glacier, and by measuring over periods of years to decades time series of geothermal power are obtained. Björnsson and Gudmundsson (1993) divided the geothermal heat flux produced in the Grímsvötn caldera into a base flux that changes little over decadal time scales, and shorter-term variations with a strong link to volcanic activity. This approach is adopted here with depressions formed in the ice surface from geothermal melting considered to be caused by thermal anomalies that are above the base level. Geothermal melting occurs in areas of increased geothermal heat flux, whereas volcanic melting occurs when the ice comes into contact with the products of volcanic eruptions. The lake at Grímsvötn is partially subglacial and partially subaerial. Changes in the lake level result in an elevation change in both the open water and the floating ice, and must be separated from the elevation changes due to melting. Thus, areas affected by either uplift or subsidence of ice or lake surface are excluded from the calorimetric estimates.

The relative change in ice surface elevation for a year-long period is calculated using a differential map, which is created by taking the topographical map for a given year and subtracting the topographical map for the previous year. This gives the rate of change of the ice volume, $\dot{V}_i$ (with a time step of one year), over the time period. The mass of ice melted, $\dot{m}_b$, is estimated from the observed volume fluxes.

$$\dot{m}_b = \rho_i \dot{V}_i \quad (1)$$

with ρ_i being the density of ice; we use a value of 917 kg m^{-3} for ice density. When this method is applied to a single ice cauldron or a very limited area (as is the case for the northern cauldrons in this study), ice flow into the depression may skew the results if not accounted for. This is done by adding an underestimation factor, U, so that $\dot{m}_b = (U + 1)\rho_i \dot{V}_i$. Jarosch and Gudmundsson (2007) found that a value of U=0.23 is appropriate to correct for the underestimation.

This method can only be used where meltwater does not accumulate beneath the glacier, and where heat is not lost directly to the atmosphere (from exposed bedrock) or to subglacial/englacial bodies of water. Several scenarios are observed at Grímsvötn where the above method does not fully apply: when the ice is floating above the subglacial lake; during eruptions that have melted through the full ice thickness; and where a patch of open water increases in area and the surrounding ice melts through the full thickness, from the bedrock to the surface. Floating ice produces a broad signal to the north of the southern caldera wall, in areas where any geothermal upflow zones at the caldera floor are obscured by open water or floating ice, and therefore they are not included in these calculations. Patches of open water show up on the topographic maps as flat areas within depressions, often partly bordered by steep ice walls. Where open water has increased in area, the ice volume melted to accommodate this increase is calculated from the ice surface from the previous year down to the surface defined by the bedrock map (Björnsson and Einarsson, 1991). During eruptions which become subaerial, no attempt is made to estimate the complete heat budget of the eruption, only the fraction lost through melting of ice is estimated while much of the heat is released into the atmosphere.

The method described above is used to calculate ice volume changes due to volcanic eruptions and localised geothermal anomalies. Aside from the geothermal anomalies, a base geothermal signal is produced at Grímsvötn. By considering the mass of ice melted or added to the system, this can be estimated using:

$$dM = M_1 - M_2 - M_3 \quad (2)$$

where dM is the change in the ice mass within the Grímsvötn ice drainage basin, M_1 is the net mass added to the area by surface accumulation (winter accumulation minus summer ablation), M_2 is the mass of ice removed by melting from volcanic eruptions and anomalous geothermal signals, and M_3 is the mass removed due to melting from the base geothermal heat. The margin of the ice drainage basin at Grímsvötn migrates slightly from year to year due to changing ice topography, so an intermediate basin is used for the calculations (figure 1). dM is estimated by subtracting the topographic map from the first year of the study period from the final year to get the volume change, and using the ice density ρ_i = 917 kg m^{-3} to convert to the change in ice mass (equation 1). Corrections are made to dM to account for the addition of eruption deposits to the area, and the change in lake level during the study period. M_1 is calculated by multiplying the Grímsvötn drainage basin area of 131 km^2 by the specific annual mass balance, which has an average of 1.35 m yr^{-1} (water equivalent) during the study period; this result is obtained from annual mass balance measurements in the Grímsvötn area (Björnsson and Pálsson, 2008; Pálsson et al., 2016).

Where the meltwater accumulation is not a consideration, the observed ice volume changes are used as a large-scale calorimeter (Gudmundsson et al., 2004; Jarosch et al., 2008). The thermal

energy (Q) required to generate the ice cauldrons is estimated from the mass of ice melted ($\dot{m}_b$) and the latent heat of fusion for ice ($L_i = 3.34\times10^5$ J kg^{-1}).

$$Q = \dot{m}_b L_i \quad (3)$$

The ice is assumed to be temperate, and therefore at the pressure melting point throughout. Although the melting point decreases slightly with pressure, this is roughly equivalent to assuming a uniform ice temperature of 0 °C.

3. Results

The ice surface changes at Grímsvötn between 1998 and 2016 are presented in photographs (figure 2), as topographic maps for selected years (figure 3), as differential maps (figure 4), and as cauldron activity maps (figure 5). The differential maps show the difference in the ice surface elevation for each one year period (from June to June), with red representing a lowering of the ice surface, and blue a higher ice surface elevation. Only the southern part of the Grímsvötn area is displayed in figure 4 as thermal anomalies in the northern part are relatively minor in comparison. Several features are observed and summarised in Table 1: melting due directly to eruptions and their deposits; deepening/infilling of ice cauldrons, which form mainly around the caldera rims; and melting around the lake, resulting in larger areas of open water. The (mostly) subglacial lake has several areas of open water along the southern caldera wall, which are observed as flat areas on the topographic maps (figure 3).

Three eruptions took place within the Grímsvötn caldera during the study period (figures 1 and 3). Melting from each of the eruptions is clearly visible in the differential maps (figure 4), and a build-up of volcanic products can be seen south of the 2011 eruption fissure as an increase in elevation. The estimates of the volumes of tephra added to the Grímsvötn basin in these eruptions are given in table 1 and figure 3, and are corrected for when calculating the ice volume change. Many jökulhlaups occurred during the study period, and three of the main flood events appear to be connected to eruptions (Table 1). A jökulhlaup followed the 1998 eruption by about four weeks, the 2004 eruption occurred during a jökulhlaup (Sigmundsson and Gudmundsson, 2004), and a jökulhlaup occurred about half a year prior to the 2011 eruption. It is suggested that the 2004 eruption was triggered by the pressure release resulting from the draining of the subglacial caldera lake (Albino et al., 2010). The rise of the level of the subglacial lake prior to the jökulhlaups is conspicuous on the difference maps (about 50 m in 2003–2004, and 30 m in 2009–2010). The increase in the level of the open water by the southern caldera wall was similar, before dropping by up to 60 m during both jökulhlaups.

Table 1: Summary of events and activity from 1998–2016

Year	Southwest corner	South area	Southeast area	North area	Significant jökulhlaups
1998–1999	Large area of melting west of eruption site	**ERUPTION 18–27 DEC 1998, producing ~ 80×10^6 m^3 of tephra (Gudmundsson et al. 2000)**	Cauldrons deepening		Jan–Feb 1999
1999–2000		Melting continues at eruption site	Cauldrons deepening		Nov 1999
2000–2001			Cauldrons deepening		
2001–2002		Melting around lake			
2002–2003		Melting around lake			
2003–2004				Increased activity	
2004–2005	**ERUPTION 1–6 NOV 2004, producing ~ 40×10^6 m^3 of tephra (Oddsson et al. 2012; Jude-Eton et al. 2012)**		Cauldrons deepening		Oct–Nov 2004
2005–2006	Cauldrons deepening, infill of ice at the 2004 eruption site				
2006–2007	Cauldrons deepening				
2007–2008	Cauldrons deepening				
2008–2009	Melting west of caldera wall			Increased activity	
2009–2010	Melting west of caldera wall		Cauldrons deepening		
2010–2011	**ERUPTION 21–28 MAY 2011, producing ~ 55×10^6 m^3 of tephra (IES unpublished data)**				Sep–Oct 2010
2011–2012	Infill of ice at the 2011 eruption site				
2012–2013				Increased activity	
2013–2014	Cauldron deepening	Melting around lake			
2014–2015	Cauldron deepening			Increased activity	
2015-2016	Cauldron deepening				

Figure 2: Photographs of the Grímsvötn southern caldera wall, taken from the western end, showing changes in the lake level and ice cover with time.

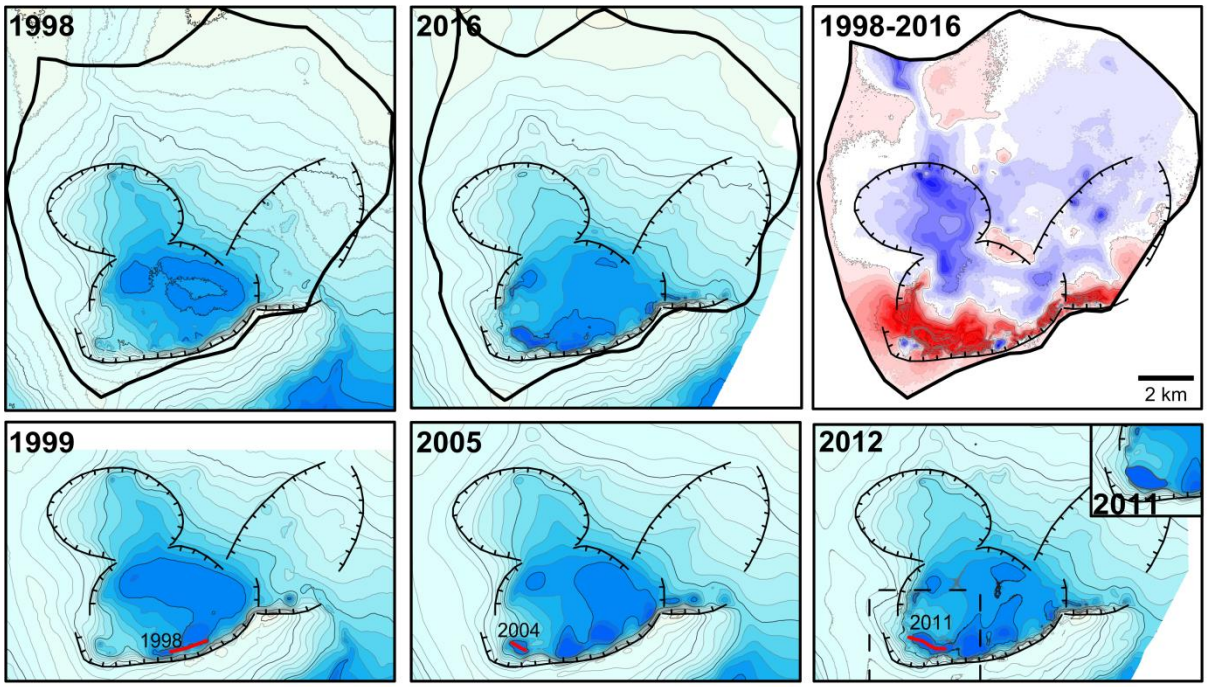

	Volume (10^6 m^3)	
Volume change (1998-2016)	318	
Corrections:		
1998 eruption tephra	-80	(Gudmundsson et al. 2000)
2004 eruption tephra	-40	(Oddsson et al. 2012; Jude-Eton et al. 2012)
2011 eruption tephra	-55	(IES unpublished data)
Lake water level	-100	
Net volume change (dV)	**43**	

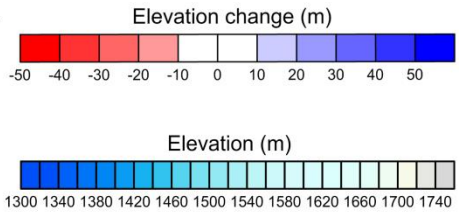

Figure 3: Topographic plots of the ice surface elevation around Grímsvötn caldera. The top row shows the first and last years of the study period (1998 and 2016), and a differential map showing the difference in ice surface elevation between these years. The black lines denote the ice drainage basins for each year, with an intermediate basin used for the differential map. The table gives the ice volume change for this region, and lists the corrections made to give the net volume change used in the base heat flux calculations. Three eruptions took place during this period and the fissures are marked in red on the second row. Depressions appear in the ice around the eruption sites and at geothermal areas around the caldera rim. Elevation change in the centre of the caldera represents changes in the subglacial lake level.

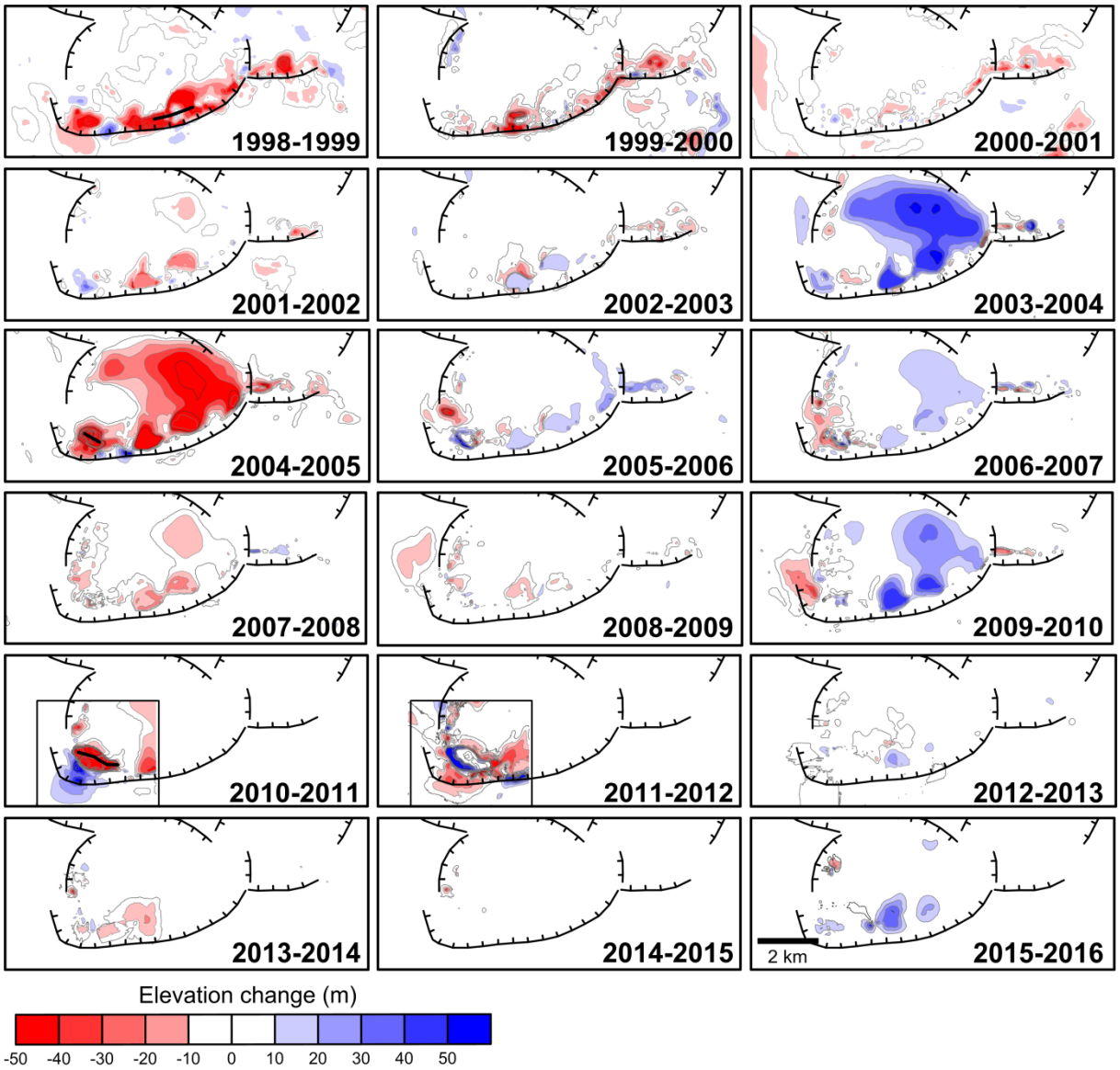

Figure 4: Differential maps showing the change in ice elevation over a one year period, as labelled. The red parts represent a lowering of the ice surface, due to ice melting or a decrease in the water level of the lake, and the blue areas show uplift of the ice, or infill of previous depressions. Black lines show eruption fissures in 1998-1999, 2004-2005, and 2010-2011. Data collection was limited following the 2011 eruption, so the 2010–2011 and 2011–2012 differential maps cover a smaller area.

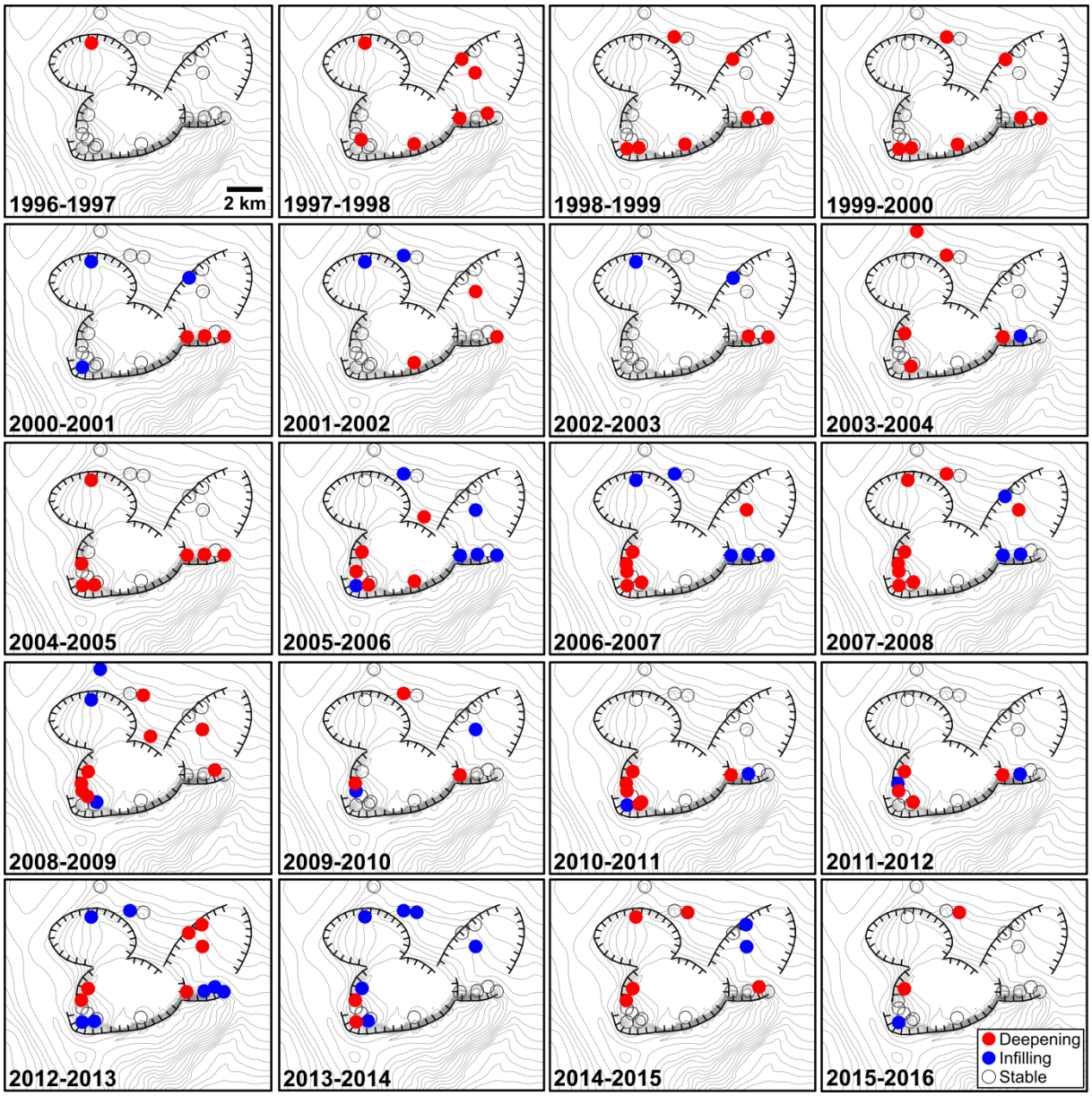

Figure 5: The activity at ice cauldrons during the study period. Red dots represent ice cauldrons that are deepening, blue dots are infilling cauldrons (power decreasing), and grey circles represent stable cauldrons.

Twenty ice cauldrons, mostly along the caldera rims, become active intermittently during the study period, each for durations of typically between one and five years, before starting to be infilled by ice flowing into the caldera. The majority of the activity is located along the south-western, southern and south-eastern caldera walls (figure 6), but eight cauldrons are observed to the north of these.

In the year prior to the 1998 eruption, the cauldrons in the north of the caldera are seen to deepen (figure 7d). Similarly, cauldrons deepened along the western caldera wall and in the south-west before the 2004 eruption (figure 4).

During the 1998 eruption (between 18-27 December), 130±25 million m^3 of ice melted at the eruption site and immediate vicinity (figure 7b). Following the eruption, significant changes were observed along the caldera wall. Major melting occurred at the south-eastern caldera wall between 1998 and 2001 (figure 7c), and a large area (~0.5 km^2) to the west of the eruption site melted out after the eruption (figure 7a). The combined volume melted at these two locations was 155±25 million m^3.

An ice volume of 70±10 million m^3 melted during the 2004 eruption (Oddsson et al., 2012), around the eruption site in the south-west of the caldera. Following the 2004 eruption, cauldrons began to form to the north of the eruption site, reaching a volume of 25±4 million m^3 (figure 4).

The 2011 eruption produced a large ice cauldron in the south-western corner of the caldera, at roughly the same location as the 2004 eruption site (figure 7a). An ice volume of 80±10 million m^3 was melted during the 2011 eruption. Cauldrons were observed to deepen along the south-western and southern caldera walls following the eruption.

The change in ice volume within the Grímsvötn ice drainage basin from 1998–2016, dV, is calculated to be 4.3×10^7 m^3 (figure 3). Using equation 1, dM is therefore 3.9×10^{10} kg. M_1, the mass of ice accumulated on the glacier surface, is estimated to be 3.2×10^{12} kg. The total mass of ice melted due to local increased geothermal activity and volcanic eruptions from 1998–2016 is 1.0×10^{12} kg, which is M_2 in equation 2, and equates to an average power of ~600 MW during this period. Using equations 2 and 3, the term M_3 is estimated as 2.1×10^{12} kg for 1998–2016, giving an average base geothermal power for the Grímsvötn basin of 1200 MW. The total power, including all contributions from volcanic eruptions, anomalous increases in geothermal activity, and the base geothermal activity, is therefore ~1800 MW. It should be noted that this value for the total power does not include heat which is transferred to the atmosphere from areas of exposed bedrock, or to the lake water, and therefore slightly underestimates the value.

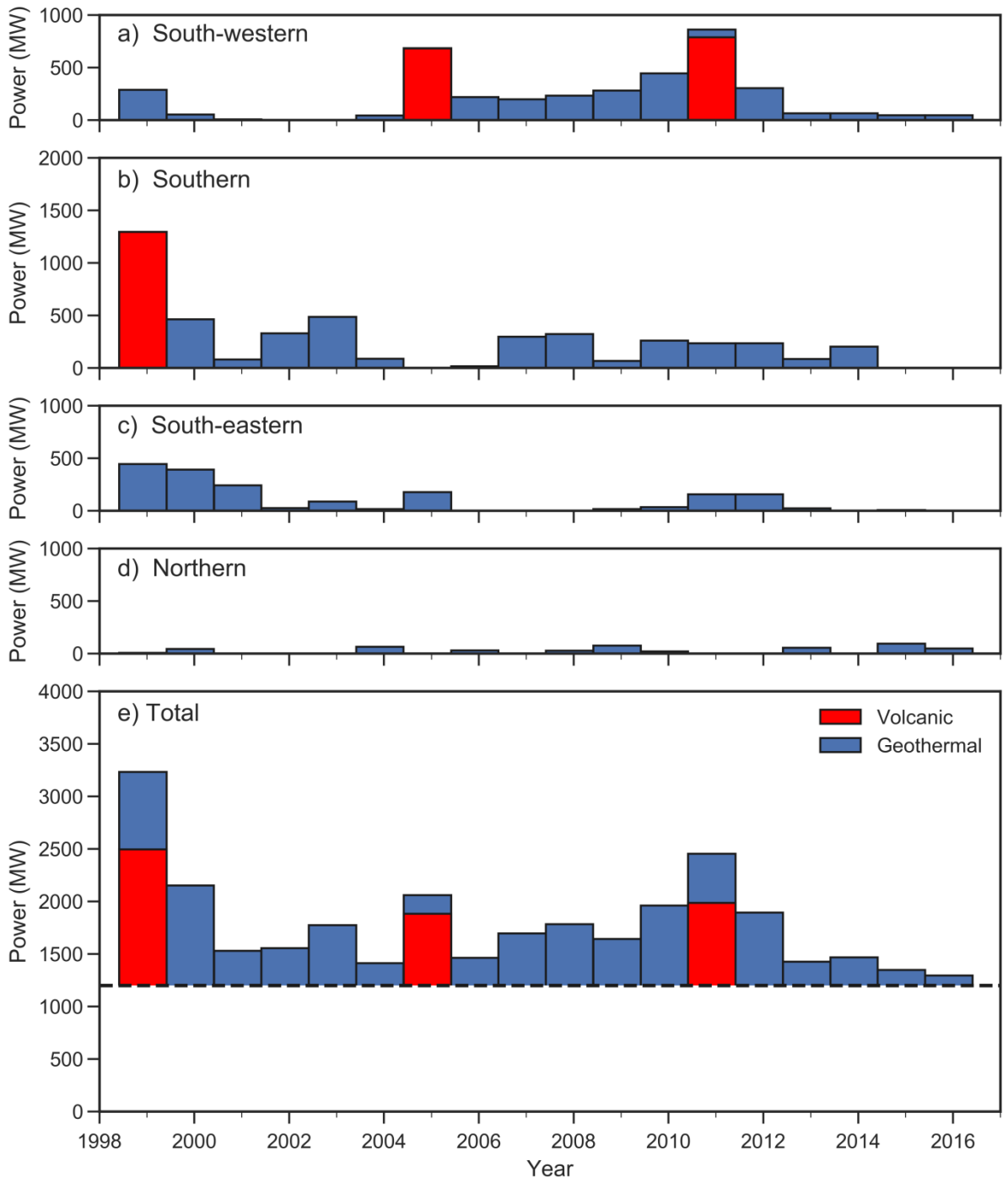

Figure 6: The power required to melt the depressions around the Grímsvötn caldera walls, split into four areas: a) south-western, b) southern and c) south-eastern as shown in the map, and d) is the power of the cauldrons lying north of these areas, referred to as the northern cauldrons. This shows the most heat flux is generated in area b), with very little produced outside of the south caldera wall. The red bars represent the power contributed directly from eruptions; most of that heat is released during the eruptions (days-weeks) but here their contribution to yearly averages are shown. e) displays the total power used to melt ice at Grímsvötn. The dashed line shows the average base geothermal power for Grímsvötn, and above this is the total power from geothermal variations (blue) and power which melted ice during volcanic eruptions (red), in the whole Grímsvötn area, i.e. the sum of graphs a) to d).

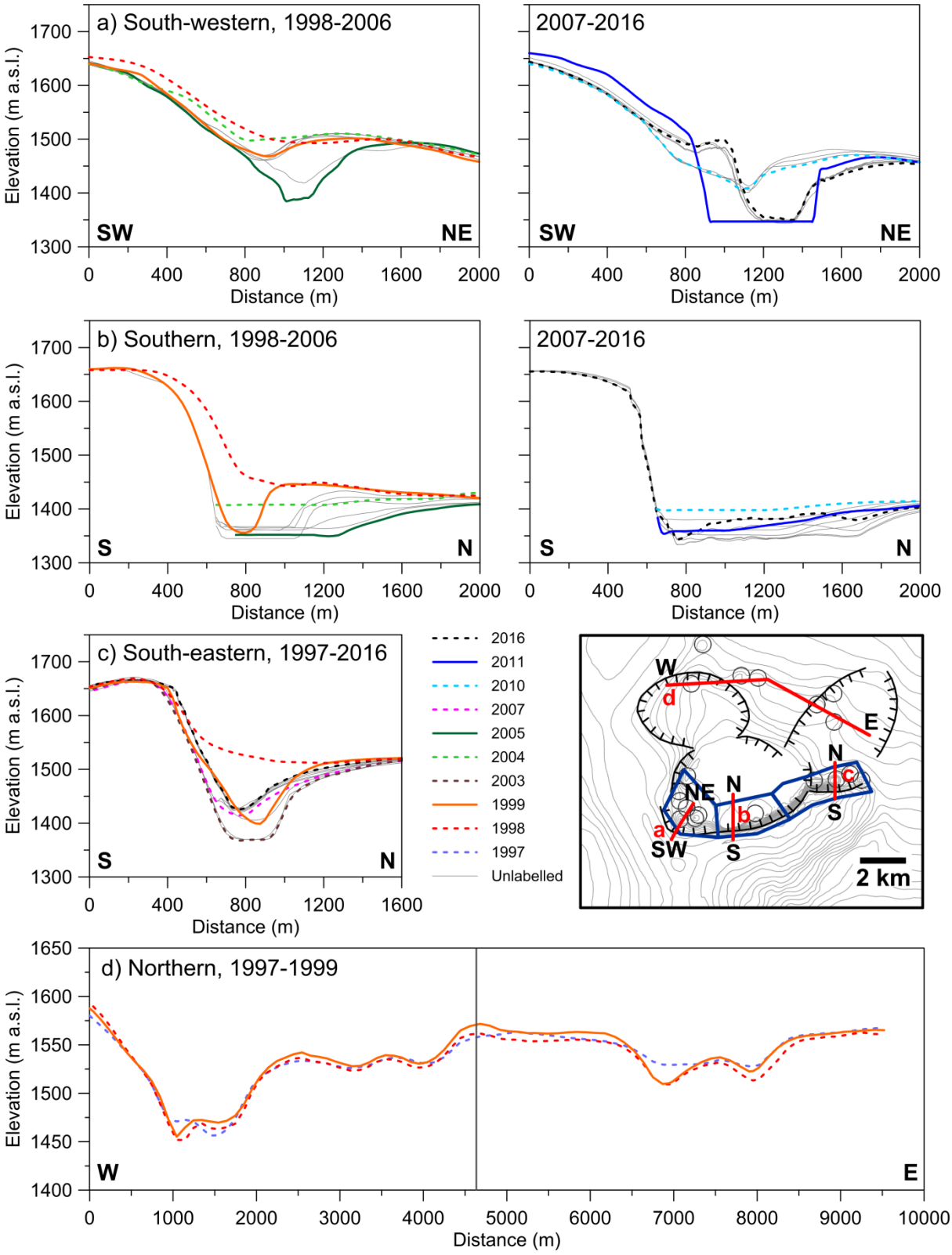

Figure 7: The graphs display four profiles, which are shown on the map as red lines. Note that a) and b) are split into two, the period from 1998–2006 on the left and 2007–2016 on the right. Years following eruptions are displayed as solid lines, years of particular interest are dashed lines, and other years are unlabelled but marked as thin grey lines to show the full range of the data. The black line in d) is the point at which the profile changes direction.

4. Discussion

Increased geothermal melting was observed in the ~1 year period prior to all three eruptions, assumed to be precursory activity, similar to the increased geothermal activity observed before the 2009 eruption at Redoubt (Bleick et al., 2013). The 2004 and 2011 eruptions were preceded by jökulhlaups, directly before the 2004 eruption and seven months before the 2011 eruption. It has been suggested that the pressure release, after the load of the subglacial lake within Grímsvötn is removed, may trigger volcanic eruptions (Thorarinsson, 1953; Björnsson, 2002; Albino et al., 2010). The increase in geothermal heat flux which followed the 2004 and the 2011 eruptions may also have been caused by the pressure release following the jökulhlaups.

The estimated total power for the Grímsvötn area between 1998 and 2016 of ~1800 MW includes all thermal heat flux from volcanic activity, increased geothermal activity, and the base geothermal output. Björnsson and Gudmundsson (1993) estimated the total power from the Grímsvötn caldera for 1922–1991. They found the highest total heat flux to be 11600 MW, from 1934–1938, which gradually decreased over the following 20 years. From 1960–1991, the total heat flux was calculated for periods of between 2 and 6 years, with a minimum value of 1600 MW, a maximum of 3000 MW, and an average value of 2270 MW. The value obtained for 1998–2016 falls on the lower end of this range, suggesting that the long-term average total heat flux from Grímsvötn has not changed significantly between 1960 and 2017.

Ice cauldrons form mostly around the rims of the caldera, suggesting that higher bedrock permeability along the caldera faults plays a role in the cauldron formation. The ice cauldrons at Grímsvötn tend to remain active for periods of more than one year, some for many decades, and these long timescales confirm that they are not the result of small subglacial eruptions. If the ice cauldrons were a direct result of a subglacial eruption, i.e. if magma came into direct contact with the basal ice beneath a cauldron, the thermal signal would last for much shorter periods and decline rapidly (Reynolds et al., 2017). The cauldrons which were observed to deepen following the 1998 and 2004 eruptions were active for ~3 years, and the increased activity began within a year of the eruptions.

Björnsson et al. (1982) suggested that for the total heat flux observed at Grímsvötn to be generated, water must penetrate into cracks within hot rocks, and since then it has been suggested that hydrothermal convection extracting heat from the roof of the Grímsvötn magma chamber and shallow intrusions is the source of the geothermal activity (Björnsson and Gudmundsson, 1993). The observed precursory and post-eruption thermal anomalies are most likely caused by the emplacement of shallow magmatic intrusions or increased permeability during periods of unrest prior and during the eruptions.

5. Conclusions

We present an 18 year record of the ice surface elevation changes at Grímsvötn caldera, from 1998 to 2016, with surface heat flux estimates. The main conclusions are:

- A net ice loss of about 1.1 km^3 (a mass of 1×10^{12} kg is observed for the Grímsvötn drainage basin over the survey period. Ice cauldrons are observed around the caldera rims, with the majority of the heat flux generated along the southern, south-eastern and south-western caldera walls.
- Some increase in geothermal activity was observed preceding all eruptions.

- Thermal anomalies were observed following all three eruptions, lasting 2–3 years. After the 1998 eruption a thermal anomaly of 650 MW was observed during the following two years, similarly thermal anomalies of 500 MW and 450 MW were observed in the two years after the 2004 and 2011 eruptions respectively. These thermal signals suggest a post-eruption link to increased geothermal activity at the caldera walls.
- The average thermal power of volcanic eruptions and associated shorter-term increases in geothermal power over the survey period is estimated as ~600 MW.
- The average base geothermal heat flux for the Grímsvötn area was estimated to be 1200 MW and the average total power of Grímsvötn from volcanic and geothermal sources ~1800 MW.

Acknowledgements

We acknowledge the support of the EU Seventh Framework Marie Curie project NEMOH no. 289976, the Research Fund of the University of Iceland and Landsvirkjun power company. GPS profiling took place in the annual expeditions of the Iceland Glaciological Society. We thank the crew of TF-FMS, the survey aircraft of Isavia for fruitful collaboration over the survey period.

References

Albino F, Pinel V, Sigmundsson F (2010) Influence of surface load variations on eruption likelihood: application to two Icelandic subglacial volcanoes, Grimsvotn and Katla. Geophysical Journal International 181:1510–1524.

Anderson CH, Behrens CJ, Floyd GA, Vining MR (1998) Crater Firn Caves of Mount St. Helens, Washington. Journal of Caves and Karst Studies 60:44–50.

Björnsson H, Björnsson S, Sigurgeirsson Th (1982) Penetration of water into hot rock boundaries of magma at Grímsvötn. Nature 295:580–581.

Björnsson H (1988) Hydrology of Ice Caps in Volcanic Regions. Soc Sci Isl, Rit 40. 139 pp.

Björnsson H, Einarsson P (1991) Volcanoes beneath Vatnajökull, Iceland: Evidence from radio-echo sounding, earthquakes and jökulhlaups. Jökull 40:147–148.

Björnsson H, Guðmundsson MT (1993) Variations in the thermal output of the subglacial Grímsvötn Caldera, Iceland. Geophysical Research Letters 20:2127–2130.

Björnsson H (2003) Subglacial lakes and jökulhlaups in Iceland. Global planet change 35:255–271.

Björnsson H, Pálsson F (2008) Icelandic glaciers. Jökull 58:365–386.

Bleick HA, Coombs ML, Cervelli PF, Bull KF, Wessels RL (2013) Volcano-ice interactions precursory to the 2009 eruption of Redoubt Volcano, Alaska. J Volcanol Geotherm Res 259:373–388.

Giggenbach WF (1976) Geothermal ice caves on Mt Erebus, Ross Island, Antarctica. New Zeal J Geol Geophys 19:365–372, doi: 10.1080/00288306.1976.10423566.

Gudmundsson MT (1997) Gosið í Vatnajökli í október 1996. Einkenni, bræðsla íss og breytingar á jöklinum (in Icelandic). In Haraldsson H, editor, Vatnajökull. Gos og hlaup 1996, pp. 37–59. Vegagerðin, Reykjavík.

Guðmundsson MT, Milsom J (1997) Gravity and magnetic studies of the subglacial Grímsvötn volcano, Iceland. Implications for crustal and thermal structure. J Geophys Res 102:7691–7704.

Gudmundsson MT, Björnsson H (1993) Eruptions in Grímsvötn 1934–1991. Jökull 41:21–46.

Gudmundsson MT, Sigmundsson F, Björnsson H, Högnadóttir Th (2004) The 1996 Eruption at Gjálp, Vatnajökull Ice Cap, Iceland: Efficiency of Heat Transfer, Ice Deformation and Subglacial Water Pressure. Bull Volcanol 66(1):46–65.

Gudmundsson MT, Högnadóttir T, Kristinsson AB, Gudbjörnsson S (2007) Geothermal activity in the subglacial Katla caldera, Iceland, 1999–2005, studied with radar altimetry. Ann Glaciol 45:66–72.

Gudmundsson MT, Jónsdóttir K, Hooper A, Holohan EP, Halldórsson SA, Ófeigsson BG, Cesca S, Vogfjörd KS, Sigmundsson F, Högnadóttir T, Einarsson P, Sigmarsson O, Jarosch AH, Jónasson K, Magnússon E, Hreinsdóttir S, Bagnardi M, Parks MM, Hjörleifsdóttir V, Pálsson F, Walter TR, Schöpfer MPJ, Heimann S, Reynolds HI, Dumont S, Bali E, Gudfinnsson GH, Dahm T, Roberts MJ, Hensch M, Belart JMC, Spaans K, Jakobsson S, Gudmundsson GB, Fridriksdóttir HM, Drouin V, Dürig T, Aðalgeirsdóttir G, Riishuss MS, Pedersen GBM, van Boeckel T, Oddsson B, Pfeffer MA, Barsotti S, Bergsson B, Donovan A, Burton MR, Aiuppa A (2016) Gradual caldera collapse at Bárdarbunga volcano, Iceland, regulated by lateral magma outflow. Science 353(6296), aaf8988.

Hreinsdóttir S, Sigmundsson F, Roberts MJ, Björnsson H, Grapenthin R, Arason P, Árnadóttir T, Hólmjárn J, Geirsson H, Bennett RA, Gudmundsson MT, Oddsson B, Ófeigsson BG, Villemin T, Jónsson T, Sturkell E, Höskuldsson Á, Larsen G, Thordarson T, Óladóttir BA (2014) Volcanic plume height correlated with magma pressure change at Grímsvötn Volcano, Iceland. Nature Geoscience 7:214–218, doi:10.1038/ngeo2044.

Jarosch AH, Gudmundsson MT (2007) Numerical studies of ice flow over subglacial geothermal heat sources at Grímsvötn, Iceland, using Full Stokes equations. J Geophys Res 112: F02008, doi: 10.1029/2006JF000540.

Jarosch AH, Gudmundsson MT, Högnadóttir T, Axelsson G (2008) Progressive cooling of the hyaloclastite ridge at Gjálp, Iceland, 1996–2005. J Volcanol Geotherm Res 170:218–229.

Jóhannesson T, Björnsson H, Magnússon E, Guðmundsson S, Pálsson F, Sigurðsson O, Thorsteinsson T, Berthier E (2013) Ice- volume changes, bias estimation of mass-balance measurements and changes in subglacial lakes derived by lidar mapping of the surface of Icelandic glaciers. Ann Glaciol 54(63):63–74.

Jude-Eton TC, Thordarson Th, Gudmundsson MT, Oddsson B (2012) Dynamics, stratigraphy and proximal dispersal of supraglacial tephra during the ice-confined 2004 eruption at Grímsvötn volcano, Iceland. Bull Volcanol 74:1057–1082, doi: 10.1007/s00445-012-0583-3.

Kiver E, Mumma M (1971) Summit firn caves, Mount Rainier, Washington. Science 173(3994):320–322.

Larsen G, Gudmundsson MT, Björnsson H (1998) Eight centuries of periodic volcanism at the center of the Iceland hot spot revealed by glacier tephrastratigraphy. Geology 26: 943–946.

Magnússon E, Björnsson H, Pálsson F, Dall J (2004) Glaciological application of InSAR topography data of western Vatnajökull acquired in 1998. Jökull 54:17–36.

Major JJ, Newhall CG (1989) Snow and ice perturbtion during historical volcanic-eruptions and the formation of lahars and floods – a global review. Bull Volcanol 52:1–27.

Montanaro C, Scheu B, Gudmundsson MT, Vogfjörd K, Reynolds HI, Dürig T, Strehlow K, Rott S, Reuschlé T, Dingwell DB (2016) Multidisciplinary constraints of hydrothermal explosions based on the 2013 Gengissig lake events, Kverkfjöll volcano, Iceland. Earth and Planetary Science Letters 434:308–319.

Oddsson B, Gudmundsson MT, Larsen G, Karlsdóttir S (2012) Monitoring the plume from the basaltic phreatomagmatic 2004 Grímsvötn eruption – application of weather radar and comparison with plume models. Bull Volcanol 74:1395–1407, doi: 10.1007/s00445-012-0598-9.

Pálsson F, Gunnarsson A, Jónsson Þ, Steinþórsson S, Pálsson HS (2016) Vatnajökull: Mass balance, meltwater drainage and surface velocity of the glacial year 2014–15. Landsvirkjun report.
Reynolds HI, Gudmundsson MT, Högnadóttir Th, Magnússon E, Pálsson F (2017) Subglacial volcanic activity above a lateral dyke path during the 2014–2015 Bárdarbunga-Holuhraun rifting episode, Iceland. Bull Volcanol 79(6):38.
Sigmundsson F, Gudmundsson MT (2004) Eldgosið í Grímsvötnum í nóvember 2004 – The Grímsvötn eruption, November 2004. Jökull 54:139–142.
Sæmundsson K (1982) "Calderas in the neovolcanic zones of Iceland." Eldur er í nor ri, Festschrift for Sigur ur órarinsson. pp. 221–239. SögufØlag, Reykjavík.
Thorarinsson S (1953) Some new aspects of the Grímsvötn problem. J Glaciology 4:267–274.
Thorarinsson S (1974) "Vötnin stríð." Saga Skeidarárhlaupa og Grímsvatnagosa [The swift flowing rivers: the history of Grímsvötn jökulhlaups and eruptions. In Icelandic]. 254 pp. Menningarsjóður, Reykjavík.
Thordarson T, Larsen G (2007) Volcanism in Iceland in historical time: volcano types, eruption styles and eruptive history. J Geodyn 43(1):118–152.
Zimbelman DR, Rye RO, Landis GP (2000) Fumaroles in ice caves on the summit of Mount Rainier—preliminary stable isotope, gas, and geochemical studies. J Volcanol Geotherm Res 97:457–473, doi: 10.1016/S0377-0273(99)00180-8

Appendix A

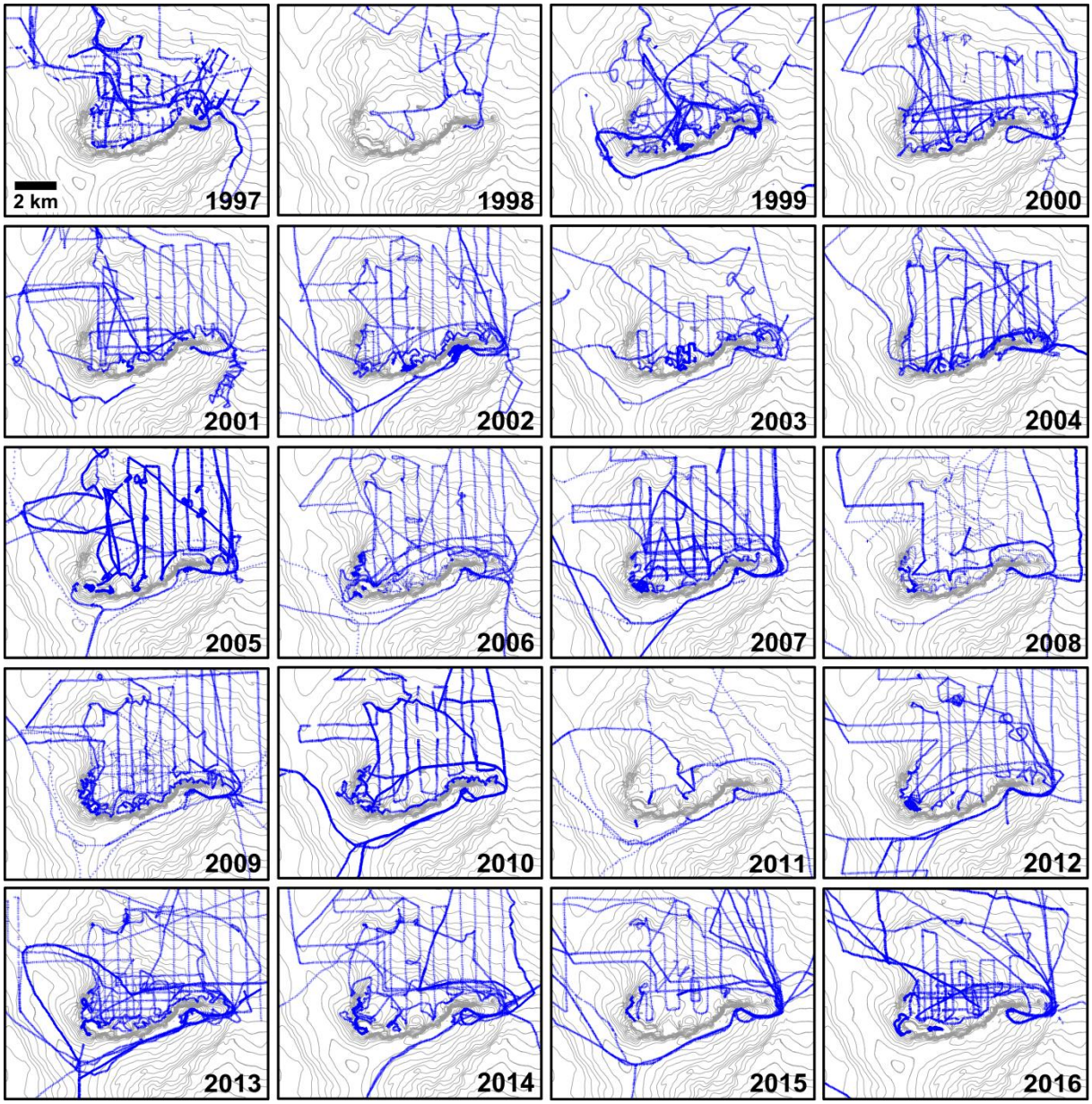

Figure A: Blue crosses show the data points taken in the ice elevation surveys during the study period.

Paper II

Subglacial volcanic activity above a lateral dyke path during the 2014–2015 Bárdarbunga-Holuhraun rifting episode, Iceland

Hannah Iona Reynolds, Magnús Tumi Gudmundsson, Thórdís Högnadóttir, Eyjólfur Magnússon, Finnur Pálsson

Bulletin of Volcanology, 79:38, doi: 10.1007/s00445-017-1122-z

Copyright 2017 Bulletin of Volcanology. Reprinted with the permission of Springer Science and Business media

Bull Volcanol (2017) 79:38
DOI 10.1007/s00445-017-1122-z

RESEARCH ARTICLE

Subglacial volcanic activity above a lateral dyke path during the 2014–2015 Bárdarbunga-Holuhraun rifting episode, Iceland

Hannah I. Reynolds[1] · **Magnús T. Gudmundsson**[1] · **Thórdís Högnadóttir**[1] · **Eyjólfur Magnússon**[1] · **Finnur Pálsson**[1]

Received: 28 November 2016 / Accepted: 13 April 2017
© Springer-Verlag Berlin Heidelberg 2017

Abstract The rifting episode associated with the Bárdarbunga-Holuhraun eruption in 2014–2015 included the first observations of major dyke propagation under ice. Three shallow ice depressions (ice cauldrons) with volumes ranging from 1 to 18 million m^3 formed in Dyngjujökull glacier above the 48-km-long lateral path of the magma, at 4, 7 and 12 km from the northern glacier edge. Aircraft-based radar altimetry profiling was used to map the evolution of the cauldrons and construct a time series of the heat transfer rates. Out of the three scenarios explored: (1) onset or increase of hydrothermal activity, (2) convection within vertical fissures filled with water overlying intruded magma and (3) subglacial eruptions, the last option emerges as the only plausible mechanism to explain the rapid heat transfer observed in a location far from known geothermal areas. The thermal signals at two of the cauldrons are consistent with effusive subglacial eruptions. The formation of the northernmost cauldron was more rapid, indicating faster heat transfer rates. Radio-echo sounding data indicate that in contrast to the other two cauldrons, an intrusion of eruptive products occurred into the glacier, reaching 50–60 m above bedrock with the increased magma-ice contact explaining the more rapid heat transfer. We propose that the ~2-m widening associated with graben formation increased the groundwater storage capacity of the bedrock, creating space for the meltwater to be stored, explaining the absence of meltwater pulses draining from Dyngjujökull.

Keywords Subglacial eruptions · Volcano-ice interaction · Rifting event · Ice cauldrons · Heat flux · Holuhraun

Editorial responsibility: J. Taddeucci

✉ Hannah I. Reynolds
hir10@hi.is

[1] Nordvulk, Institute of Earth Sciences, University of Iceland, Sturlugata 7, 101 Reykjavík, Iceland

Introduction

A major rifting episode took place in central Iceland in 2014–2015, between the central volcanoes Bárdarbunga and Askja (Sigmundsson et al. 2015; Hjartardóttir et al. 2016). Such episodes are known at divergent plate boundaries (e.g. Wright et al. 2012) with the frequency being approximately one or two every century in Iceland (Thordarson and Larsen 2007). The 2014–2015 episode involved collapse of the Bárdarbunga caldera (Gudmundsson et al. 2016; Riel et al. 2015) and resulted in a flood basalt eruption of 1.4–1.5 km^3 of lava at the Holuhraun eruption site (Pedersen et al. 2017; Gudmundsson et al. 2016). This rifting episode took place predominantly beneath the northern part of the Vatnajökull glacier, where ice thickness is typically several hundred metres, and is the first subglacial rifting episode that has been monitored (Björnsson and Einarsson 1990; Sigmundsson et al. 2015). The aims of this paper are to describe the thermal effects of the dyke propagation under the glacier, and study the sources causing the thermal signals manifested by formation of three shallow depressions (ice cauldrons) in the ice surface above the sites of basal melting.

Regional setting

The Bárdarbunga central volcano belongs to the Bárdarbunga-Veidivötn system, which includes a fissure swarm, approximately 190 km in length, with segments extending into both the northern and eastern volcanic zones (Jóhannesson and Sæmundsson 1998). The system is one of the most active in

Published online: 05 May 2017

Iceland with over 20 known eruptions in the last 1200 years (Larsen et al. 1998; Óladóttir et al. 2011). Bárdarbunga itself is a subglacial central volcano, located beneath the Vatnajökull glacier, with a caldera approximately 65 km^2 in area and filled with 700–800 m thick ice (Björnsson and Einarsson 1990). Geochemical data indicates that the fissure eruption which produced the Holuhraun lava field in 1797 AD originated from the Bárdarbunga-Veidivötn system (Hartley and Thordarson 2013).

Ice cauldrons are shallow depressions, which form on the glacier surface due to basal melting, as a manifestation of heat flux from below (e.g. Björnsson 1976; Jarosch and Gudmundsson 2007). Several small geothermally generated ice cauldrons existed at the Bárdarbunga caldera rim prior to the 2014–2015 unrest (Fig. 1). Two short-lived cauldrons were observed at the south-eastern extent of the Bárdarbunga caldera following the Gjálp eruption of 1996 (Gudmundsson et al. 2004), which may have been formed by minor eruptive activity beneath the glacier (Kristmannsdóttir et al. 1999). Sustained geothermal activity is observed at several other locations beneath Vatnajökull, at Grímsvötn and Kverkfjöll volcanoes and the Skafta cauldrons, but not along the path of the 2014 dyke intrusion beneath Dyngjujökull outlet glacier.

Course of events in August–September 2014

Increased seismic activity was observed within the caldera of Bárdarbunga on 16 August 2014 (Fig. 1). During the following 2 weeks, seismic activity and ground deformation indicated the path of a lateral dyke for more than 45 km, initially propagating to the south east of Bárdarbunga, before changing course and continuing beyond the northern extent of the glacier (Sigmundsson et al. 2015; Hjartardóttir et al. 2016; Gudmundsson et al. 2016). A short fissure eruption occurred at the site of the pre-existing Holuhraun lavas on 29 August, lasting for approximately 5 h and producing less than 1 million m^3 of lava, before the onset of the main basaltic effusive eruption on 31 August. During the next 6 months, a lava field

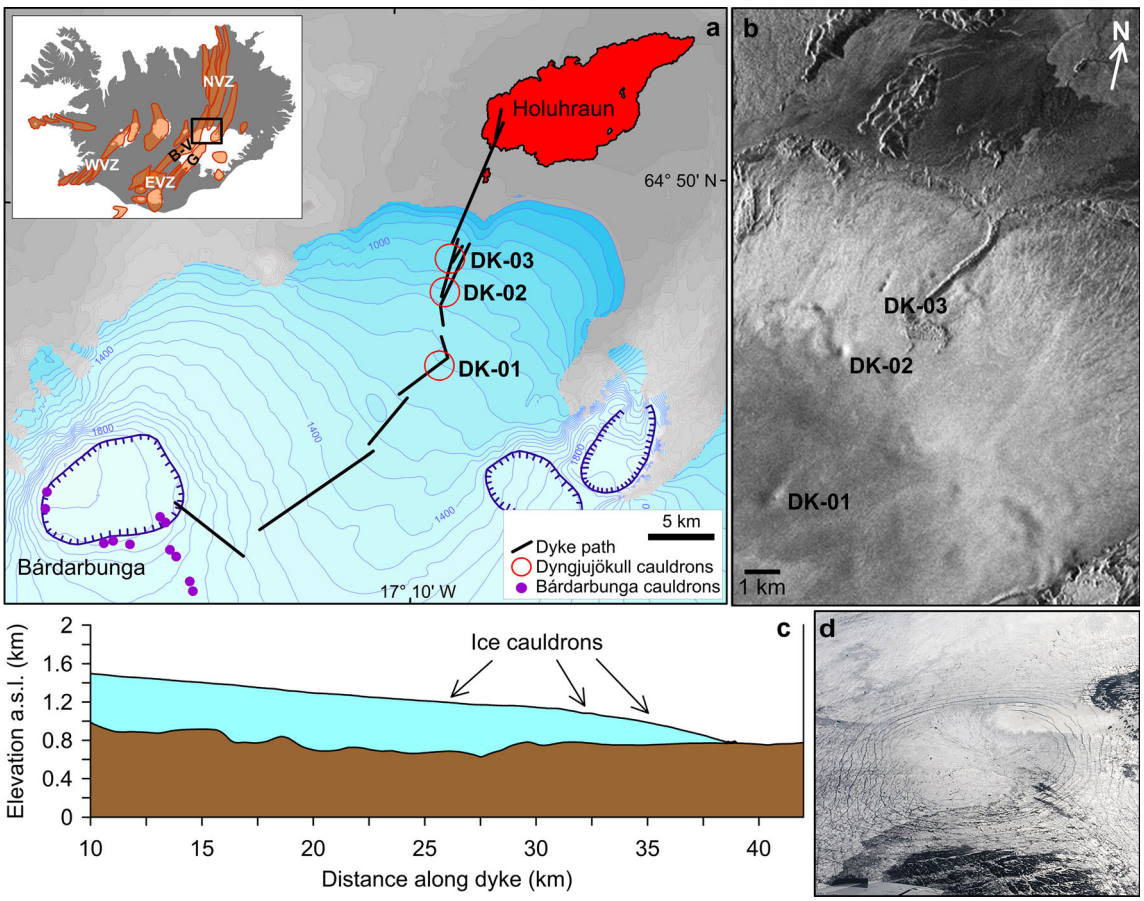

Fig. 1 Bárdarbunga-Holuhraun: **a** northwestern part of Vatnajökull, Iceland. The *segmented line* denotes the path of the lateral dyke after Sigmundsson et al. (2015). Ice cauldrons formed above the path of the dyke on Dyngjujökull (*red circles*) and at the caldera rim (*purple circles*). *Inset* shows location in central Iceland and the volcanic systems. **b** TerraSAR-X image of Dyngjujökull. **c** Cross section of the dyke path, showing the position of the cauldrons. Bedrock surface from Björnsson and Einarsson (1990). **d** Aerial photograph of DK-02, taken on 5 September 2014

of 1.4–1.5 km^3 was produced, before the eruption ended on 27 February 2015 (Gíslason et al. 2015; Gudmundsson et al. 2016, Pedersen et al. 2017). During the first several days at least, shallow conduit plumbing was not yet consolidated, as one further subaerial eruption began on 5 September 2014, approximately 2 km to the south of the main eruption (Fig. 1a), and lasted for about 2 days.

Ice subsidence was detected above Bárdarbunga, where a down-sag subsidence bowl extended beyond the margins of the pre-existing caldera. The caldera collapse was gradual, its formation coinciding with the eruption, eventually reaching a maximum depth of 65 m in February 2015, when the eruption ceased (Gudmundsson et al. 2016). No evidence of significant basal melting was found within the caldera. During the dyke propagation, a graben formed above the distal part of the lateral flow path of magma, with subsidence observed from about 13 km from the glacier edge beneath Dyngjujökull outlet glacier and extending towards Holuhraun (Sigmundsson et al. 2015; Hjartardóttir et al. 2016; Rossi et al. 2016).

Ice cauldrons formed above the path of the dyke on Dyngjujökull glacier and along a line extending towards southeast from the southeast corner of the Bárdarbunga caldera (Fig. 1), and the heat output of pre-existing minor subglacial geothermal areas at the caldera rim increased. The three ice cauldrons that formed at Dyngjujökull were located at 4, 7 and 12 km to the south of the glacier edge, where no signs of previous geothermal activity can be found in satellite photos or ice surface maps. We therefore assume that the ice cauldrons that emerged on Dyngjujökull at the end of August and beginning of September 2014 were caused by heat released from magma. Interestingly, no increased discharge or unusual hydrological or geochemical signals were detected in the autumn of 2014 in the river Jökulsá á Fjöllum that drains from Dyngjujökull (Galeczka et al. 2016).

This study aims to discern the most plausible heat transfer mechanism in the formation of the three ice cauldrons on Dyngjujökull, and the following possible scenarios are considered (Fig. 2): increased geothermal activity following the emplacement of a magmatic intrusion, a magmatic intrusion within a vertical fracture that extends from the surface and a minor subglacial eruption.

Methods

Ice surface monitoring

NW Vatnajökull was monitored aerially in August–September 2014, after the onset of heightened seismic activity. Changes in the glacier surface were first identified by visual inspection, and the evolution of these features was monitored by repeated airborne radar altimetry profiling, visual observations, aircraft-based synthetic aperture radar (SAR) and satellite images (Gudmundsson et al. 2016). Measurements were made using a C-band radar altimeter to record the aircraft elevation, and kinematic GPS to simultaneously record the precise position. Data collection was limited by weather conditions and the availability of the aircraft. The surface elevation measurements have an absolute accuracy of 3 m, with a relative consistency of 1–2 m (Gudmundsson et al. 2007). A LiDAR map of the Vatnajökull ice cap from 2011 (Jóhannesson et al. 2013) provided a good match to the ice surface prior to the onset of increased seismic activity on 16 August 2014, as although the ice surface elevation had changed by up to 18 m, the form of the surface was unchanged. The volumes of the ice cauldrons were estimated by interpolating radar profile data and comparing them with the 2011 LiDAR map, vertically corrected for the difference in ice surface elevation observed in the area outside the ice cauldrons.

Radio-echo sounding

On 4 June 2015, the Dyngjujökull ice cauldrons were surveyed with low frequency (1–5 MHz receiver bandwidth) radio-echo sounding (RES). Continuous profiles of RES measurements were obtained by placing a transmitter and a receiver on sledges, 47 m apart, at the centre of the antenna. This setup was towed by a snow-scooter, equipped with an L1-L2

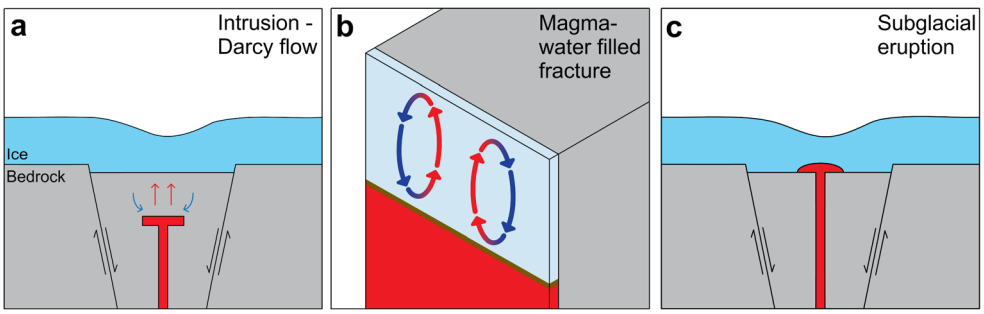

Fig. 2 Schematic cross-sectional diagrams of the three scenarios considered: **a** increased geothermal activity induced by a shallow intrusion; **b** heat transfer across a thin thermal boundary layer (*brown* layer in the diagram), separating magma and water at the bottom of a fluid-filled fracture; and **c** subglacial eruptions

GPS receiver. Radar backscatter images were obtained and migrated with 2-D Kirchhoff migration (e.g. Schneider 1978) to compensate for the width of the radar beam (200–300 m) in the along-track direction of the survey line. The propagation velocity of the radar wave in the ice was assumed to be 1.69×10^8 m s^{-1} (Björnsson et al. 2000). The 2-D migration applied accounts for the elevation changes at the surface, enhancing the imaging of the features beneath the radar in areas of high surface topography such as at ice cauldrons. The RES profiles are however too sparse to allow for 3-D migration which would also compensate for the width of the radar beam in the across direction of the survey. The 2-D migrated images give a satisfactory along-track image of features >100 m in diameter. However, uncertainty in dimensions of smaller scale features (diameter < 100 m) within the ice is high.

Modelling of heat sources

Darcy flow

Darcy's law can be employed to estimate the fluid velocity of the groundwater as it rises due to increased buoyancy, from a heated area around an intrusion towards the relatively cold bedrock-ice interface. Groundwater flow velocity is highly dependent on permeability (κ), which is not known for the bedrock beneath Dyngjujökull glacier, so a range of permeabilities have been considered. The Darcy velocity (q_w) gives the volumetric flow rate per unit area (Ingebritsen and Sanford 1999):

$$q_w = \frac{\kappa \rho_{w,0} g \alpha_w (T_1 - T_0)}{\mu_w} \quad (1)$$

Where $\rho_{w,0}$ is fluid (water) density, g is the gravitational acceleration, α_w the linear coefficient of thermal expansion for water, T_1 and T_0 are the water temperatures adjacent to the heat source (intrusion) and glacier base, respectively, and μ_w the dynamic viscosity of water. The fluid propagation velocity, v, is obtained by dividing the Darcy velocity with the formation porosity, n:

$$v = \frac{\kappa \rho_{w,0} g \alpha_w (T_1 - T_0)}{n\, \mu_w} \quad (2)$$

Equation (2) may be applied to estimate the minimum time for the buoyant rise of heated liquid groundwater to the surface.

Numerical modelling using Hydrotherm

Hydrotherm, a computer program developed by the United States Geological Survey to simulate groundwater flow and heat transfer (Hayba and Ingebritsen 1997), was used to simulate a two-phase groundwater system. Two coupled governing partial differential equations are solved: (1) the water-component flow equation, which combines the conservation of mass in both liquid and gas phases of groundwater with Darcy's law for fluid flow in porous media, and (2) the thermal-energy transport equations, derived from the conservation of enthalpy in the groundwater fluid (Kipp et al. 2008). A 2-D time-dependent numerical model was created to simulate the solidification and cooling of a dyke, into porous host rock saturated with pure water. Heat transfer through both conduction and convection is included; as the porous fluid heats up, a convection cell forms around the intrusion, transferring heat far more efficiently than by conduction alone. Hydrotherm takes full account of the temperature and pressure dependence of the thermodynamic properties of water.

Numerical modelling using COMSOL

COMSOL Multiphysics, a commercial finite element method modelling software, was used to simulate the solidification and cooling of subglacial lava. A phase change temperature of 1100 °C was used, with a transition interval between the phases of 100 °C to simulate gradual crystallisation. The upper boundary of a subglacial lava flow was considered to be in contact with the glacial ice and held at 0 °C so that all heat transferred through this boundary was spent on melting ice. A thermal conductivity of 2 W m^{-1} K^{-1} was used for lava.

The model is based on conductive heat flow and assumes that the thermal properties within the lava flow are homogeneous, although fracturing at the lava margins would increase the surface area available for heat transfer, leading to an underestimate in the simulated initial heat flux. We assume instant drainage of meltwater at the boundaries and no further heat transferred to the water once it has melted. We do not consider the possible accumulation of magmatic gas at the water-ice boundary above the edifice, which would act as insulator and decrease the heat transfer to the ice above the edifice. This should result in ice melting over a wider area (Höskuldsson and Sparks 1997) and may be a contributing factor in explaining the width of the cauldrons.

Conductive heat transfer through a boundary layer (the water-magma filled fracture)

As an end member case, we consider a vertical intrusion (dyke) filling the lower part of a fracture while the upper part is filled with water. In this scenario, the maximum heat flux at the surface is controlled by the heat flux through the upper margin of the cooling intrusion. Heat is conductively transferred through a thin thermal boundary layer of solidified magma separating the liquid magma underneath from permeable, newly formed, solidified and water-saturated intrusion within the fracture. Observations from lava lakes (Wright et al.

1976) and the solidification of lava from the Heimaey eruption in 1973 (Arnórsson et al. 2008) indicate a very thin conductive layer, of the order of metres. The temperature at the upper edge of the thermal boundary layer can be assumed to be the boiling point of water. In order to estimate the maximum heat flux in such a setting, we use a high temperature gradient estimate of $\frac{dT}{dz}$ = 1000 °C m^{-1} and assume a 1-m-thick boundary layer. Fourier's law of thermal conduction gives the heat flux (q) to be:

$$q = -k\frac{dT}{dz} \quad (3)$$

A value of k = 1.5 W m^{-1} °C^{-1} is used for the thermal conductivity for solid basalt at high temperatures (Robertson 1988; Clauser and Huenges 1995).

Calorimetry in subglacial eruptions

Melting at the glacier base is assumed to correspond exactly to the ice volume change on the surface, in cases where all meltwater drains instantaneously. The observed ice volume changes are used as a large-scale calorimeter (Gudmundsson et al. 2004; Jarosch et al. 2008). The thermal energy (Q) required to generate the ice cauldrons is estimated by considering the volume of ice melted (V_i), ice density ρ_i and the latent heat of fusion for ice (L_i). The ice is assumed to be temperate and therefore at the pressure melting point throughout. Although the melting point decreases slightly with pressure, this is roughly equivalent to assuming a uniform ice temperature of 0 °C.

$$Q = \rho_i V_i L_i \quad (4)$$

In the case of a subglacial eruption, the efficiency (f) of heat transfer from the magma to melt ice is defined by Gudmundsson et al. (2004) to be $f = \frac{\dot{E}_i}{\dot{E}_m}$, where $\dot{E}_i$ is the heat released from magma per unit time, and $\dot{E}_m$ is the total heat content of the magma erupted during the same time period. Considering full efficiency (f = 1), where no heat is lost to the bedrock below or to the meltwater, the volume of magma (V_m) required to generate the observed heat flux can be estimated directly from the volume of ice melted using the following equation:

$$V_m = \frac{\rho_i L_i V_i}{\rho_m (L_m + C_m \Delta T)} \quad (5)$$

with ρ_m, L_m and C_m being respectively the density, latent heat of fusion and the specific heat capacity of magma, and ΔT the temperature change of the cooling magma. Full efficiency may be approximately reached over long timescales compared to the time it takes to cool the volcanic products, although in most cases f is considerably less than 1 (Gudmundsson 2003; Tuffen 2007).

The size of the heating area beneath the glacier is not well constrained by ice surface data, although it must be considerably smaller than the width of the cauldrons at the surface. In the Gjálp eruption, the volcanic formation covered about 6 km^2, while the depressions in the ice surface, formed over weeks (Gudmundsson et al. 2004), were ~35 km^2 in area, or ~6 times larger than the contact area; this is ~17% of the area of the surface depression. In this study, we will assume a heating area 15% of the area of ice subsidence.

Results

The course of events and most significant aerial observations of the glacier surface are summarised in Table 1, from the onset of activity at Bárdarbunga to the cessation of the eruption at Holuhraun.

The cauldrons DK-01, DK-02 and DK-03 (Fig. 1) reached volumes of 18, 4 and 1 million m^3, respectively. Cauldron DK-01 was first detected on 5 September 2014 when its diameter was 1.2 km. It is located 12 km from the edge of the glacier, where the ice thickness is 500 m. By 24 October, the diameter had reached its maximum of 1.4 km. Cauldron DK-02 is located ~6.5 km to the south of the glacier edge, where the ice is 300 m thick. It was first observed on 27 August, but first measured on 5 September when it had an apparent diameter of 680 m. DK-02 grew to 780 m by 21 January 2015. The smallest cauldron, DK-03, was observed on 5 September, 4 km from the glacier edge where the ice was 250 m thick. Unlike the other two cauldrons, DK-03 is elongated along the strike of the dyke, with an along strike length of about 560 m and a width of 250–300 m. Increased seismic tremor signals were observed on four separate occasions, on the 23, 27 and 29 August and 3 September (Icelandic Meteorological Office 2014). These signals may have been associated with rapid melting and cauldron formation.

The majority of the melting, and therefore the highest heat flux, was observed at the beginning of cauldron formation; DK-01 and DK-02 were fully formed within 2 months, and DK-03 formed very rapidly, over a period of days (Figs. 3 and 5a). It is not clear when each of the cauldrons first appeared, as they were first observed by visual monitoring and were difficult to identify in their initial, shallow and mostly crevasse-free stages. The date of initial formation of the cauldrons was estimated by scrutinising photographs from previous observation flights and using the timing of the dyke progression to each cauldron location to constrain the earliest possible date for the formation of each cauldron (Fig. 4). The most likely date is then suggested based on tremor measurements recorded by the Icelandic Meteorological Office as tremor is often associated with volcanic eruptions or vigorous geothermal activity beneath glaciers (e.g. McNutt 1992;

Table 1 A summary of significant events during the period of unrest at Bárdarbunga

Date	Event description	Data type	Reference
16 August 2014	Onset of activity at Bárdarbunga	Seismicity	(1)
19 August	Dyke propagation halts 26 km from caldera rim	Seismicity	(1)
23 August	Dyke propagation recommences	Seismicity	(1)
23 August	Tremor detected	Seismicity	(2)
27 August	Ice cauldrons observed 1–5 km SE of Bárdarbunga	Aircraft	
27 August	Ice cauldron (DK-02) observed on Dyngjujökull, above dyke path	Aircraft	
27 August	New fractures delineating graben formation north of the Vatnajökull glacier	Aircraft	(3)
27 August	Tremor detected	Seismicity	(2)
29 August	Small eruption at Holuhraun, 6 km north of Vatnajökull, lasting approximately 4 h	Ground, webcam, aircraft	(1)
29 August	Tremor detected	Seismicity	(2)
31 August	Start of large eruption at Holuhraun at the same place as on 29 August	Ground and webcam	(1)
3 September	Tremor detected	Seismicity	(2)
5 September	Small eruption begins approximately 3 km north of Vatnajökull glacier	Aircraft	
5 September	Ice cauldrons observed (DK-01 and DK-03) on Dyngjujökull, above the dyke path. Likely formation date of DK-01 significantly earlier	Aircraft	
7 September	Small eruption stopped	Aircraft	
27 February 2015	Main eruption ceases	Aircraft and ground	(4)

References: (1) Sigmundsson et al. (2015), (2) Iceland Meteorological Office (2014), (3) Hjartardóttir et al. (2016), (4) Gíslason et al. (2015)

Vogfjörd et al. 2013; Montanaro et al. 2016). DK-01 is estimated to start forming on 23 August, DK-02 on 27 August and DK-03 on 3 September (Figs. 4 and 5a). Due to uncertainty over the dates when melting commenced and the time between measurements, it is not clear how high the heat flux was initially. An average power for each measurement

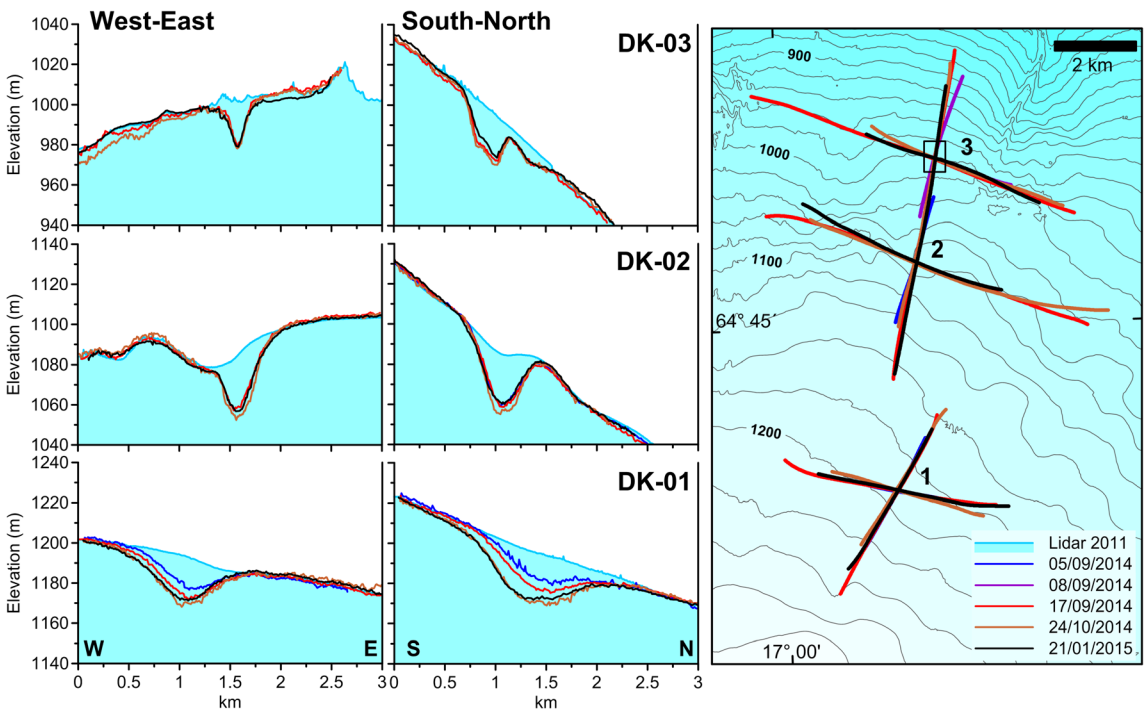

Fig. 3 Profiles of the evolution of the Dyngjujökull ice cauldrons measured using airborne altimetry profiling. Profiles DK-01, DK-02 and DK-03 are labelled. The map shows the profiles measured on each date, indicated by colour. The *box* shows the map location in Fig. 6

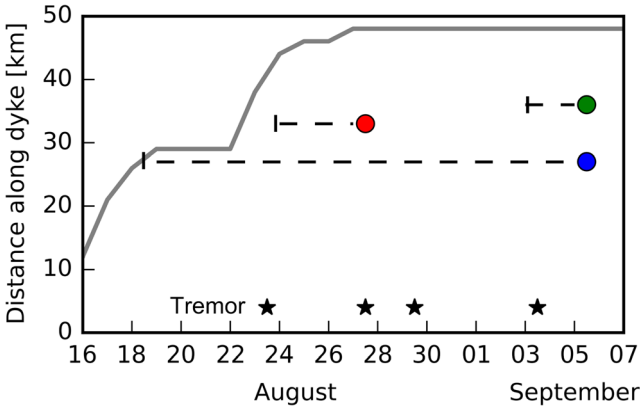

Fig. 4 *Coloured dots* show the dates when the cauldrons were first observed: *blue* for DK-01, *red* for DK-02 and *green* for DK-03. The *dashed lines* cover the period during which the cauldrons could have been active before being observed, based on previous visual inspections and the timing of the dyke reaching the cauldron locations (*grey line*). *Stars* denote days when increased tremor signals were measured (Iceland Meteorological Office 2014)

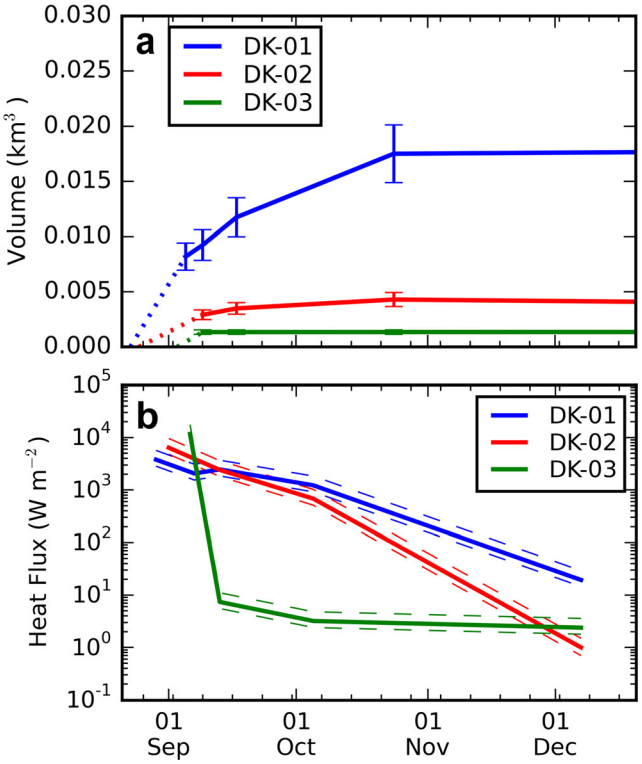

Fig. 5 **a** Volumes of the cauldrons with time—the *dotted line* connects the estimated start date of the cauldron development until the date it was first observed. The minor ticks on the horizontal axis represent weeks. **b** The average heat fluxes for each measurement period, calculated as the heat required to melt the observed change in ice volume for each time period. This gives an average heat flux, which is plotted in the middle of each time period. *Solid lines* represent the flux if the heating area is assumed to be 15% that of the cauldron, *dashed lines* show the flux if a heating area of 10 or 20% is considered. All dates are from 2014

period has been calculated. From the trend of decreasing power for these cauldrons, it can be deduced that the initial heat flux was higher than this average value (Fig. 5).

Radio-echo surveys were conducted at the ice cauldrons on Dyngjujökull, on 4 June 2015 (Fig. 6). The survey results for DK-1 and DK-02 show possible anomalous signals approximately 10 m above the level of the bedrock, although they are on the limit of what is detectable using this technique and are therefore inconclusive. DK-03 showed a clearer signal, of an anomaly 300–400 m in length and up to 60 m high. The fact that it blocks reflections from the bed below suggests that width is likely of the order of tens of metres. The exact form and extent is, however, not well constrained as the data is not dense enough to allow 3-D migration.

Constraints from thermal modelling

The exact nature of the heat source required to generate the Dyngjujökull cauldrons is not obvious and three scenarios are explored (Fig. 2): (a) increased geothermal activity following the emplacement of a magmatic intrusion, where groundwater convection sets in and heat is transferred through fluid flow; (b) a magmatic intrusion meets the end of a vertical fracture which extends from the surface; and (c) a subglacial eruption occurs, resulting in direct contact between magma and the glacial ice.

Increased geothermal activity

All three cauldrons observed on Dyngjujökull are located above the dyke, which is expected to heat the surrounding bedrock and groundwater. As the groundwater is heated, convection cells develop which carry heat towards the surface. Darcy's law is used to estimate the fluid velocity of the groundwater as it rises due to increased buoyancy (Eq. 1). The ice-bedrock interface is considered to have a temperature $T_{surface}$ of 0 °C, the freezing point of water, and the density $\rho_{w,0}$ of water at 0 °C is used. $T_{boiling}$ is set at the boiling point of water at the depth of the intrusion, as this is the highest temperature the groundwater can reach without becoming superheated.

The fluid propagation velocity (Eq. 2) can be used to estimate the minimum travel time for the heated groundwater to reach the surface, producing an elevated heat flux (Fig. 7). A shallow intrusion into bedrock with permeability of the order 10^{-11} m^2 could produce a signal within the time frame of 1 month. However, thermal signals were observed at Dyngjujökull within days of the dyke emplacement, and the permeabilities required to generate a signal on this timescale are for heavily fractured rock. Although there may be a highly fractured damage zone around the intrusion, this is unlikely to extend far enough to significantly influence the time it would take heated groundwater to flow to the surface. Therefore, onset of geothermal activity at the glacier base due to the

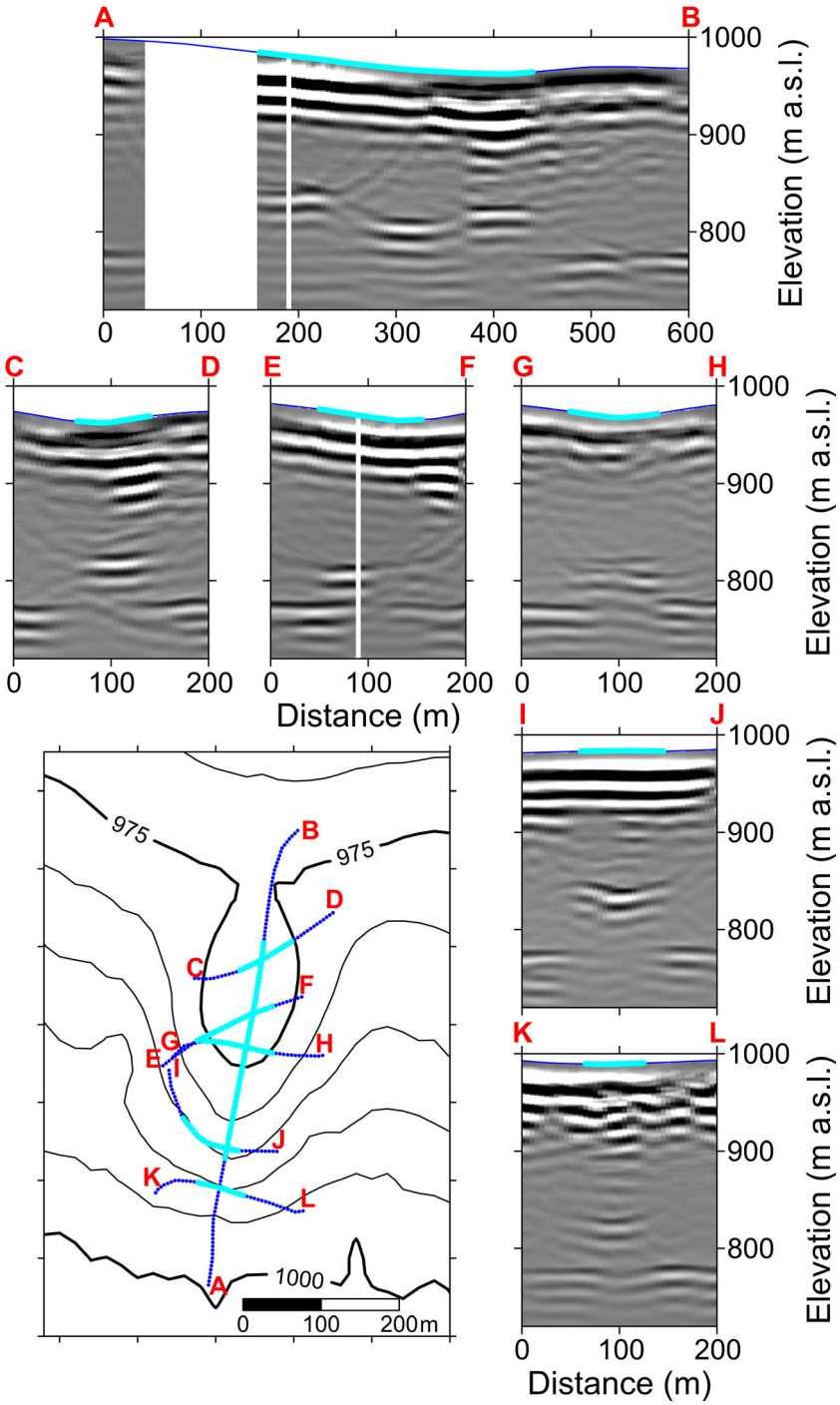

Fig. 6 Radio-echo sounding over cauldron DK-03. The map shows the survey profiles, each of which are displayed with letter corresponding to their location. For map location, see Fig. 3. The *lighter blue sections* highlight the anomaly observed 30–60 m above the typical ice-bedrock boundary at ~780 m a.s.l.

emplacement of the dyke is not considered as an explanation for the heat source which generated the ice cauldrons.

The analytical model described above considers only single-phase convection, in this case liquid water. Although the dyke entered a 'cold' area beneath Dyngjujökull, the magma may heat some of the surrounding groundwater to steam. Thus, a two-phase system must also be considered, and a model was developed in Hydrotherm for this purpose. The Hydrotherm simulations do not produce timescales consistent with observations on Dyngjujökull which show a thermal signal just days into the event. The Hydrotherm results suggest that for permeabilities $<10^{-13}$ m^2, a two-phase system could transport heat to the surface within a timeframe of more than one order of magnitude lower than that of times calculated using the analytical model. However, for higher permeabilities, this difference largely disappears, indicating that at heat transfer becomes liquid dominated and effectively single-phase as water flow becomes faster and more efficient.

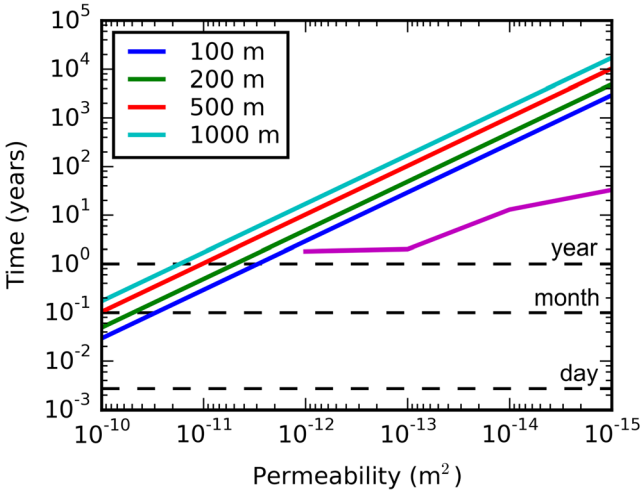

Fig. 7 Minimum time for fluid to reach the surface for different intrusion depths and bedrock permeabilities (Fig. 2a), using porosity of 0.2 in Eq. 2. The *pink line* shows results for a Hydrotherm model with an intrusion at 200 m depth. The *dashed lines* show 1 day, month and year on the logarithmic time axis. Thermal signals at Dyngjujökull were observed within days

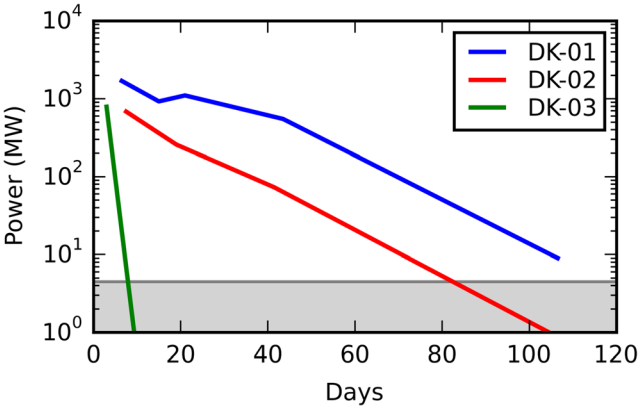

Fig. 8 The power output required to melt enough ice to produce the observed ice cauldrons. The *grey-shaded area* represents the maximum power output from a fluid-magma-filled fissure (Fig. 2b), for a fracture with aperture up to 3 m and length up to 1 km

We consider the bedrock to be fully saturated with water up to the bedrock-ice boundary, although following the intrusion of magma beneath Dyngjujökull, an increase in overall porosity due to the dilation of the crust may result in a decrease in the water table beneath the glacier. However, this change would result in a maximum drop in the groundwater level of several metres, which would not have a significant effect on the transport time of heat via convection. Heat may also be transported through cracks, formed during the intrusion of magma and graben subsidence, and an end member case of this will be discussed in the next section.

Heat transfer through partly magma-filled open fissures

Another mechanism of heat transfer from a magmatic intrusion to the surface is through convection in fluid-filled cracks in the bedrock. The heat flux is calculated using Eq. 3 and can be converted to a total power by multiplying the thermal heat flux by the exposed area of the fracture at the surface; here we consider fracture apertures up to 3 m and length 1 km being the upper limit imposed by the dimension of the cauldrons and the assumed width of the dyke (Sigmundsson et al. 2015).

Figure 8 shows that even the maximum possible heat flux through this scenario produces power values orders of magnitude lower than the conservative estimates of initial heat flux derived from the observed cauldron formation. From these calculations, it is found that convection of fluid within fractures cannot provide the heat flux required. Thus, we consider this mechanism implausible as the heat source for the observed signal.

Subglacial eruptions

The magma volumes required to melt enough ice to form the three cauldrons on Dyngjujökull are listed in Table 2. These volumes (~0.1 to 1.8 million m^3) are similar in magnitude to the erupted volumes observed for two subaerial eruptions during this event: the initial eruption at the Holuhraun site on 29 August 2014 which produced ~0.6 million m^3 and an isolated fissure which erupted for approximately 2 days on 5 September 2014, producing ~2 million m^3 of lava.

Discussion

In the "Constraints from thermal modelling" section, we conclude that neither increased geothermal activity, nor heat transfer through cracks, can explain the observed heat flux, whereas the subglacial eruption scenario does produce the observed thermal signal. We therefore conclude that small subglacial eruptions led to the formation of all three ice cauldrons observed on Dyngjujökull. Eibl et al. (2017) found shallowing seismicity beneath cauldrons DK-01 and DK-02 before 27 August 2014, suggesting the movement of magma towards the surface and providing further evidence of subglacial eruptions. They also find that a source or tremor beneath DK-02 shallows and changes in character on 3 September, consistent with what would be expected from magma reaching the bedrock surface, raising the possibility of reactivation of this vent on this date. Ground deformation is not considered as a mechanism for the formation of the ice cauldrons, as no local bedrock subsidence was observed in the radio-echo sound profiles beneath the cauldrons.

Table 2 The volume of each ice cauldron on Dyngjujökull, with heat energy required to generate the cauldron, and the corresponding volume of magma

Cauldron	Ice thickness (m)	Max. cauldron depth (m)	Max. cauldron diameter (m)	V_{ice} (10^6 m^3)	E_{heat} (J)	V_{magma} (10^6 m^3)
DK-01	510	25	1400	18	5.4×10^{15}	1.8
DK-02	320	31	780	4	1.2×10^{15}	0.4
DK-03	250	24	560	1	0.4×10^{15}	0.1

Effusive or explosive eruptions

Subglacial eruptions may be explosive or effusive, and it is not obvious which style was dominant in the small Dyngjujökull eruptions. Confining pressure is a critical factor in eruption style and is principally controlled by the lithostatic load generated by the ice thickness. Several estimates have been published for the pressure threshold, above which only effusive activity will occur, from 3 to 5 MPa which corresponds to ~320–550 m of ice (Wilson and Head 2002; Gudmundsson et al. 2004; Tuffen 2007). The Dyngjujökull eruptions took place beneath the following approximate initial ice thicknesses and corresponding maximum pressures (P_{max}): 510 m, 4.5 MPa (DK-01); 320 m, 3.0 MPa (DK-02); and 250 m, 2.2 MPa (DK-03).

Subglacial explosive eruptions

During explosive subglacial eruptions, it is likely that 70–80% of the heat content of the magma is released before burial of the erupted particles, suggesting that roughly this percentage of magmatic heat is transferred to the surrounding during the eruption (Gudmundsson 2003; Woodcock et al. 2012). The eruptions at Gjálp in 1996 and Eyjafjallajökull in 2010 produced approximately 1 and 4 MW m^{-2}, respectively, during their initial subglacial phases (Jarosch et al. 2008; Magnusson et al. 2012), producing fluxes approximately two orders of magnitude greater than those estimated for the Dyngjujökull eruptions (Fig. 9). Based on the continued melting over the month following the formation of DK-01 and DK-02, it is unlikely that they were formed by explosive subglacial eruptions. Moreover, the absence of floods may be regarded an argument against a significant explosive component in these events.

Subglacial lava flow

Subglacial lava flows transfer heat both to the ice above the lava flow and the bedrock at the base. Assuming that meltwater drains continuously, the upper margin of the lava flow will be in contact with ice at its melting point of 0 °C. Experiments where ice and molten lava come into direct contact show that

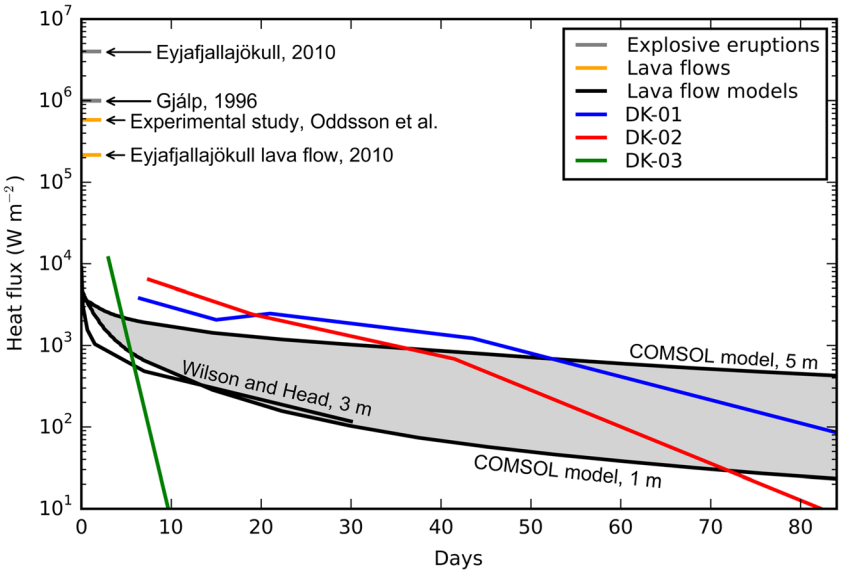

Fig. 9 Comparison of observed heat flux for each Dyngjujökull cauldron (assuming a heating area of 15% of the cauldron area), with empirical data for the initial subglacial phase of the Eyjafjallajökull 2010 and Gjálp 1996 explosive eruptions (Magnusson et al. 2012; Jarosch et al. 2008), and for the Eyjafjallajökull 2010 lava flow (Oddsson et al. 2016b). Modelling results are also displayed: experimental study data from Oddsson et al. (2016a), and numerical models of subglacial lava flow cooling from Wilson and Head (2007) and using COMSOL Multiphysics. The *shaded area* shows the heat flux expected for lava flows between 1 and 5 m thick (using COMSOL); the Wilson and Head model is for a 3-m-thick lava flow

the heat flux was highest in the first 10 s, reaching 400–770 kW m^{-2}, but dropped by an order of magnitude within several minutes (Oddsson et al. 2016a). These values are similar to those observed at lava flows during the Eyjafjallajökull 2010 eruption, of 125–310 kW m^{-2} (Oddsson et al. 2016b). The data from Dyngjujökull, however, do not capture the initial highest heat fluxes, so it is not clear if these subglacial eruptions reach heat fluxes similar to these values.

The results of the COMSOL Multiphysics lava cooling model, and a model from Wilson and Head (2007), are used to compare longer-term subglacial lava flow cooling to the thermal data from Dyngjujökull. These results provide a good fit to the observations for DK-01 and DK-02 (Fig. 9).

Intrusion into ice

Wilson and Head (2002) proposed that a basaltic dyke which reaches the base of a glacier could penetrate through 20–30% of the ice thickness, before stalling to form a dyke-like intrusion within the ice. However, as far as we are aware, no such event has been confirmed although an ice intrusion is suspected to have occurred during the beginning of the Gjálp eruption in 1996 (Gudmundsson et al. 2004). Radio-echo sounding revealed a deposit with dyke-like geometry beneath DK-03, with a length of 300–400 m and a height of approximately 60 m where the glacier is around 250 m thick. This indicates dyke penetration through about 25% of the ice, in keeping with Wilson and Head's model. Three intrusion geometries are presented in Fig. 10. Scenario c, showing a dyke penetrating upwards into the ice before spreading horizontally, is the most likely, as it would explain the reflection observed. The increased surface area achieved in this scenario also better explains the rapid heat output observed at DK-03. The rapid cooling is much faster than expected from conduction of a single coherent body. However, this would not cool as a cohesive block; rather, cooling cracks and fractures would develop, with the breakup of the intrusion further aided by deformation and collapse due to ice melting. This process would continually expose fresh magma and cause the temperature gradient to propagate through the deposit at a much accelerated rate, creating the fast cooling observed. It is also possible that some explosive activity took place, as the lithostatic pressure decreased while the dyke propagated through the ice.

Meltwater

No jökulhlaup (glacial flood) was observed in connection to the Holuhraun 2014–2015 event, or any significant chemical signal in the local river water to indicate magma-water interaction prior to the main eruption at Holuhraun (Galeczka et al. 2016). Nevertheless, formation of the Dyngjujökull cauldrons resulted in the melting of about 23 million m^3 of ice.

The meltwater from the subglacial eruptions may have been stored as groundwater, rather than draining into rivers. This additional groundwater could have been accommodated by increased storage capacity of the bedrock due to movement along faults during dyke propagation and graben reactivation. The established graben subsided a further 4 m during the unrest period, extending at least 12 km beneath the glacier to DK-01, the southernmost cauldron on Dyngjujökull (Rossi et al. 2016). Although an exact value of the increase in the bedrock storage capacity is unknown, an estimation can be made based on measurements of the dilation of the crust north of Vatnajökull, of approximately 2.5 m and the fractures reaching a minimum depth of ~1.2–1.8 km (Hjartardóttir et al. 2016). Using a conservative estimate of 1 km for the depth of fractures, this calculation gives an estimate of 30 million m^3 increased water storage capacity, which would accommodate the 23 million m^3 volume of meltwater from the small subglacial eruptions.

Conclusions

- Three ice cauldrons, ranging from 1 to 18 million m^3 in volume, formed on Dyngjujökull glacier at the end of August and beginning of September 2014, associated with the slow collapse of Bárdarbunga caldera and the Holuhraun fissure eruption. The southernmost cauldron is located about 20 km to the SSW of the main eruption site.

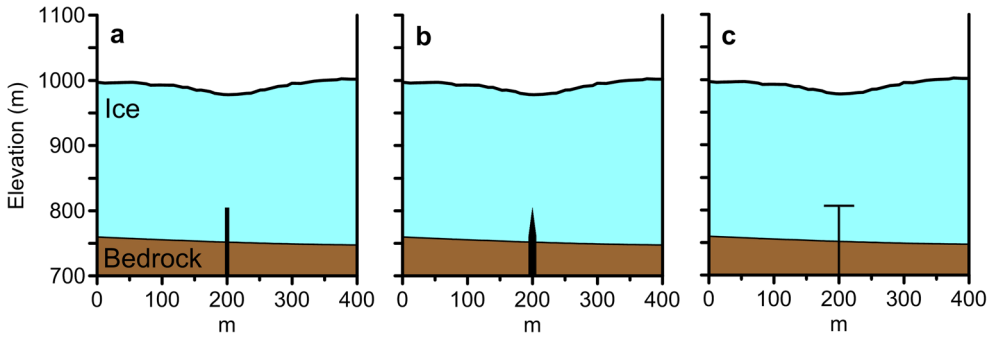

Fig. 10 Scaled diagrams of possible intrusion geometries beneath DK-03: **a** dyke of uniform 6 m width, **b** dyke which tapers from 12 m width to a point, **c** dyke of uniform 3 m width which spreads into a sill-like body

- Neither convection of groundwater within the bedrock, nor heating of fluid-filled cracks within the bedrock or ice, could have produced enough heat to generate the observed ice cauldrons.
- The Dyngjujökull cauldrons were generated as a result of small, most likely effusive subglacial eruptions during the Holuhraun 2014–2015 event.
- Radio-echo soundings of the northernmost cauldron (DK-03) reveal that it was likely to have formed when a dyke intruded into the base of the glacier, penetrating approximately 50 m.

Acknowledgements We acknowledge the support of the EU Seventh Framework Marie Curie project NEMOH no. 289976, the Research Fund of the University of Iceland and Landsvirkjun power company. Fieldwork was supported with crisis response funding from the Icelandic government through the Civil Protection Department of the National Commissioner of the Iceland Police, and through the European Community's Seventh Framework Programme grant no. 308377 (Project FUTUREVOLC). We thank The Icelandic Coast Guard who provided assistance in monitoring from their TF-SIF aircraft and ISAVIA (Icelandic Aviation Operation Services) and their crew on board the TF-FMS which was used for altimeter-DGPS profiling. The Iceland Glaciological Society assisted with fieldwork logistics in June 2015.

References

Arnórsson S, Axelsson G, Sæmundsson K (2008) Geothermal systems in Iceland. Jökull 58:269–302

Björnsson H (1976) Subglacial water reservoirs, jökulhlaups and volcanic eruptions. Jökull 25:1–15

Björnsson H, Einarsson P (1990) Volcanoes beneath Vatnajökull, Iceland: evidence from radio-echo sounding, earthquakes and jökulhlaups. Jökull 40:147–148

Björnsson H, Pálsson F, Guðmundsson MT (2000) Surface and bedrock topography of the Mýrdalsjökull ice cap, Iceland: the Katla caldera, eruption sites and routes of jökulhlaups. Jökull 49:29–46

Clauser C, Huenges E (1995) Thermal conductivity of rocks and minerals. Rock physics & phase relations: a handbook of physical constants, 105–126

Eibl EPS, Bean CJ, Vogfjörd KS, Ying Y, Lokmer I, Möllhoff M, O'Brien GS, Pálsson F (2017) Tremor-rich shallow dyke formation followed by silent magma flow at Bárðarbunga in Iceland. Nat Geosci. doi:10.1038/ngeo2906

Galeczka I, Sigurdsson G, Eiriksdottir ES, Oelkers EH, Gislason SR (2016) The chemical composition of rivers and snow affected by the 2014/2015 Bárðarbunga eruption, Iceland. J Volcanol Geotherm Res 316:101–119

Gíslason SR, Eiríksdóttir ES, Galeczka I et al (2015) Environmental pressure from the 2014–15 eruption of Bárðarbunga volcano, Iceland. Geochemical Perspectives Letters 1:84–93

Gudmundsson MT (2003) Melting of ice by magma-ice-water interactions during subglacial eruptions as an indicator of heat transfer in subaqueous eruptions. In: White JDL, Smellie JL Clague D (eds) Geophysical monograph 140, Explosive subaqueous volcanism, AGU, 61–72

Gudmundsson MT, Sigmundsson F, Björnsson H, Högnadóttir T (2004) The 1996 eruption at Gjálp, Vatnajökull ice cap, Iceland: efficiency of heat transfer, ice deformation and subglacial water pressure. Bulletin Volcanol 66(1):46–65

Gudmundsson MT, Högnadóttir T, Kristinsson AB, Gudbjörnsson S (2007) Geothermal activity in the subglacial Katla caldera, Iceland, 1999–2005, studied with radar altimetry. Ann Glaciol 45:66–72

Gudmundsson MT, Jónsdóttir K, Hooper A et al (2016) Gradual caldera collapse at Bárdarbunga volcano, Iceland, regulated by lateral magma outflow. Science 353:aaf8988. doi:10.1126/science.aaf8988

Hartley ME, Thordarson T (2013) The 1874–1876 volcano-tectonic episode at Askja, North Iceland: lateral flow revisited. Geochem Geophys Geosyst 14(7):2286–2309

Hayba DO, Ingebritsen SE (1997) Multiphase groundwater flow near cooling plutons. J Geophys Res 102(B6):12,235–12,252

Hjartardóttir Á, Einarsson P, Gudmundsson MT, Högnadóttir T (2016) Fracture movements and graben subsidence during the 2014 Bárðarbunga dike intrusion in Iceland. J Volcanol Geotherm Res 310:242–252

Höskuldsson Á, Sparks RSJ (1997) Thermodynamics and fluid dynamics of effusive subglacial eruptions. Bull Volcanol 59:219–230

Icelandic Meteorological Office (2014) Bárðarbunga and Holuhraun—overview. Accessed 13 July 2016. http://en.vedur.is/earthquakes-and-volcanism/volcanic-eruptions/holuhraun/

Ingebritsen SE, Sanford WE (1999) Groundwater in geologic processes. Cambridge University Press, Cambridge

Jarosch AH, Gudmundsson MT (2007) Numerical studies of ice flow over subglacial geothermal heat sources at Grímsvötn, Iceland, using full Stokes equations. J Geophys Res 112:F02008

Jarosch AH, Gudmundsson MT, Högnadóttir T, Axelsson G (2008) Progressive cooling of the hyaloclastite ridge at Gjálp, Iceland, 1996–2005. J Volcanol Geotherm Res 170:218–229

Jóhannesson H, Saemundsson K (1998) Geological map of Iceland. Bedrock geology, scale 1:500.000. Icelandic Institute of Natural History, Reykjavík (2nd edition)

Jóhannesson T, Björnsson H, Magnússon E, Guðmundsson S, Pálsson F, Sigurðsson O, Thorsteinsson T, Berthier E (2013) Ice-volume changes, bias estimation of mass-balance measurements and changes in subglacial lakes derived by lidar mapping of the surface of Icelandic glaciers. Ann Glaciol 54(63):63–74

Kipp KL, Hsieh PA, Charlton SR (2008) Guide to the revised groundwater flow and heat transport simulator: HYDROTHERM — Version 3: U.S. Geological Survey Techniques and Methods 6 −A25, p.160

Kristmannsdóttir H, Björnsson A, Pálsson S, Sveinbjörnsdóttir ÁE (1999) The impact of the 1996 subglacial volcanic eruption in Vatnajökull on the river Jökulsá Á Fjöllum, North Iceland. J Volcanol Geotherm Res 92(3–4):359–372

Larsen G, Gudmundsson MT, Björnsson H (1998) Eight centuries of periodic volcanism at the center of the Iceland hotspot revealed by glacier tephrostratigraphy. Geology 26:943–946

Magnusson E, Gudmundsson MT, Roberts MJ, Sigurdsson G, Höskuldsson F, Oddsson B (2012) Ice-volcano interactions during the 2010 Eyjafjallajökull eruption, as revealed by airborne imaging radar. J Geophy Res 117:B07405

McNutt SR (1992) Volcanic tremor. Encyclopedia of earth system science 4:417–425

Montanaro C, Scheu B, Gudmundsson MT et al (2016) Multidisciplinary constraints of hydrothermal explosions based on the 2013 Gengissig lake events, Kverkfjöll volcano, Iceland. Earth Planet Sci Lett 434: 308–319

Oddsson B, Gudmundsson MT, Sonder I, Zimanowski B, Schmid A (2016a) Experimental studies of heat transfer at the dynamic magma ice/water interface: application to subglacially emplaced lava. J Geophys Res Solid Earth. doi:10.1002/2016JB012865

Oddsson B, Gudmundsson MT, Edwards BR, Thordarson T, Magnússon E, Sigurðsson G (2016b) Subglacial lava propagation, ice melting and heat transfer during emplacement of an intermediate lava flow in the 2010 Eyjafjallajökull eruption. Bull Volcanol 78(7):1–17

Óladóttir BA, Larsen G, Sigmarsson O (2011) Holocene volcanic activity at Grímsvötn, Bárdarbunga and Kverkfjöll subglacial centres beneath Vatnajökull, Iceland. Bull Volc 73(9):1187–1208

Pedersen GBM, Höskuldsson A, Dürig T, Thordarson T, Jónsdóttir I, Riishuus MS, Óskarsson BV, Dumont S, Magnusson E, Gudmundsson MT, Sigmundsson F, Drouin VJPB, Gallagher C, Askew R, Guðnason J, Moreland WM, Nikkola P, Reynolds HI, Schmith J (2017) Lava field evolution and emplacement dynamics of the 2014–2015 basaltic fissure eruption at Holuhraun, Iceland. J Volcanol Geotherm Res. doi:10.1016/j.jvolgeores.2017.02.027

Riel B, Milillo P, Simons M et al (2015) The collapse of Bárðarbunga caldera, Iceland. Geophys J Int 202:446–453

Robertson EC (1988) Thermal properties of rocks. USGS Open-File Report 88-441, p. 106

Rossi C, Minet C, Fritz T, Eineder M, Bamler R (2016) Temporal monitoring of subglacial volcanoes with TanDEM-X—application to the 2014–2015 eruption within the Bárðarbunga volcanic system, Iceland. Remote Sens Environ 181:186–197

Schneider WA (1978) Integral formulation for migration in two and three dimensions. Geophysics 43:49–76

Sigmundsson F, Hooper A, Hreinsdóttir S et al (2015) Segmented lateral dyke growth in a rifting event at Bárðarbunga volcanic system, Iceland. Nature 517:191–195

Thordarson T, Larsen G (2007) Volcanism in Iceland in historical time: volcano types, eruption styles and eruption history. J Geodyn 43:118–152

Tuffen H (2007) Models of ice melting and edifice growth at the onset of subglacial basaltic eruptions. J Geophys Res 112:B03203

Vogfjörd K, Bean C, Roberts M, Ofeigsson B, Guralp Systems Ltd. (2013) Extending Icelandic volcanological network operations into the ice caps. In: EGU General Assembly Conference Abstracts, Vienna, vol. 15, p13319

Wilson L, Head JW (2002) Heat transfer and melting in subglacial basaltic volcanic eruptions: implications for volcanic deposit morphology and meltwater volumes. In: Smellie, JL, Chapman MG (eds) Volcano-ice interaction on Earth and Mars. Geol Soc London, Special Publications, vol. 202, pp. 5–26

Wilson L, Head JW (2007) Heat transfer in volcano–ice interactions on earth. Ann Glaciol 45(1):83–86

Woodcock DC, Gilbert JS, Lane SJ (2012) Particle-water heat transfer during explosive volcanic eruptions. J Geophys Res 117:B10205

Wright TL, Peck DL, Shaw HR (1976) Kiluea lava lakes: natural laboratories of study of cooling, crystallization and differentiation of basaltic magma. In: Sutton GH, Manghnani MH, Moberly R (eds) The geophysics of Pacific Ocean basin and its margin. American Geophysical Union, Washington DC, pp 375–390

Wright TJ, Sigmundsson F, Pagli C et al (2012) Geophysical constraints on the dynamics of spreading centres from rifting episodes on land. Nat Geosci 5:242–250

Paper III

Heat flux at Bárdarbunga, Iceland, following the 2014-15 caldera collapse, investigated using geothermal system modelling

Hannah Iona Reynolds, Magnús Tumi Gudmundsson, Thórdís Högnadóttir, Gudni Axelsson
Manuscript in preparation for Journal of Geophysical Research

Changes in geothermal activity at Bárdarbunga, Iceland, following the 2014–15 caldera collapse, investigated using geothermal system modelling

Hannah I. Reynolds[*1], Magnús T. Gudmundsson[1], Thórdís Högnadóttir[1], Gudni Axelsson[2]

1: Nordvulk, Institute of Earth Sciences, University of Iceland, Sturlugata 7, Reykjavík 101, Iceland.

2: Iceland GeoSurvey, Grensásvegur 5, 108 Reykjavík, Iceland.

*corresponding author: hir10@hi.is

Keywords: Volcano-ice interaction, Ice cauldrons, Heat flux, Bárdarbunga, Numerical modelling

Abstract

The gradual collapse of the subglacial Bárdarbunga caldera in 2014–2015, provided an opportunity to explore the geothermal signals produced by such large-scale subsidence. During the start of the activity in August 2014, four ice cauldrons (shallow depressions on the ice surface) formed on the south-eastern flank of Bárdarbunga caldera. These cauldrons reached their maximum size very quickly and then declined, indicating that they were created during minor subglacial eruptions. A few weeks after the start of the collapse, rapid growth occurred in three cauldrons on the caldera rims, with four smaller cauldrons forming in 2015–2017. The shortest-lived cauldron on the caldera rim was active for 7 months, and several continue to increase in volume after 3 years. The cauldrons have reached volumes in the range of 1.0±0.2 to 17±2 million m^3. HYDROTHERM numerical simulations of fluid flow and heat transport in the uppermost 1 km of the crust were performed to assess the role of shallow magmatic intrusions, for a range of likely permeability values and initial bedrock and groundwater temperatures. The heat transfer required to create the more rapidly formed non-eruption cauldrons, at or near the caldera rims, can be reproduced with shallow intrusions and high permeability pathways, which were found to greatly enhance the surface thermal signal. The delay in onset time for some of the cauldrons suggests, however, that such pathways are not always present. The pre-intrusion temperature of the surrounding bedrock has a major effect on heat transfer to the surface, with cold bedrock causing a buffering effect, whereas temperature conditions close to the boiling point of water produce far more efficient heat transfer due to the formation of steam plumes. Not all behavior observed is reproduced our models, suggesting that changes to geothermal reservoirs below 1 km depth may play a significant role in the observed thermal anomalies.

1. Introduction

Many calderas host geothermal areas (Newhall and Dzurisin, 1988) and changes in geothermal activity at volcanoes are linked with intrusive and volcanic activity (e.g. Ingebritsen et al. 2001; Bleick et al. 2013). Caldera collapses are relatively rare but large increases in geothermal activity have been associated with collapses, both through phreatic and hydrothermal activity (Nakada et al., 2005). However, only limited records exist of such signals, i.e. the quantification of thermal output, timing of the onset of geothermal activity, and how increased activity relates to faulting and subsidence. The 2014–15 gradual collapse of the Bárdarbunga caldera offered a rare opportunity to study these processes (Gudmundsson et al. 2016; Sigmundsson et al. 2015). Importantly, the full ice cover of the Bárdarbunga caldera ensures that thermal signals can be quantified through ice calorimetry.

Increased seismicity was observed at Bárdarbunga central volcano from 16 August 2014, signifying the start of a major rifting episode (Sigmundsson et al. 2015). As a lateral dyke propagated beneath Vatnajökull glacier towards the northeast, a slow collapse of the Bárdarbunga caldera began around 20 August (Gudmundsson et al 2016). On 29 August, a small eruption took place at Holuhraun, north of the glacier, followed by the main eruption, which started on 31 August and lasted for six months (Pedersen et al. 2017). Movement on a graben above the distal part of the dyke path was identified by new fractures and subsidence on the ice surface (Hjartardóttir et al. 2016; Rossi et al. 2016). Three ice cauldrons (depressions on the ice surface formed by melting at the base) formed within the graben, due to small subglacial eruptions (Reynolds et al. 2017). A set of shallow cauldrons formed along a line extending towards the southeast from the caldera rim during the dyke propagation. Moreover, ice cauldrons also formed around the caldera rims during the following months and years.

Ice cauldrons caused by subglacial thermal activity are not unique to this event, they have been observed at many subglacial volcanoes in Iceland, both as a result of eruptive processes, e.g. Gjálp 1996 (Gudmundsson et al. 2004), and due to subglacial geothermal activity, e.g. Grímsvötn (Björnsson and Gudmundsson, 1993, Jarosch and Gudmundsson, 2007), Kverkfjöll (e.g. Montanaro et al., 2016) and Katla (Gudmundsson et al. 2007). Similar manifestations of thermal activity on ice-covered volcanoes have been reported from many regions where glaciers are found on the slopes of volcanoes (e.g. Major and Newhall, 1989).

This study describes and quantifies the thermal activity around the caldera rims during and following the Bárdarbunga caldera collapse, and explores the possible heat sources that could produce such thermal signals. We use the HYDROTHERM code from the USGS to perform fluid flow and heat transport simulations to explore the potential heat flux produced by a shallow magmatic intrusion (Hayba and Ingebritsen, 1997; Kipp et al. 2008). We explore through simulations the fundamental question of the relationship between intrusions as heat sources in the uppermost crust (here defined as <1 km depth) and thermal signals at the solid earth's surface (the base of the glacier in this case). In particular, we look at how heat flow magnitude and time delay before the onset of a thermal anomaly at the surface depend upon shallow crust reservoir properties: permeability, permeability anisotropy, and pre-intrusion temperatures in the bedrock adjacent and overlying an intrusion. For the caldera setting of Bárdarbunga, emphasis is placed on the role of faults and weakness zones associated with caldera boundaries.

2. Regional Setting

The Bárdarbunga volcanic system comprises a central volcano which is located beneath the north-western part of Vatnajökull (figure 1), and an associated fissure system. The Bárdarbunga caldera is entirely subglacial, and covers an area of ~70 km^2. The caldera walls rise up to ~700 m over the floor, and the ice thickness reaches ~850 m. There have been more than 20 confirmed eruptions from the Bárdarbunga volcanic system in the last 1,200 years, making it one of the most active volcanoes in Iceland (Larsen et al., 1998; Óladóttir et al., 2011). These eruptions have taken place outside the caldera, on the fissure swarms on both sides of the central volcano; no eruptions from within the ice-filled caldera have been recorded (Thordarson and Larsen, 2007). In 1996 the Gjálp eruption took place between Bárdarbunga and Grímsvötn, and is likely to have been triggered by the Bárdarbunga volcanic system (Einarsson et al., 1997; Pagli et al., 2007), possibly with minor volcanic activity on the SE-margin of Bárdarbunga (Gudmundsson et al., 2004).

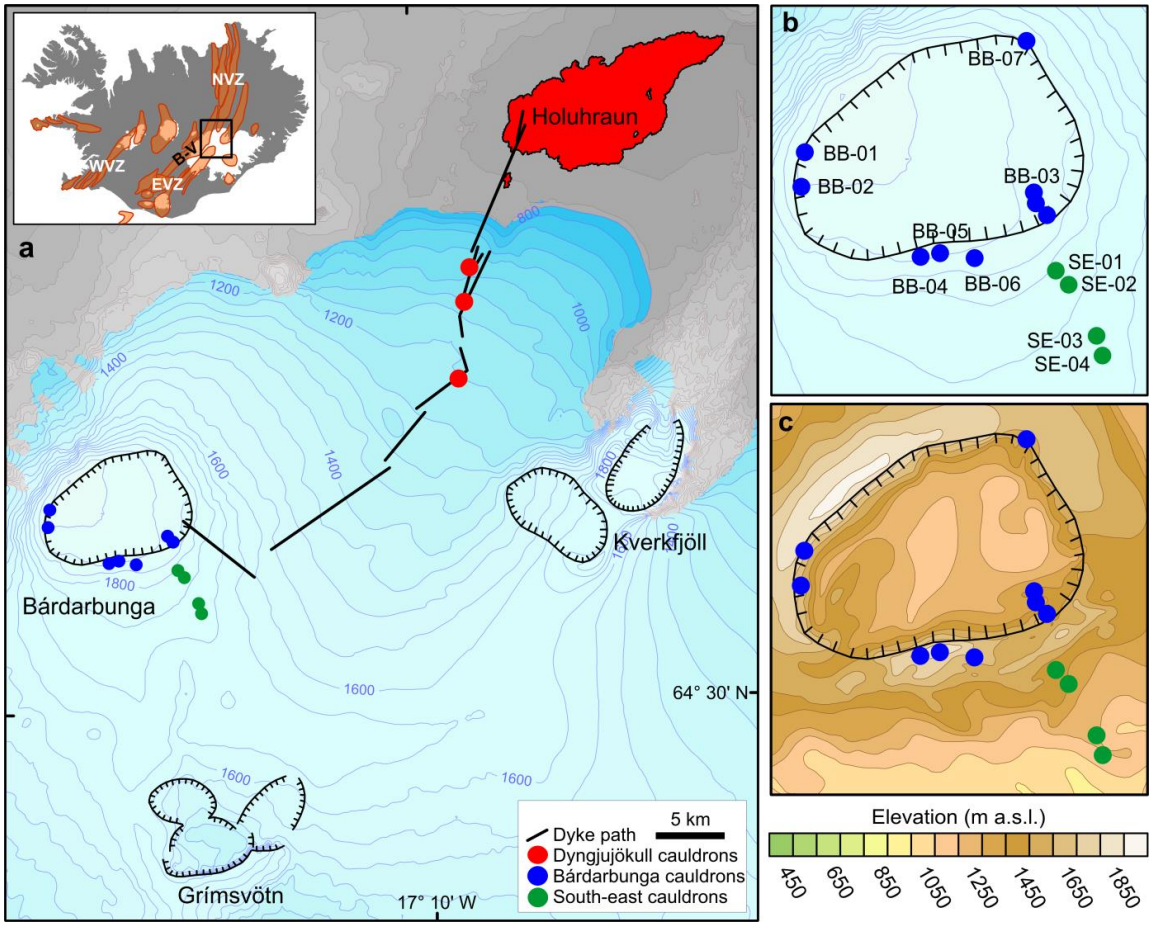

Figure 1: a) The north-western part of Vatnajökull ice cap, showing the Bárdarbunga, Grímsvötn and Kverkfjöll central volcanoes, and the path of the dyke which produced the 2014-15 eruption at Holuhraun (Sigmundsson et al., 2015). Red circles show the locations of cauldrons formed during small subglacial eruptions which took place during the dyke propagation (Reynolds et al., 2017). The green circles denote ice cauldrons which formed to the south-east of the Bárdarbunga caldera rim after the period of unrest began in August 2014, and the blue circles show the locations of cauldrons which formed around the caldera rim. b) Ice surface map of Bárdarbunga caldera with the ice cauldrons names labelled. c) Bedrock map of Bárdarbunga caldera (after Björnsson and Einarsson, 1990).

Small ice cauldrons have been observed at Bárdarbunga prior to those associated with the 2014 unrest. A cauldron has been sustained above the western caldera rim for a minimum of several decades (Eiríksdóttir, 2012). Two shorter-lived cauldrons were observed at the south-eastern extent of the Bárdarbunga caldera following the Gjálp eruption (Gudmundsson et al., 2004), and may have been formed by minor eruptive activity beneath the glacier as a magmatic signature was found in the meltwater from this area (Kristmannsdóttir et al., 1999). One further cauldron has been observed at the south-eastern extent of the caldera since 2010. As there have not been any jökulhlaups associated with these sustained ice cauldrons, it is likely that they drain continuously with only insignificant volumes of meltwater accumulating beneath them.

3. Methods

3.1 Cauldron monitoring

The Bárdarbunga caldera has been monitored from the air since the onset of heightened seismic activity in August 2014. Ice cauldrons are generally first identified by visual inspection of the ice surface, during observation overflights, and are monitored using airborne radar altimetry profiling, aircraft-based Synthetic Aperture Radar (SAR), and satellite images (Gudmundsson et al., 2016). The cauldron volumes are calculated by interpolating profiles of the ice surface elevation, measured using C-band radar altimeter and kinematic GPS on board a low-flying aircraft. The measurements of the ice surface elevation have a relative consistency of 1-2 metres (Gudmundsson et al., 2007). The depth of penetration of the radar within the glacier surface depends on the temperature and density of the surface layer, and varies from zero in summer to several meters in winter (Gudmundsson et al., 2016, supplementary materials). For this reason, the ice surface profiles are not used here as an absolute measurement, but instead are used to monitor the relative changes in elevation, compared to the ice surface outside of the depression. A LiDAR map of Vatnajökull was produced for 2011 (Jóhannesson et al., 2013), which provides a good reference surface, accurately recording details of surface form at the time of surveying. The cauldron profile data are compared to the LiDAR map, and shifted vertically to match the map where the ice surface is unaffected by geothermal activity, thus removing all other signals from the data e.g. ice flow into the collapsed caldera, surface accumulation, and inconsistencies arising from variations in the penetration depth of the radar.

3.2 Ice calorimetry

In subglacial geothermal areas ice melting can be used as a calorimeter, if it is assumed that no heat is lost to the atmosphere (Gudmundsson et al. 2004; Jarosch et al. 2008). The volume of the depression on the surface of the ice is proportional to the volume of ice melted at the base of the glacier, if the cauldrons are isolated from other sources of ice deformation. The contribution to the deformation from the caldera collapse is removed in this study by normalising the elevation profiles using the LiDAR map from 2011. The thermal energy required to melt a volume of ice (V_i) is calculated from the density (ρ_i) and latent heat of fusion (L_i) for ice. The ice is assumed to be at the pressure melting point throughout, of roughly 0°C, and therefore no energy is required to increase the temperature of the ice to the melting point. We use 917 kg m^{-3} for the ice density, and $3.34 \cdot 10^5$ J kg^{-3} for the latent heat of fusion for ice. If the inflow of ice into the cauldron area is not accounted for, estimates of geothermal heat flux are underestimated. Jarosch and Gudmundsson (2007), using a Full Stokes ice flow model, calculate the underestimation as $U = \frac{q_{av} - q_{start}}{q_{start}} \times 100$ %, where q_{start} is the average heat flux when inflow is ignored, and q_{av} is the estimated heat flux from their model. q_{av} is dependent

on the rate factor in Glen's flow law, which varies with ice properties including temperature, impurities and anisotropy. Jarosch and Gudmundsson estimate q_{av} for several values of the rate factor; using a rate factor value derived for an area very close to the area of this study, an underestimation factor of 23% was found to be most appropriate. This value is used here. Therefore, the heat required to melt the observed ice cauldrons is calculated by:

$$Q = (U + 1)\rho_i V_i L_i \tag{1}$$

3.3 HYDROTHERM modelling

HYDROTHERM is a numerical modelling program which simulates multi-phase ground-water flow and thermal energy transport (Hayba and Ingebritsen, 1997; Kipp et al. 2008). We use HYDROTHERM, version 3.2.0, to simulate heat flow from a shallow dyke to the surrounding bedrock, focusing on the surface heat flux.

Two governing partial differential equations solved are: the water-component flow equation, which combine the conservation of mass of the groundwater in both liquid and gas phase and Darcy's law for fluid flow in porous media (equation 2); and the thermal-energy transport equation, which is formed using the conservation of enthalpy for both the groundwater and the porous medium (equation 3). For the spatial and temporal discretization of the equations, finite-difference techniques are employed.

The equation for groundwater flow is given by:

$$\frac{\partial}{\partial t}[\phi(\rho_w S_w + \rho_s S_s)] - \nabla \cdot \frac{\mathbf{k} k_{rw} \rho_w}{\mu_w}[\nabla p_w + \rho_w g \hat{\mathbf{e}}_z] - \nabla \cdot \frac{\mathbf{k} k_{rs} \rho_s}{\mu_s}[\nabla p_s + \rho_s g \hat{\mathbf{e}}_z] = 0 \tag{2}$$

The subscripts *w* and *s* refer to the phases of liquid water and steam respectively. Here ϕ is the porosity, ρ the fluid density, S_w and S_s are respectively the saturation of liquid water and steam with $S_w + S_s = 1$, $\mathbf{k}$ the porous-medium permeability tensor, k_r the relative permeability, μ the fluid viscosity, p_w is the fluid pressure in the liquid phase, p_s the fluid pressure in the gas phase, g the gravitational constant, $\hat{\mathbf{e}}_z$ the unit vector in the z direction, t is the time, and ∇ is the spatial gradient (Kipp et al. 2008).

The heat transfer equation is given by:

$$\frac{\partial}{\partial t}[\phi(\rho_w h_w S_w + \rho_s h_s S_s) + (1 - \phi)\rho_r h_r] - \nabla \cdot K_a \mathbf{I} \nabla T + \nabla \cdot \phi(S_w \rho_w h_w \mathbf{v}_w + S_s \rho_s h_s \mathbf{v}_s) - q_{sh} = 0 \tag{3}$$

Here, *h* is the specific enthalpy of the fluid phases, h_r the specific enthalpy of the porous-matrix solid phase, ρ_r the density of the porous-matrix solid phase, K_a the effective thermal conductivity of the bulk porous medium, **I** the identity matrix of rank 3, *T* the temperature, and q_{sh} is the flow-rate intensity of an enthalpy source (Kipp et al. 2008).

We use two-dimensional symmetric models where a heat source is inserted at a shallow depth: (1) To investigate the magnitude and timescales of thermal signals produced by a heat source (magmatic intrusion) within a zone of homogeneous permeability, and (2) to explore the effect of anisotropy in the form of a highly permeable (fault) conduit as a pathway for fluid and energy flow.

Model 1 – homogeneous permeability

The homogeneous half-space model features a vertical heat source in the lower-left corner, within a body with porosity 0.2 and homogeneous permeability. The heat source is 500 m in vertical length, has a half width (1/2·w) of 2.5 m, and an initial temperature of 1200 °C. The model is run for heat sources at two depths, 200 m and 500 m (Table 1). The initial temperature gradient in the rest of the domain increases linearly, from 0 °C at the surface to 200°C at 200 m (temperature gradient of 0.4 °C m^{-1} in the uppermost 200 m; figure 2). The upper boundary is held at the initial temperature of 0 °C and atmospheric pressure.

Table 1: List of simulations using model 1, with a heat source within a zone of homogeneous permeability. All models were run with a vertical heat source with half width of 2.5 m, and initial bedrock temperature gradient of 0-200 °C (see figure 2).

Depth of heat source (m)	**Permeability (m^2)**
200	1×10^{-13}
200	1×10^{-14}
500	1×10^{-13}
500	1×10^{-14}

Model 2 – high-permeability conduit

Three separate rock units are defined for model 2 (figure 2). The main part of the domain is set to a permeability of 1×10^{-14} m^2, and porosity of 0.2, and represents the main part of the bedrock. In the lower left corner, a narrow high-temperature zone represents an intrusion. This unit is 500 m long vertically and has a width of 1/2·w = 0.5 or 2.5 m (the half-width of the intrusion), and set to have an initial temperature of 1200 °C. On the upper left side of the model, a high-permeability zone, with a porosity of 0.2, ranges in permeability from 1×10^{-13} to 1×10^{-10} m^2. The depth of the high-temperature zone (intrusion) is varied between d = 200, 500 and 1000 m. This model assumes that the porous-matrix is fully saturated, with pure water. The simulations included in this study are summarized in Table 2.

The effects of pre-intrusion temperatures are explored, for a range of temperature gradients (figure 2), from an initially cold bedrock, to an initially hot bedrock slightly below the pressure boiling point, similar to conditions in geothermal areas.

The model domain is divided into a grid, with columns (horizontal dimension) varying in width from 0.5 m to 2 m, and rows (vertical dimension) of thickness 10 or 20 m. It should be noted that during the simulations with the narrower high-temperature zone and corresponding high-permeability zone, these zones are only one cell-width wide, making that part of the model essentially one-dimensional. This is due to instabilities that develop in the model when run with a narrower cell-width.

A constant pressure-temperature condition is applied to the upper boundary, based on the initial conditions. The initial temperature at the upper boundary is 0 °C, and the initial pressure varies from atmospheric pressure, to 1.3 MPa and 2.7 MPa (which represent the ice load from glacier thicknesses of 150 and 300 m respectively). The initial temperature in the high-temperature zone is 1200 °C, and outside of that an initial temperature gradient is applied which starts at 0 °C at the upper boundary and increases linearly downwards to 50, 100 or 200°C at -200 m, where it becomes uniform down to the lower boundary. The lower host-rock boundary layer is impermeable with a basal heat flux, which maintains the initial temperature gradient. The boundaries at the left and right-hand sides are impermeable and thermally insulating.

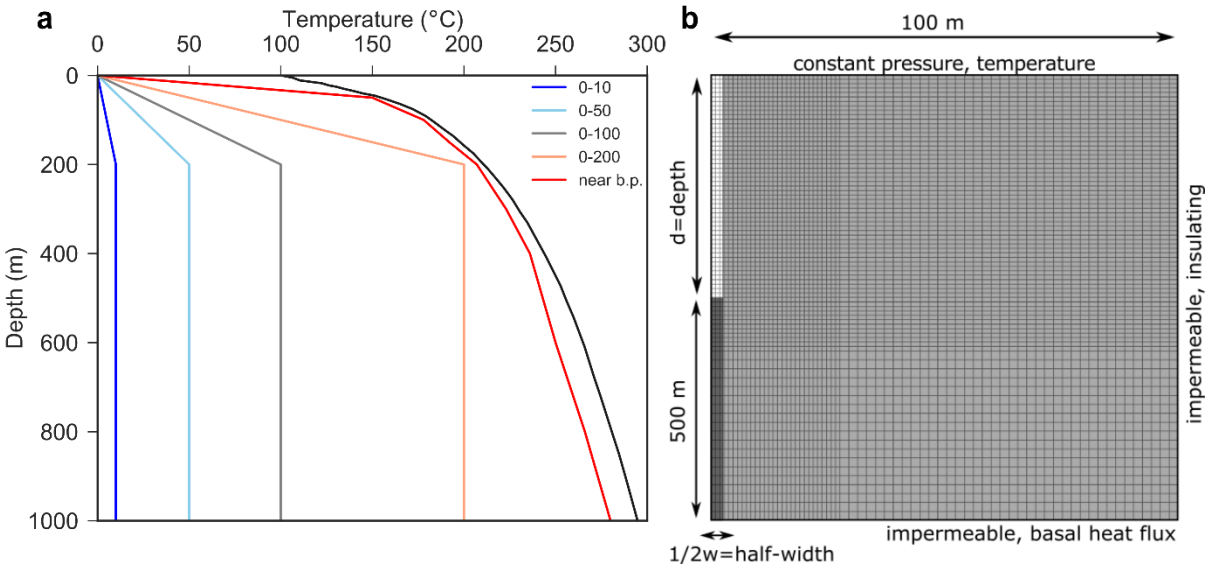

Figure 2: a) Initial temperature gradients used in the modelling. The black curve is the boiling point curve, and the red line is the temperature gradient for the near boiling point (near b.p.) scenario. b) Model geometry in the HYDROTHERM model, showing the finite difference grid, boundary conditions, and the rock units used in the models, which are indicated by shading. The narrow, vertical rock unit in the lower corner left is a high temperature zone with temperature dependent permeability (dark grey). Model 1 is the case of homogeneous permeability (conduit same as surroundings); for this model, the area outside of the high-temperature zone (white and light grey) has a permeability of 10^{-13} or 10^{-14} m^2. Model 2 is used to explore high permeability conduits, and for this model the light grey rock unit is a relatively low permeability zone of 10^{-14} m^2, and above it the vertical conduit (white) is given a range of permeabilities from 10^{-13} to 10^{-10} m^2. Constant pressure and temperature are imposed on the upper boundary, and the other boundaries are impermeable and insulating. The half-width and depth of the dyke are varied for different simulations, as are the permeability and initial temperature of the bedrock.

Table 2: List of simulations using model 2, a vertical intrusion with high-permeability zone.

Heat source half-width (m)	Depth of heat source (m)	Surface pressure (MPa)	Ice thickness (m)	Initial temp. at 200 m depth (°C)	Vertical Zone Permeability (m^2)
0.5	500	0.1	0	200	1×10^{-10}
0.5	500	0.1	0	200	1×10^{-11}
0.5	500	0.1	0	200	1×10^{-12}
0.5	500	0.1	0	200	1×10^{-13}
2.5	200	0.1	0	200	1×10^{-10}
2.5	200	0.1	0	200	1×10^{-11}
2.5	200	0.1	0	200	1×10^{-12}
2.5	200	0.1	0	200	1×10^{-13}
2.5	500	0.1	0	50	1×10^{-10}
2.5	500	0.1	0	50	1×10^{-11}
2.5	500	0.1	0	50	1×10^{-12}
2.5	500	0.1	0	50	1×10^{-13}
2.5	500	0.1	0	100	1×10^{-10}
2.5	500	0.1	0	100	1×10^{-11}
2.5	500	0,1	0	100	1×10^{-12}
2.5	500	0.1	0	100	1×10^{-13}
2.5	500	0.1	0	200	1×10^{-10}
2.5	500	0.1	0	200	1×10^{-11}
2.5	500	0.1	0	200	1×10^{-12}
2.5	500	0.1	0	200	1×10^{-13}
2.5	500	1.5	150	200	1×10^{-10}
2.5	500	1.5	150	200	1×10^{-11}
2.5	500	1.5	150	200	1×10^{-12}
2.5	500	1.5	150	200	1×10^{-13}
2.5	500	1.5	300	200	1×10^{-10}
2.5	500	2.85	300	200	1×10^{-11}
2.5	500	2.85	300	200	1×10^{-12}
2.5	500	2.85	300	200	1×10^{-13}
2.5	1000	0.1	0	200	1×10^{-10}
2.5	1000	0.1	0	200	1×10^{-11}
2.5	1000	0.1	0	200	1×10^{-12}
2.5	1000	0.1	0	200	1×10^{-13}

4. Results

4.1 Ice cauldrons

The cauldrons being studied here can be divided into four groups (figure 1): (1) on the south-eastern flank, (2) in western part of caldera, (3) the southeast part, and (4) the southern caldera rim. A small cauldron began to emerge in a new area, at the northeast rim in early 2017 (BB-07 in figure 1).

Cauldrons on the south-eastern flank

Four ice cauldrons on the south-eastern flank of Bárdarbunga were first observed on 27 August 2014 (figures 1, and 3). They initially grew very rapidly, before reaching their maximum volumes within 5 months (figures 4 and 7). Three of the cauldrons have been infilling with ice since then, with the exception of SE-01 which was reactivated in July 2016 (figure 7). These cauldrons are thought to have formed during small subglacial eruptions due to the initially large thermal signal which gradually decreased within months, similar to those observed at Dyngjujökull (Reynolds et al., 2017). The date that the eruptions took place is not known; the earliest possible date is 16 August 2014 (when seismicity at Bárdarbunga increased), but it is likely to be later than this. The later growth at SE-01 may be due to geothermal activity.

Cauldrons on the western caldera rim

The growth of the two western cauldrons (BB-01 and BB-02) was first observed in October 2014, about two months after the beginning of unrest in mid-August 2014. They are located in an area of known geothermal activity (figures 5 and 6). BB-01 and BB-02 grew to volumes of 7.6±1.1 and 7.2±1.1 million m^3, respectively (figure 7). BB-01 was one of the longest-lived of the cauldrons, remaining active for over two years. BB-02 remained active for a shorter time, and began to infill ~7 months after its growth was observed.

Cauldrons in the south-eastern part of the caldera

The growth of BB-03 was first observed within a month of the onset of heightened activity. It is located where geothermal activity had previously been observed. BB-03 grew to the largest volume of the cauldrons, peaking at 17±2 million m^3 (figure 7). It initially formed as two cauldrons side-by-side (figure 3d), and the more northerly of the two began to migrate northwards in 2017. These cauldrons continue to increase in volume in 2017.

Cauldrons on the southern caldera rim

In July 2015, approximately a year after the event started, three more cauldrons were observed on the southern caldera rim. BB-04, BB-05 and BB-06 were much smaller in size, reaching only 1.0±0.2, 2.0±0.3 and 1.4±0.2 million m^3, respectively (figure 7). These southern cauldrons are located where the ice is thinner, up to 150 m compared to several hundreds of metres at the other cauldron locations (figure 6). During the period when bedrock is exposed at the bottom of the cauldrons, some of the heat will have been lost to the atmosphere, and therefore the power output for these cauldrons is underestimated. The cauldrons along the southern rim (BB-04, BB-05, and BB-06) grew for over a year, and have remained similar in size since, although BB-05 has grown somewhat. Bedrock was observed at the bottom of BB-05 in late summer 2016 and in late summer 2017 this opening had grown wider. Steam has occasionally been observed rising from these cauldrons since the summer of 2016.

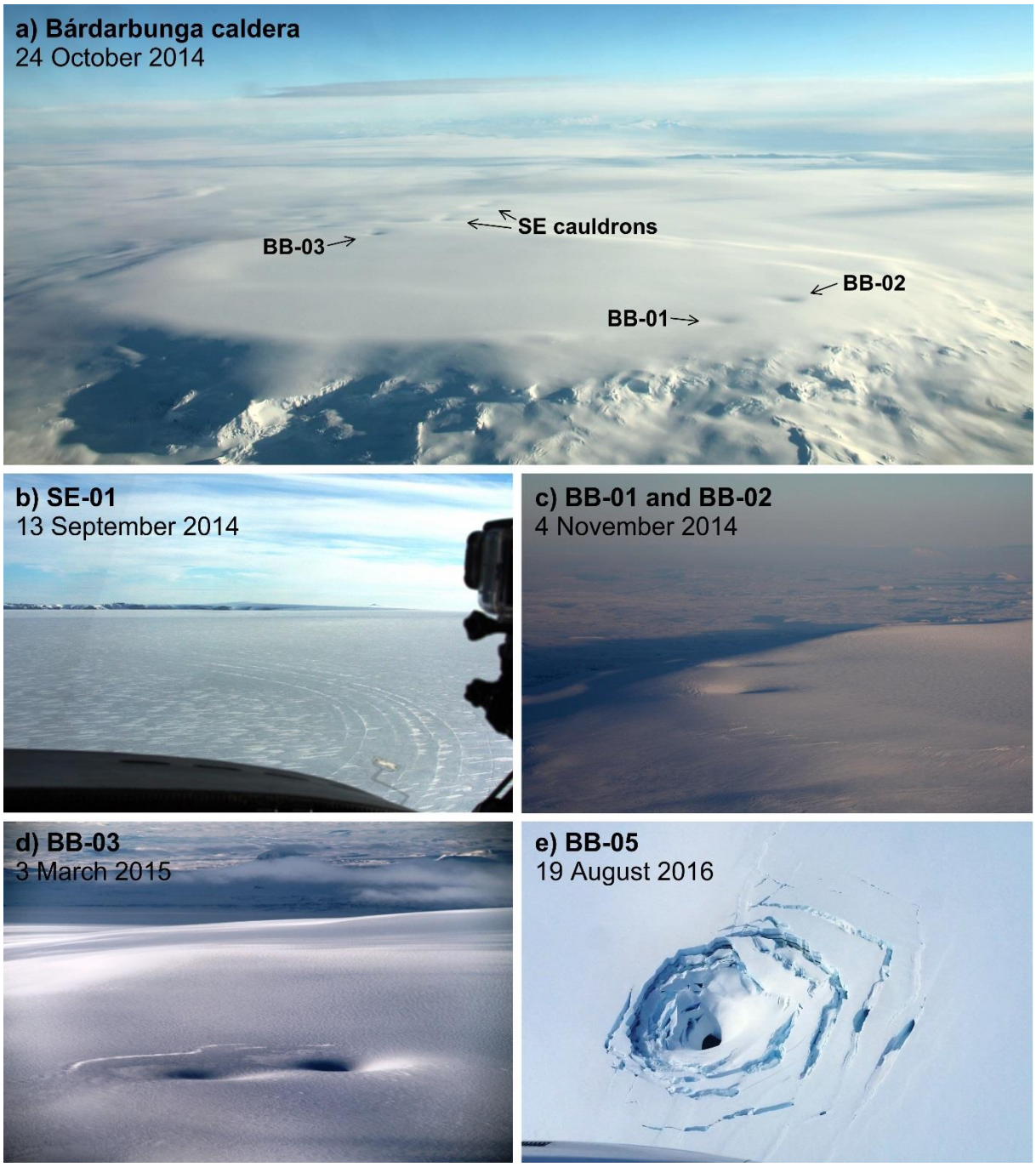

Figure 3: Aerial photographs of ice cauldrons at Bárdarbunga, which formed during and following the 2014–15 rifting episode. a) The Bárdarbunga caldera, view towards SE, b) SE-01, on the caldera flank, with a view towards Grímsvötn, c) BB-01 and BB-02, view towards north, d) BB-03, and d) BB-05 which is one of the cauldrons on the southern caldera rim where a hole exposing bedrock formed in 2016.

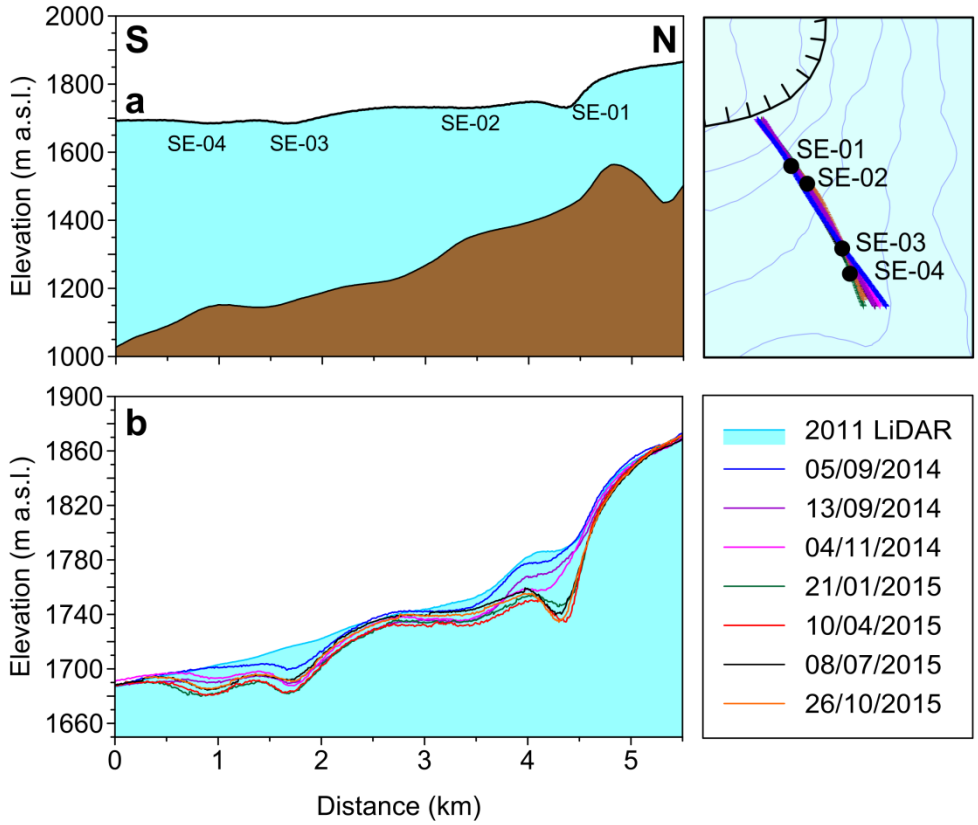

Figure 4: a) The ice surface with bedrock beneath, for a profile through the ice cauldrons on the south-eastern flank of Bárdarbunga caldera, and b) the same profile, but a close-up of the ice surface, with survey lines showing the evolution of the cauldrons. The map shows the paths of the survey lines.

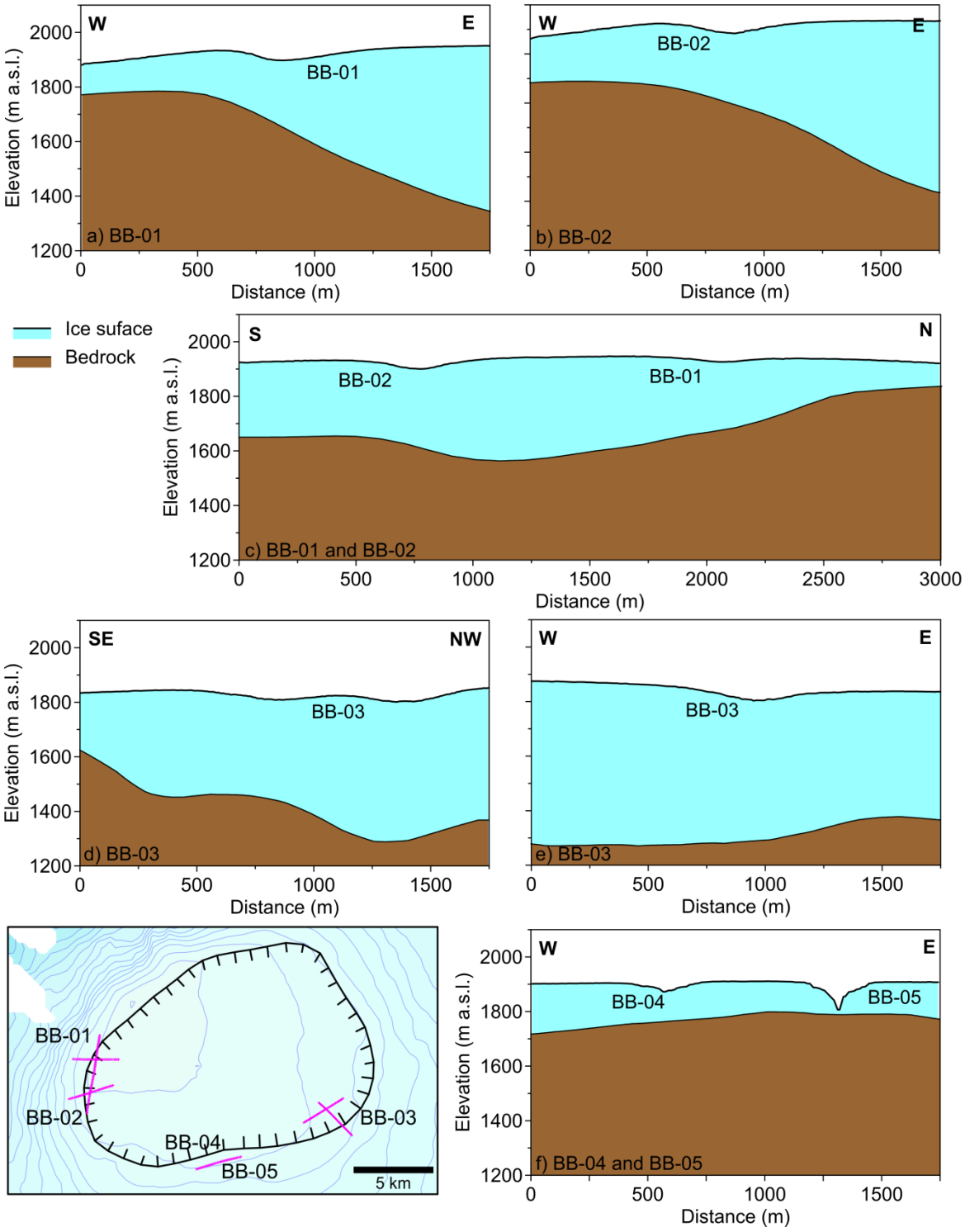

Figure 5: The setting of the cauldrons around the Bárdarbunga caldera rim, with the bedrock beneath, showing the scale of the cauldrons compared with the ice thickness and caldera wall. The map shows the profiles lines in relation to the caldera rim.

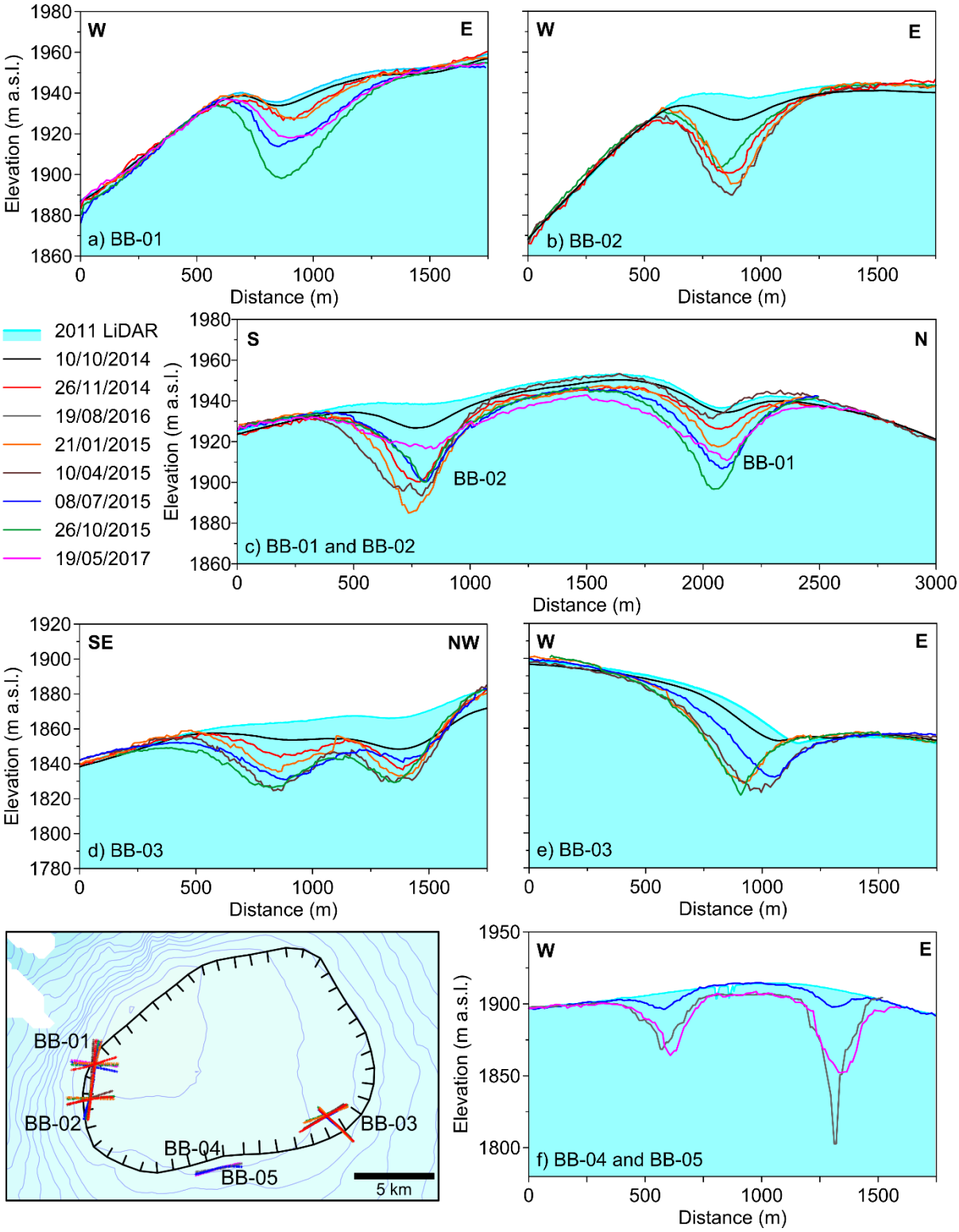

Figure 6: Selected profiles showing the time evolution of the ice cauldrons at Bárdarbunga caldera. The profile data are from airborne radar altimetry measurements, except the profiles from 10/10/2014, which were acquired from a Pleiades satellite image. The survey lines are displayed on the map, showing slight variation in repeated lines, which accounts for some differences in the profiles. The cauldron numbers and profile orientations are labelled.

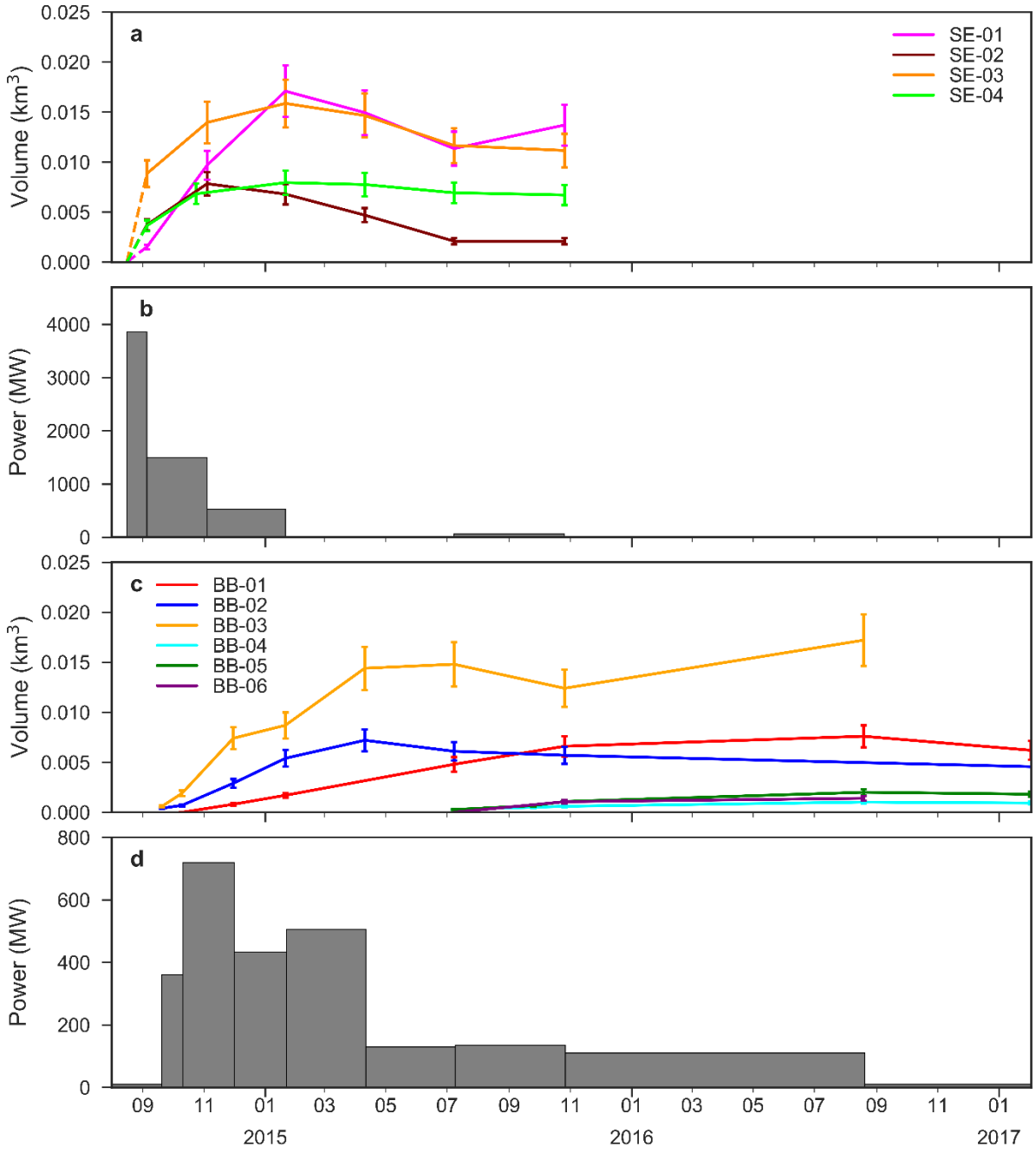

Figure 7: a) The volumes of the SE cauldrons with time, with dashed lines from the earliest possible eruption date of 16th August 2014. b) The total power for all the SE cauldrons with time, calculated using equation 1. The power for the first segment is an underestimate if the eruptions took place later than August 16th, and because it is an average over the period it does not capture the highest power which occurs during the eruptions. c) The volumes of the BB cauldrons with time. d) The combined power of the BB cauldrons.

4.2 Heat transfer results

Model 1 – homogeneous permeability

Here only an example of a run for domain temperature of 0–200°C is shown. The onset of the surface thermal signal at the upper boundary of the model occurs ~1.4 years after start of simulation for the heat source at 200 m depth within a zone of 1×10^{-13} m^2, and ~2.1 years for the heat source at a depth of 500 m; the shallower heat source produced a slightly larger peak power, and the duration of the signal is twice that produced by the heat source at 500 m depth (figure 8). No significant surface signal is produced when the heat source is within a zone of 1×10^{-14} m^2 permeability. This indicates how strong a control the permeability has for the onset of convection within a porous medium. The phase field is shown in figure 9, for a vertical heat source at 500 m depth, within a homogeneous medium with a permeability of 1×10^{-13} m^2. For a 500 m long vertical intrusion the peak power at the surface would be ~20 MW (= 500 m x 40,000 W m^{-1}).

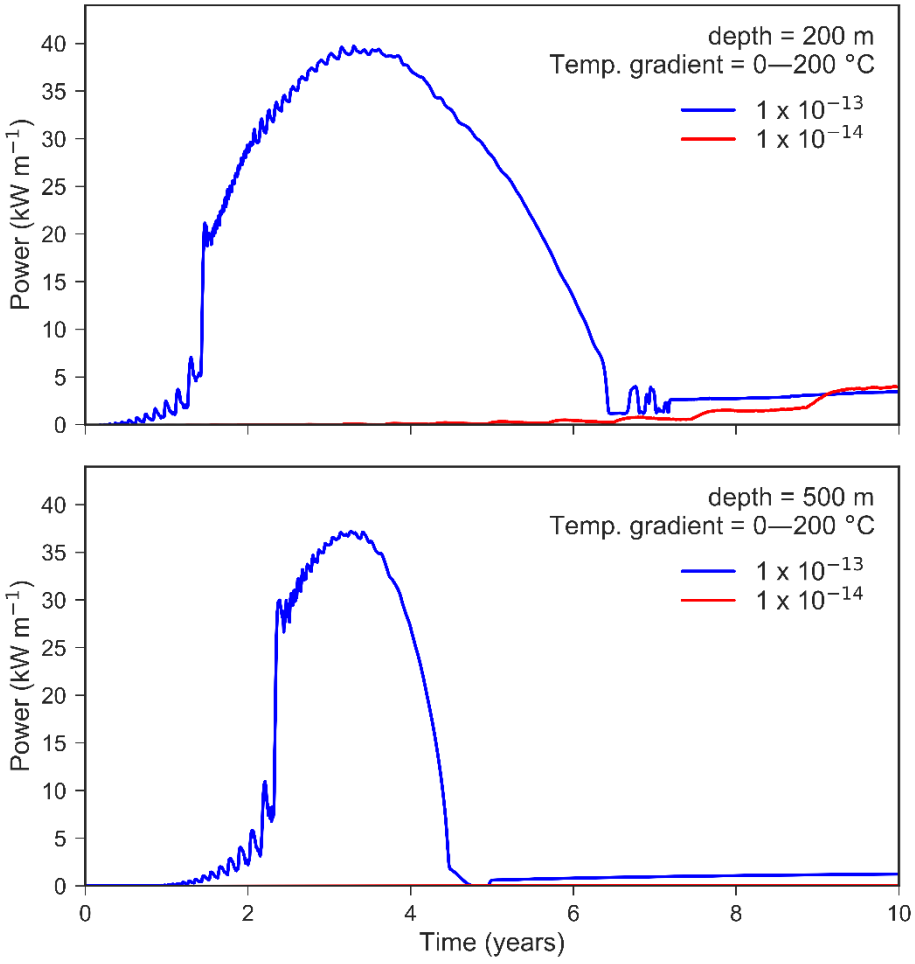

Figure 8: Surface thermal power per metre length produced by a vertical heat source within a zone of homogeneous permeability.

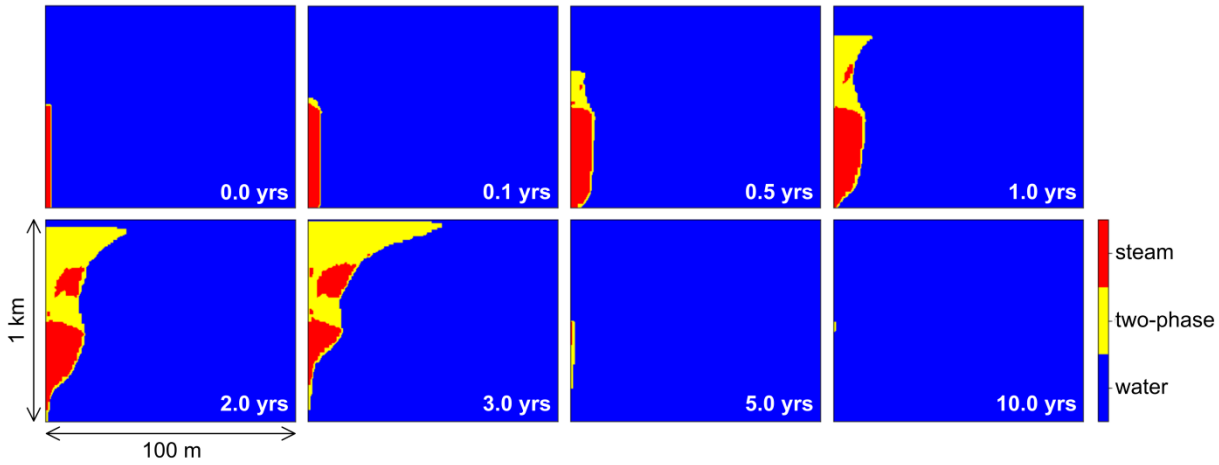

Figure 9: The phase field for a vertical heat source within a homogeneous medium with permeability of 1×10^{-13} m^2, at 500 m depth.

Model 2 – high-permeability conduit

The simulation results presented include several values of permeability for the high-permeability zone, and pre-intrusion temperatures range from 10 °C to near the pressure-boiling point for water.

Both the maximum surface heat flux magnitude and the total thermal output due to an intrusion increase with permeability (figure 10). Permeability had the least effect on the shallowest dyke, of a depth of 200 m, but the effect was very significant for the deeper dykes. Only a minor surface thermal signal is produced where a high permeability zone of 1×10^{-13} m^2 is used. The total surface heat output decreases with increasing depth of the intrusion.

The narrower ($1/2 \cdot w = 1$ m) high-temperature zone produced a smaller total surface thermal signal than the wider ($1/2 \cdot w = 5$ m) high-temperature zone with otherwise identical initial parameters, for all permeabilities simulated (figure 10). The difference in total surface heat output is more significant with decreasing permeability; the narrower high-temperature zone produced 26%, 18%, 6% and 1% of the total surface heat output produced by the wider high-temperature zone, when run with the permeabilities of 1×10^{-10} m^2, 1×10^{-11} m^2, 1×10^{-12} m^2, and 1×10^{-13} m^2 respectively.

The peak in heat flux occurs after the shortest duration for the simulations run with the intrusion at 200 m depth, and those with the thinner 1 m intrusion, with the shortest time to the peak being around 15 days for the highest permeabilities. The other simulations peak at between 40 and 80 days. The highly permeable zone focuses the hot fluid upwards, producing a surface signal after a significantly shorter onset time than those seen using model 1, which had onset times of 1.5–2.5 years (figure 8).

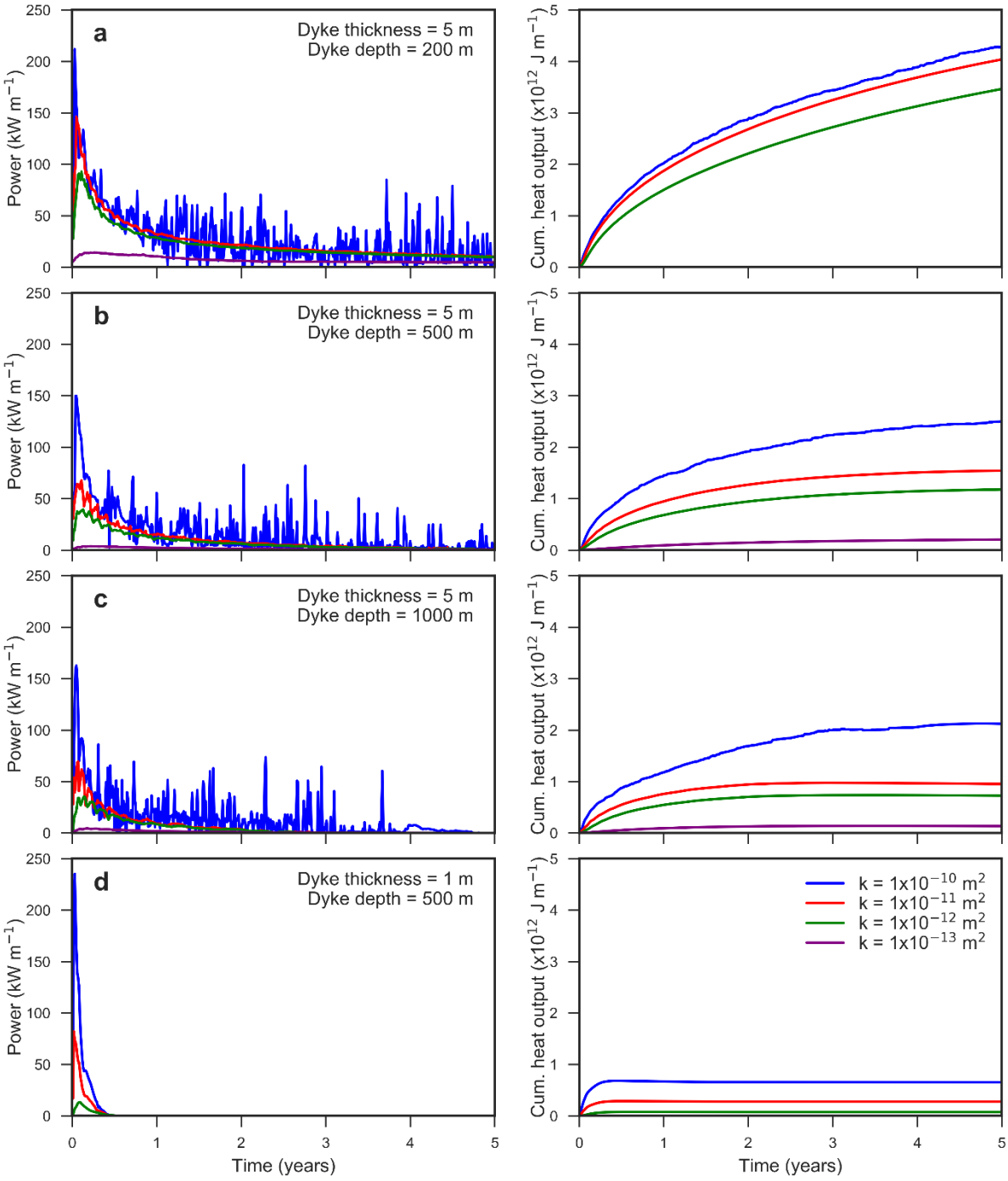

Figure 10: Results from HYDROTHERM simulations for the potential power output at the surface for a dyke segment with a length of 1 m, and the cumulative heat output with time. a), b) and c), are the results for a 5 m thick dyke, reaching a depth of 200 m, 500 m and 1 km respectively. d) Shows results for a 1 m thick dyke at 500 m depth. The colours represent runs using different permeabilities, as specified in the legend. All of these simulations were run for atmospheric pressure at the upper boundary.

Initial bedrock temperature has a significant effect on the maximum surface heat flux magnitude, and the total thermal output at the surface (figure 11). When an initial bedrock of temperature of 200 °C is used below 200 m (and a uniform gradient from 0 to 200 °C from the

surface to 200 m), the heat flux maximum and total heat output are respectively ~4 and ~6 times greater than for initial bedrock temperature of 100 °C. The signal also lasts for a far longer period when the initial bedrock temperature is higher. This is not due to the extra heat within the bedrock, as this contribution to the surface heat flux is subtracted, leaving only the signal from the dyke. Rather, it is due to more efficient heat transfer from the intrusion to the surface. In the near boiling point bedrock temperature case, the signal is very much greater, and lasts for more than 5 years.

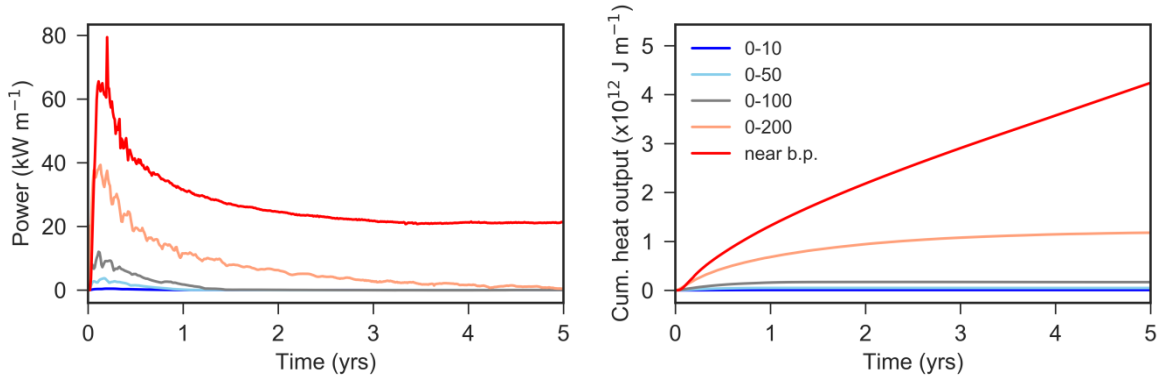

Figure 11: Surface power per metre length of intrusion and cumulative heat output with time for different initial bedrock temperatures, as specified in the legend. These simulations were run for a heat source of half-width 2.5 m, depth of 500 m, and a domain permeability of 1×10^{-12} m^2.

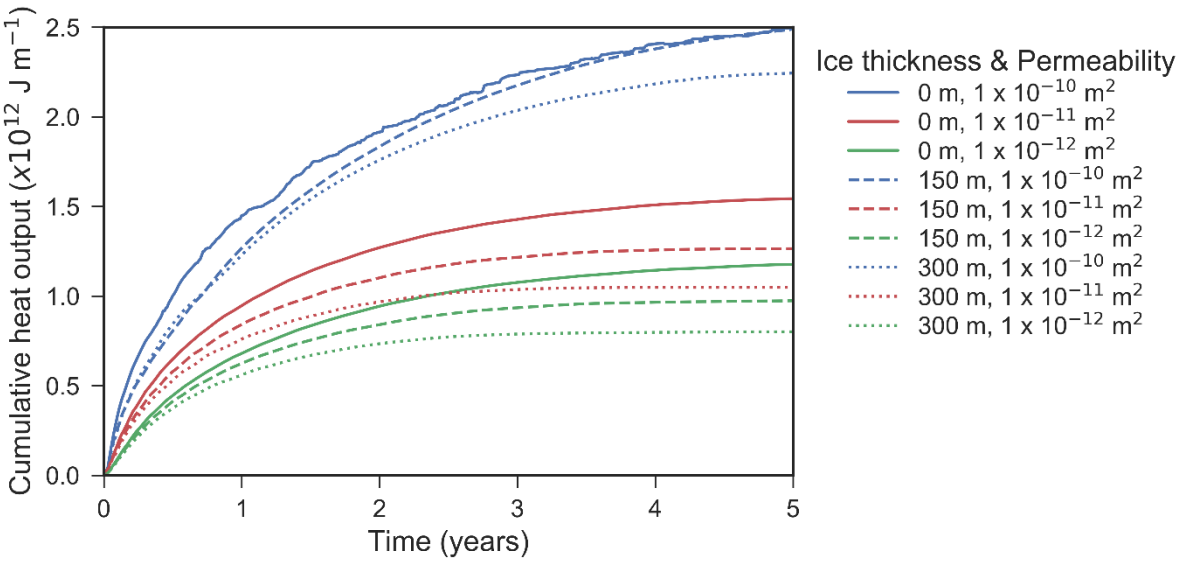

Figure 12: The effect of the pressure at the surface on the simulated thermal signal (cumulated thermal energy released per meter length of intrusion) for different permeabilities, with an initial bedrock temperature of 0-200 °C.

If a higher pressure is applied to the upper boundary, this reduces the heat flow to the surface (figure 12). When a pressure of 1.4 MPa was applied, representing an ice thickness of 150 m, this reduced the total heat output by ~18 % for permeabilities of 1×10^{-11} m^2 and 1×10^{-12} m^2. The total heat output doesn't change for the highest permeability of 1×10^{-10} m^2, but it should

be noted that these simulations were less stable and therefore the results may not be reliable. The runs for an upper boundary pressure of 2.7 MPa (representing 300 m of ice) reduced the heat output by 32 % compared to the results for atmospheric pressure conditions.

5. Discussion

The ice cauldrons formed in August 2014 on the south-eastern flank of the caldera display the characteristics of small subglacial eruptions. They formed very rapidly, with the heat flux peaking in the first days/weeks after their formation. The heat flux quickly dropped off and the cauldrons had stopped growing within five months. This is very similar to the thermal signals observed on Dyngjujökull glacier in August/September 2014, where subglacial eruptions took place as the lateral dyke propagated from Bárdarbunga towards the main eruption site at Holuhraun (Reynolds et al., 2017).

The ice cauldrons which formed at Bárdarbunga caldera rim during and following the 2014–15 eruption at Holuhraun were active for between 7 months and two years, which is relatively long-lived when compared to those on the south-eastern flank or at Dyngjujökull. Therefore, subglacial eruptions have been ruled out as the heating mechanism for the ice cauldrons around the Bárdarbunga caldera rim.

During the two years following the onset of seismicity and caldera subsidence at Bárdarbunga in 2014, the total power at the caldera rim has averaged ~270 MW. This is similar to the geothermal signal produced at Katla, which is of the order of hundreds of Megawatts (Gudmundsson et al. 2007). In contrast, Grímsvötn produces a much higher geothermal signal, having been sustained in the Gigawatts range for several centuries (Björnsson and Gudmundsson, 1993; Björnsson 1988).

From the HYDROTHERM simulations, both the permeability of the high-permeability zone, and the initial temperature of the porous matrix, are major controls on the efficiency of heat transfer to the surface. Reducing the temperature of the bedrock means that the fluids within the porous matrix are further from the pressure boiling point, and therefore have a higher capacity to absorb heat energy without changing phase, which is a major driver in convection due to the large change in density. Therefore, it should be expected that shallow magmatic intrusions in low temperature regions have a muted thermal response.

Comparison of the results of model 1 and model 2 show that onset time is greatly reduced when a high permeability pathway is added to the system, and that the surface heat flux magnitude increases significantly as the permeability in this zone increases. Vertical zones of high permeability could be expected around the ring faults at calderas due to fractures, explaining the prevalence of ice cauldrons around caldera rims. Hemmings et al. (2016) conducted a study into the surface heat flux associated with hydrothermal perturbation, and also find that high-permeability zones have a significant effect on the onset time and magnitude of the surface thermal signals produced by a heat source at depth.

The results for simulations run at the highest permeability of 1×10^{-10} m^2 are more erratic than those for lower permeabilities. Instabilities may be caused as the scenario reaches the limits of the Darcy equation, which requires that fracture spacing be on a much smaller scale than the area of interest.

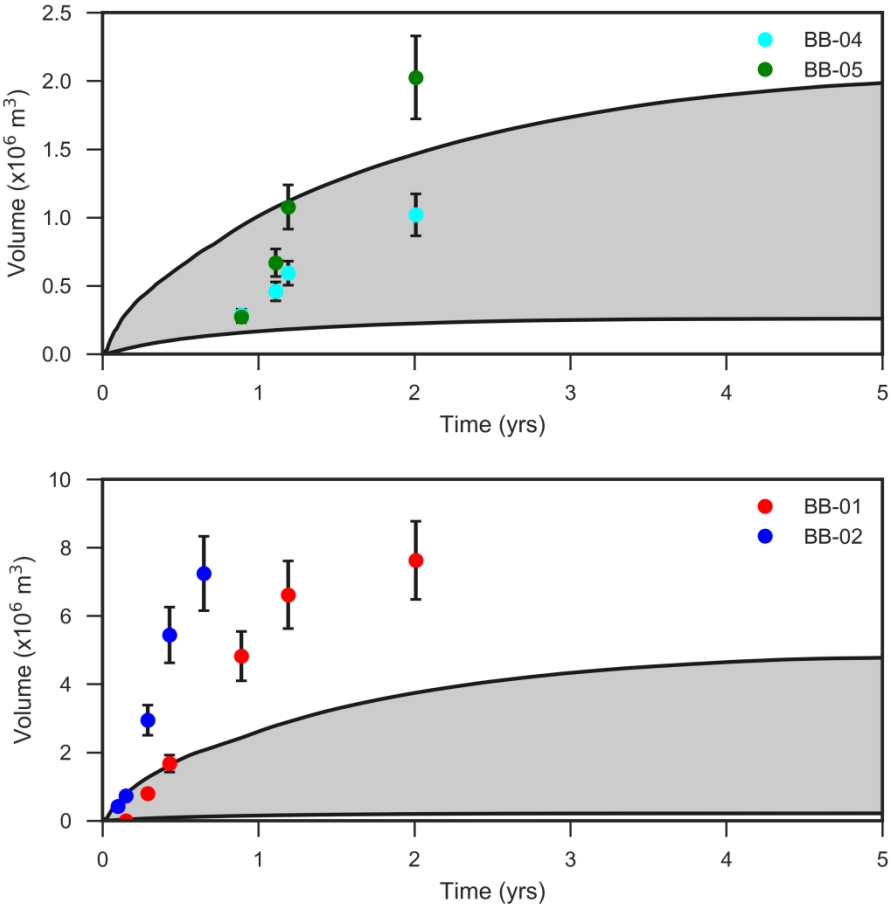

Figure 13: Modelling results converted to the equivalent volume of melted ice, for an intrusion 500 m below the surface, of width 5 m, plotted with the observed volumes of ice cauldrons in Bárdarbunga. A high permeability zone of 1×10^{-12} m^2 is used and the pre-intrusion bedrock temperature gradient is 0-200°C. a) Shaded area gives range in ice melt for an intrusion of between 100 and 300 m in length, beneath an ice thickness of 150 m, plotted with the volume of BB-04 and BB-05. b) Shaded area gives the potential ice melt based on an intrusion of between 100 and 800 m in length, below an ice thickness of 300 m, plotted with the volume of BB-01 and BB-02.

To explore the potential for the modelled scenario to be the heat source for the observed ice cauldrons, we compare the observed ice cauldron volumes with the potential ice melt from the thermal output of the simulations. BB-01 and BB-02 are located where the ice thickness is ~250 and ~350 m respectively, so the modelling results for the scenario for an initial pressure of 2.7 MPa (equivalent to 300 m ice thickness) are considered to be appropriate. Similarly, BB-04 and BB-05 are located above an ice thickness of ~150 and ~120 m respectively so these cauldrons are compared with the potential ice melt in the simulations with a pressure of 1.3 MPa (equivalent to 150 m ice thickness; figure 13). The results used for figure 13 are from simulations of a 5 m wide intrusion at 500 m depth, with an initial bedrock temperature of up to 200 °C. The modelling results give the cumulative heat output for a 1 m length of intrusion. The extent of the heating area beneath the ice cauldrons is not known from the surface measurements, so the modelled heat output is plotted for a range of dyke lengths, from 100 m

to the approximate diameter of the cauldrons, which is 800 m for BB-01 and BB-02 and 300 m for BB-04 and BB-05.

It is found that the range of potential ice melt from the simulations could produce cauldrons BB-04 and BB-05, although these cauldrons were first observed one year after the beginning of the event yet there is no delay in the onset of the surface signal in the results of a model 2 type. The delay times, however, are similar to the ones seen for the model 1, where a vertical high permeability zone is present. The ice volumes melted at BB-01 and BB-02 are not reproduced by the modelling results, so other heating mechanisms must contribute to the observed thermal signal. The modelling results do however shows a surface signal within the timeframe of the onset of melting at BB-01 and BB-02.

The modelling results obtained can be broadly fitted with the observed signals. Some cauldrons (BB-01, 02, 03) fit to model 2 type behaviour of a vertical high permeability conduit while the onset times of BB-04, 05, 06, 07 suggest they fit better with a model 1 type scenario. The behaviour of SE-01 seems to start with a minor subglacial eruption followed by later onset time that can be fitted to either model. Notably, the size of the cauldrons that fit to the high permeability conduit is much greater than for the other cauldrons.

Finally, it should be noted that it is not to be expected that our modelling can reproduce all behaviour observed at Bárdarbunga. The caldera faults reach down ~10 km into the crust and dilatation and stretching of the upper few kilometres near caldera faults can have had a significant effect on the geothermal reservoirs that may be present in the shallow crust. The effect of such dilatation would be an increase in porosity (faults and cracks opening) and that may have resulted in pressure drop, boiling and increased convection. Any combination of this effect and the intrusion-fed thermal signals is possible. Our results demonstrate the importance of pathways of high permeability for transient thermal signals and major effect of pre-intrusion bedrock temperature on whether such signals reach to the surface or are absorbed by groundwater.

6. Conclusions

- Six ice cauldrons formed at the Bárdarbunga caldera rim in the two years following the onset of increased seismicity in the area in 2014. A seventh ice cauldron was observed at the beginning of 2017, 2.5 years after the start of the event.
- The maximum volume of the individual ice cauldrons ranged between 1.0±0.2 and 17±2 million m^3.
- The ice cauldrons around the caldera rim formed due to increased geothermal activity. HYDROTHERM was used to investigate the potential surface heat flux produced by shallow magmatic intrusions, and compared to the observed thermal signals.
- It was found that permeability provides strong control on the surface heat flux, as does the initial temperature of the porous matrix where lower temperatures result in a muted surface thermal signal compared to the higher initial temperatures.
- Modelling results show that high-permeability pathways have a very significant effect on both the magnitude of the surface heat flux, and the onset time for the signal. The distribution of ice cauldrons suggests that these high permeability pathways correspond to fault zones associated with the caldera collapse.
- The smaller ice cauldrons (BB-04 and BB-05) could have been produced by the total thermal output from the modelling results and the delay in onset time may be a result of

limited permeability. However, the thermal signals measured at BB-01 and BB-02 can only be partly explained by the modelling results, suggesting that additional heating mechanisms must contribute to these signals, e.g. from deeper intrusions or increased permeability at greater depth than modelled in this study.

- In contrast, the cauldrons which formed in August 2014 to the southeast of the caldera display characteristics of minor subglacial eruptions, as they initially grew very rapidly followed by a gradual decline.

Acknowledgements

We acknowledge the support of the EU Seventh Framework Marie Curie project NEMOH no. 289976, the Research Fund of the University of Iceland and Landsvirkjun power company. Fieldwork was supported with crisis response funding from the Icelandic government through the Civil Protection Department of the National Commissioner of the Iceland Police, and through the European Community's Seventh Framework Programme grant no. 308377 (Project FUTUREVOLC). We thank The Icelandic Coast Guard who provided assistance in monitoring from their TF-SIF aircraft and ISAVIA (Icelandic Aviation Operation Services) and their crew on board the TF-FMS which was used for altimeter-DGPS profiling. The Iceland Glaciological Society assisted with fieldwork logistics in June 2015.

References

Björnsson H (1988) Hydrology of Ice Caps in Volcanic Regions. Societas Scientarium Islandica. Reykjavík 45, 139 pp.

Björnsson H, Guðmundsson MT (1993) Variations in the thermal output of the subglacial Grímsvötn caldera, Iceland. Geophys Res Lett 20(19): 2127-2130.

Bleick HA, Coombs ML, Cervelli PF, Bull KF, Wessels RL (2013) Volcano–ice interactions precursory to the 2009 eruption of Redoubt Volcano, Alaska. J Volcanol Geotherm Res 259:373-388.

Einarsson P, Brandsdóttir B, Gudmundsson MT, Björnsson H, Grínvold K, Sigmundsson, F (1997) Center of the Iceland hotspot experiences volcanic unrest. Eos, Transaction American Geophysical Union 78(35):369–375.

Eiríksdóttir VS (2012) Þróun sigkatla í Bárðarbungu (Bachelor´s thesis). Retrieved from http://skemman.is/stream/get/1946/11961/30211/1/BS.pdf.

Gudmundsson MT, Sigmundsson F, Björnsson H, Högnadóttir Th (2004) The 1996 Eruption at Gjálp, Vatnajökull Ice Cap, Iceland: Efficiency of Heat Transfer, Ice Deformation and Subglacial Water Pressure. Bull Volcanol 66(1):46–65. doi:10.1007/s00445-003-0295-9.

Gudmundsson MT, Högnadóttir T, Kristinsson AB, Gudbjörnsson S (2007) Geothermal activity in the subglacial Katla caldera, Iceland, 1999–2005, studied with radar altimetry. Ann Glaciol 45:66–72.

Gudmundsson MT, Jónsdóttir K, Hooper A, Holohan EP, Halldórsson SA, Ófeigsson BG, Cesca S, Vogfjörd KS, Sigmundsson F, Högnadóttir Th, Einarsson P, Sigmarsson O, Jarosch AH, Jónasson K, Magnússon E, Hreinsdóttir S, Bagnardi M, Parks MM, Hjörleifsdóttir V, Pálsson F, Walter TR, Schöpfer MPJ, Heimann S, Reynolds HI, Dumont S, Bali E, Gudfinnsson GH, Dahm T, Roberts MJ, Hensch M, Belart JMC, Spaans K, Jakobsson S, Gudmundsson GB, Fridriksdóttir HM, Drouin V, Dürig T, Aðalgeirsdóttir G, Riishuus MS, Pedersen GBM, van Boeckel T, Oddsson B, Pfeffer MA, Barsotti S, Bergsson B, Donovan A, Burton MR, Aiuppa A (2016) Gradual caldera collapse at Bárdarbunga volcano, Iceland, regulated by lateral magma outflow. Science 353(6296): aaf8988.

Hayba, DO, Ingebritsen SE (1997) Multiphase groundwater flow near cooling plutons. J Geophys Res 102(B6): 12,235-12,252.

Hemmings B, Whitaker F, Gottsmann J, Hawes MC (2016) Non-eruptive ice melt driven by internal heat at glaciated stratovolcanoes. J Volcanol Geother Res 327: 385-397.

Hjartardóttir Á, Einarsson P, Gudmundsson MT, Högnadóttir T (2016) Fracture movements and graben subsidence during the 2014 Bárðarbunga dike intrusion in Iceland. J Volcanol Geotherm Res 310:242–252.

Jarosch AH, Gudmundsson MT (2007) Numerical studies of ice flow over subglacial geothermal heat sources at Grímsvötn, Iceland, using Full Stokes equations. J Geophys Res-Earth 112(F2).

Jarosch A, Gudmundsson MT, Högnadóttir Th, Axelsson G (2008) Progressive cooling of the hyaloclastite ridge at Gjálp, Iceland, 1996–2005. J Volcanol Geotherm Res 170(3): 218-229.

Jóhannesson T, Björnsson H, Magnússon E, Guðmundsson S, Pálsson F, Sigurðsson O, Thorsteinsson T, Berthier E (2013) Ice-volume changes, bias estimation of mass-balance measurements and changes in subglacial lakes derived by lidar mapping of the surface of Icelandic glaciers. Ann Glaciol 54(63):63–74.

Kipp KL, Hsieh PA, Charlton SR (2008) Guide to the revised ground-water flow and heat transport simulator: HYDROTHERM — Version 3: U.S. Geological Survey Techniques and Methods 6–A25, 160 p.

Kristmannsdóttir H, Björnsson A, Pálsson, S, Sveinbjörnsdóttir ÁE (1999) The Impact of the 1996 Subglacial Volcanic Eruption in Vatnajökull on the River Jökulsá Á Fjöllum, North Iceland. J Volcanol Geotherm Res 92(3–4): 359–72. doi:10.1016/S0377-0273(99)00056-6.

Larsen G, Gudmundsson MT, Björnsson H (1998) Eight centuries of periodic volcanism at the center of the Iceland hotspot revealed by glacier tephrostratigraphy. Geology 26:943–946.

Major JJ, Newhall CG (1989) Snow and ice perturbation during historical volcanic eruptions and the formation of lahars and floods. Bull Volcanol 52(1):1-27.

Montanaro C, Scheu B, Gudmundsson MT, Vogfjörd K, Reynolds HI, Dürig T, Strehlow K, Rott S, Reuschlé T, Dingwell DB (2016) Multidisciplinary constraints of hydrothermal explosions based on the 2013 Gengissig lake events, Kverkfjöll volcano, Iceland. Earth Planet Sci Lett 434:308-319.

Nakada S, Nagai M, Kaneko T, Nozawa A, Suzuki-Kamata K (2005) Chronology and products of the 2000 eruption of Miyakejima Volcano, Japan. Bull Volcanol 67(3):205-218.

Newhall CG, Dzurisin D. (1988) Historical unrest at the large calderas of the world (No. 1855). Department of the Interior, US Geological Survey.

Óladóttir BA, Larsen G, Sigmarsson O (2011) Holocene volcanic activity at Grímsvötn, Bárdarbunga and Kverkfjöll subglacial centres beneath Vatnajökull, Iceland. Bull Volcanol 73(9):1187–1208.

Pagli C, Sigmundsson F, Pedersen R, Einarsson P, Árnadóttir Th, Feigl KL (2007) Crustal deformation associated with the 1996 Gjálp subglacial eruption, Iceland: InSAR studies in affected areas adjacent to the Vatnajökull ice cap. Earth Planet Sci Lett 259:24–33.

Pedersen GBM, Höskuldsson A, Dürig T, Thordarson T, Jónsdóttir I, Riishuus MS, Óskarsson BV, Dumont S, Magnusson E, Gudmundsson MT, Sigmundsson F, Drouin VJPB, Gallagher C, Askew R, Guðnason J, Moreland WM, Nikkola P, Reynolds HI, Schmith J (2017) Lava field evolution and emplacement dynamics of the 2014–2015 basaltic fissure eruption at Holuhraun, Iceland. J Volcanol Geotherm Res. doi:10.1016/j.jvolgeores.2017.02.027

Reynolds HI, Gudmundsson MT, Högnadóttir Th, Magnússon E, Pálsson F (2017) Subglacial volcanic activity above a lateral dyke path during the 2014–2015 Bárdarbunga-Holuhraun rifting episode, Iceland. Bull Volcanol 79(6):38.

Rossi C, Minet C, Fritz T, Eineder M, Bamler R (2016) Temporal monitoring of subglacial volcanoes with TanDEM-X—application to the 2014–2015 eruption within the Bárðarbunga volcanic system, Iceland. Remote Sens Environ 181:186–197.

Sigmundsson F, Hooper A, Hreinsdottir S, Vogfjord KS, Ofeigsson BG, Heimisson ER, Dumont S, Parks M, Spaans K, Gudmundsson GB, Drouin V, Arnadottir T, Jonsdottir K, Gudmundsson MT, Hognadottir Th, Fridriksdottir HM, Hensch M, Einarsson P, Magnusson E, Samsonov S, Brandsdottir B, White RS, Agustsdottir Th, Greenfield T, Green RG, Hjartardottir AR, Pedersen R, Bennett RA, Geirsson H, La Femina PC, Bjornsson H, Palsson F, Sturkell E, Bean CJ, Mollhoff M, Braiden AK, Eibl EPS (2015) Segmented lateral dyke growth in a rifting event at Bardarbunga volcanic system, Iceland. Nature 517(7533):191–195.

Thordarson T, Larsen G (2007) Volcanism in Iceland in historical time: Volcano types, eruption styles and eruptive history. J Geodyn 43(1):118-152.